UNIVERSITÀ DI PISA

DIPARTIMENTO DI BIOLOGIA
CORSO DI LAUREA MAGISTRALE IN
BIOLOGIA APPLICATA ALLA BIOMEDICINA

Tesi di Laurea Magistrale

Insights into the mechanisms of plasmidic DNA nuclear delivery by confocal microscopy in living cells

Relatori:
Dott. Francesco Cardarelli
Prof. Mario Pellegrino

Correlatori:
Prof.ssa Renata Batistoni
Prof. Giovanni Casini

Candidato:
Giuseppe Fiume

Anno Accademico
2014/2015

To my friends

and family

Index

ABSTRACT **1**

1 AIM OF THE THESIS **3**

2 INTRODUCTION **4**

2.1 Gene therapy and DNA delivery systems **4**

2.1.1 Viral vectors 5

2.1.2 Non-viral vectors 5

2.2 Cellular transfection barriers involved in gene delivery **10**

2.2.1 Uptake pathways for non-viral Gene Delivery 11

2.2.2 Endosomal Escape 11

2.2.3 Fate of plasmidic DNA in the cytoplasm 12

2.2.4 Nuclear delivery 13

2.2.5 Transcription efficiency 14

2.3 Focusing on the nucleus as a barrier for non-viral gene delivery **16**

2.3.1 Nuclear entry of viruses 17

2.3.2 Transcription factor-binding sites promote DNA nuclear translocation 18

2.3.3 Cell division and nuclear uptake of plasmidic DNA 20

2.4 Lipid-polymer hybrid system as an additional non-viral gene delivery vector **23**

2.4.1 Protamine as an enhancer of lipid-mediated gene transfer 23

2.4.2 Comparison between Lipoplexes and Lipid/Protamine/DNA Nanoparticles 25

3 MATERIALS AND METHODS **34**

3.1 Cell culture **34**

3.2 Transfection with Lipofectamine® Reagent **34**

3.3 Transfection with Lipid/Protamine/DNA nanoparticles **35**

3.4 Plasmids **36**

3.5 Fluorescence phenomenon **36**

3.6 Green fluorescent proteins as transfection efficiency reporters **37**

3.7 Other fluorescent dyes used in this work **40**

3.7.1 Hoechst 40

3.7.2 NBD 40

3.7.3 FM4-64 41

3.7.4 Propidium iodide 41

3.8 Confocal microscopy 42
3.8.1 Fluorescence Recovery After Photobleaching (FRAP) 43
3.8.2 Z-stacks of optical sections 45
3.8.3 Time lapse 46
3.9 Flow cytometry 46
3.9.1 Fluorescence expression analysis of transfected cells as a parameter for transfection efficiency 48
3.9.2 Cell cycle analysis 49
3.9.3 How to study transfection efficiency in synchronized CHO cells 50

4 RESULTS 52
4.1 Characterization of transfection phenotypes 52
4.1.1 Dc-Chol/DOPE/Protamine Nanoparticles 52
4.1.2 Lipofectamine 67
4.2 Transfection Efficiency measured with Flow Cytometry 69
4.3 CHO cells synchronization with mimosine 72
4.4 Live cell imaging with confocal microscopy 76

5 DISCUSSION 79

6 REFERENCES 83

7 ACKNOWLEDGMENTS 88

Abstract

Transfection allows the introduction of foreign genetic material into cells to study gene function and regulation, investigate protein function and, potentially, cure diseases by delivering the gene of interest into the target cells of patients. Although virus-mediated gene delivery methods show high transfection efficiency, they are mostly limited by their hazardous immunogenicity. That is the reason why, lately, chemical and physical approaches have been developed to overcome this huge disadvantage, though displaying a low efficiency. The use of cationic lipids as a chemical method is very common today because of their ease to use: such a system just exploits the capability of liposomes to trap hydrophilic molecules, like DNA, and facilitate their delivery into the cells. More recently, complexes made of lipids and polycations (e.g. protamine) have been deeply investigated because of a promising improvement in transfection efficiency as compared to cationic lipids alone. A general feeling coming from the recent literature is that the mechanisms involved in the cellular delivery of DNA with non-viral gene delivery methods are not clear, especially those concerning the intracellular trafficking and transport into the nucleus. In this Master's thesis project two transfection nanoformulations are compared to give a deeper insight into one of the most important cellular barrier that plasmidic DNA encounters at the end of its intracellular trafficking: the entry into the nucleus. The first nanoformulation chosen is Lipofectamine, a gold standard for transfection; the second one is the complex between cationic lipids and the polycationic agent protamine, which is used to condense DNA before formulation with lipids. Observations coming from laser scanning confocal microscopy and flow cytometry allowed studying the different mechanisms of DNA nuclear delivery among these two nanoformulations. The most important finding is the understanding of the crucial role played by the cell cycle during transfection: data show that all the cells go through mitosis before being transfected. This prompts us to speculate that the breakdown of the nuclear envelope during the mitotic phase may facilitate trapping of plasmidic DNA within the nucleus. Another important observation is the establishment of a different transfection phenotype after mitosis, between the two transfection formulations: cells transfected with Lipofectamine show high transfection efficiency and symmetry of the fluorescent signal between the two daughter cells after cell division; by contrast, cells transfected with the lipids/protamine complexes typically show a lower characteristic transfection efficiency, and marked asymmetry of the fluorescent signal between the two daughter cells (along with the existence of big clusters of plasmidic DNA colocalizing inside the nucleus). From the literature, it is known that condensation of DNA with protamine before mixing with cationic liposomes increases transfection efficiency (as measured by the luciferase assay) in comparison with the use of liposomes only. The observations coming from my experiments may help elucidating the differences between the two formulations: transfection with lipids/protamine could yield lower transfection efficiency, compared to Lipofectamine, because of a lower bioavailability of plasmidic DNA, which is clustered in a few "big" aggregates. These clusters may explain the asymmetry described before: in other words, a limited number of plasmidic DNA molecules can be segregated into the two daughter nuclei after the nuclear envelope breakdown, giving rise to a pronounced asymmetry of the fluorescence signal between daughter cells. These insights provided by confocal microscopy and flow cytometry on the relationship between transfection and cell

division may help guiding the development of a new class of non-viral gene delivery systems with higher performances.

1 Aim of the Thesis

In this Master's thesis project fluorescence-based, state-of-the-art techniques, such as confocal microscopy and flow cytometry, are used to get insights into the cellular processes involved in protamine-mediated transfection. Indeed, a special focus is given on the nuclear envelope barrier and correlation between the transfection process and the cell cycle. In order to get a deeper understanding of these phenomena, the gold standard transfection formulation Lipofectamine is used in comparison with lipid-protamine nanoparticles to elucidate, through live cell imaging and large cell population analysis, the mechanisms responsible for the different transfection efficiency of these two nanoformulations. The methods and results described in this work offer a powerful additional protocol to evaluate, compare and analyze further non-viral transfection vectors with the expectation of a better comprehension of intracellular mechanisms and improvement of gene delivery performances.

2 Introduction

2.1 Gene therapy and DNA delivery systems

Gene therapy is a promising therapeutic strategy for the treatment of a wide range of acquired and inherited diseases. This therapeutic model depends on either replacing a dysfunctional gene by a healthy one, or complementing a missing gene in order to express the required protein.[1] A transgene used as a pharmaceutical must overcome several obstacles avoiding degradation in order to reach the cell nucleus where it should be correctly expressed **Figure 1**. A perfect delivering system should have the following characteristics:

- it must not interact with vascular endothelial cells and blood components;
- it must be capable of avoiding uptake by the reticuloendothelial system;
- it must be small enough to pass through the cell membrane and reach the nucleus.

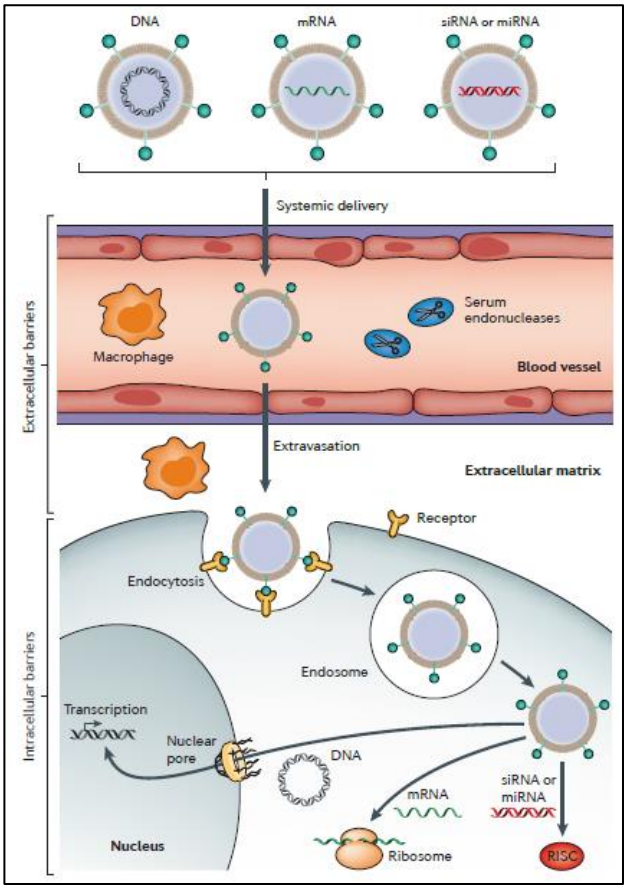

Figure 1 Barriers to successful *in vivo* delivery of nucleic acids. These vectors need to prevent degradation by serum endonucleases and evade immune detection. They also need to avoid renal clearance from the blood and prevent nonspecific interactions. Moreover, the vectors need to extravasate from the bloodstream to reach target tissues, and mediate cell entry and endosomal escape.

At present, treatment using genes is preferable to enzyme/protein replacement therapy because gene therapy ensures the lasting production of a stable quantity of proteins and allows specific transgene-expression localization, which permits to avoid the unwanted effects caused by the systematic presence of a protein.

Vectors are vehicles carrying the genetic material into cells. The optimal vector depends on the target cells and its characteristics, duration of expression and size of the genetic material incorporated. The first vectors used in gene therapy were viruses, due to their ability to deliver and protect the therapeutic gene and ensure long-term expression. However, the risk of provoking immune responses, the high cost and difficulty relating to their preparation, and the limited size of the genetic material that can be incorporated limited the use of these vectors, and led to research into cheaper and safer alternatives.

This is the reason why non-viral vectors have appeared and they can be divided into two groups:

1. **physical approaches** like needle injection, electroporation, gene gun, ultrasound and hydrodynamic delivery. These methods depend on a physical force that weakens the cell membrane and help facilitate the penetration of the gene inside the nucleus;
2. **chemical vectors** like lipoplexes and polyplexes. These are particles prepared by electrostatic interaction between polycationic derivatives like lipids or polymers with the anionic phosphate of DNA.[2,3]

2.1.1 Viral vectors

A **virus** is a biological entity that can penetrate into the cell nucleus of the host cell and exploit the cellular machinery to express its own genetic material and replicate it, before spreading to neighbour cells. Researchers have used different viruses to deliver therapeutic genes by exploiting their particular life cycle. The most used viruses are retroviruses, adenoviruses, adeno-associated viruses (AAV) and simplex herpes virus. To use a virus as a vector, it must be modified by removing the pathogenic part of its genes and replacing it by the therapeutic gene. At the same time, the virus retains its non-pathogenic structures which allow it to infect the cell (like envelope proteins, fusogenic proteins, etc.). To date, viral vectors are the vectors most often used to transfer genes. **Table 1** shows advantages and disadvantages of viral vectors.[2]

Advantages	Disadvantages
High transfection efficiency *in vivo*	Carcinogenesis and immunogenicity
	Difficult and expensive production in large quantities
	Limited size of gene that can be delivered

Table 1

2.1.2 Non-viral vectors

The drawbacks of viral vectors, especially severe immune response and insertional mutagenesis, have led scientists to find safer alternatives. Consequently, **non-viral vectors** have been designed for transferring DNA and their use in clinical trials increased from 2004 to 2013, while that of viral vectors saw significant decrease. Research in this field has attracted great attention as a result of the advantages that they offer in comparison to viral vectors. **Table 2** shows advantages and disadvantages of non-viral vectors.[2,4]

Advantages	Disadvantages
Relatively safe	Low transfection efficiency
Low immune response	
Easy and cheap production in large quantities	
Transfer of different and large transgenes	
Long period storage due to their stability	

Table 2

Despite all these advantages, only a few of these non-viral vectors have so far been tested clinically owing to their low delivery efficiency compared to viral vectors. Whereas viruses have evolved to deliver their genomes efficiently to mammalian cells, most synthetic vectors are unable to effectively transport their payloads through the multiple barriers they have to confront.[5]

As briefly described before, non-viral DNA delivery systems are classified into two groups: physical methods and chemical methods.

Physical Methods

The principle of physical gene delivery systems is to use mechanical, ultrasonic, electric, hydrodynamic or laser-based energy in order to create temporary weak points in the membrane of the target cell, by causing transient injuries or defects in it and facilitates DNA intracellular delivery by diffusion. The most important physical methods are:

- **electroporation**: the principle is to induce the uptake of DNA into the cell by increasing the permeability of the cell membrane through exposure to a controlled electric field and pulse duration. Intense electric pulses affect the cell membrane and cause temporary localized destabilization, like pores formation, allowing DNA to pass easily into the cell;
- **gene gun** (or ballistic DNA transfer): first employed in plant cells, in this method transgene delivery into the target cell and tissue is carried out by using accelerated particle carriers made of biocompatible heavy metals such as gold, tungsten or silver. These carriers are coated with plasmid DNA, and the required acceleration is provided either by vaporization, water under high-voltage electric spark, or by using helium discharge;
- **ultrasound** (or **sonoporation**): depends on increasing the permeability of cell membrane by using ultrasound waves that create pores or acoustic cavitation in the exposed cell membrane to allow cellular uptake of DNA.[2]

Chemical Methods

Chemical vectors are proposed as promising alternatives to viral ones to overcome the drawbacks of the latter. These vectors have three objectives that improve gene transfer into the cell nucleus. They:

- mask DNA-negative charges;
- compress the DNA molecule to make it smaller;
- protect it from degradation by intracellular nucleases.

These objectives can be achieved through packing DNA either by electrostatic interaction between anionic DNA and polycations, or encapsulating it with biodegradable polymers, or by adsorbing it.

Examples include inorganic particles like engineered nanoparticles that may vary in size, shape and porosity: calcium phosphate, silica, gold, magnetic compounds, quantum dots, carbon nanotubes are among the most studied in this category.

Using electrostatic attraction between anionic DNA and a cationic lipid or polymer lead to positive complexes known respectively as **lipoplexes** and **polyplexes**.

• Lipoplexes: A cationic lipid consists of three parts **Figure 2**:

1) a hydrophobic anchor (two aliphatic chains (saturated/unsaturated), or a cholesterol derivative),
2) a hydrophilic positively charged head,
3) a space (linker).

The linker connects the anchor to the head and plays and important role in determining the lipid's biodegradability.

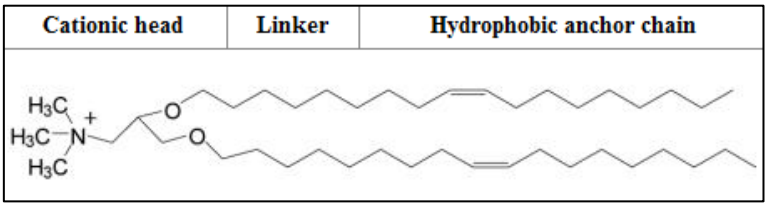

Figure 2 DOTMA as an example of cationic lipid.

The hydrophobic moieties and head groups cause the cationic lipids to assemble into bilayer vesicles (liposomes) when are dispersed in aqueous solutions. When cationic liposomes condense with anionic DNA, they form positively charged lipoplexes because of the positively charged head group of cationic lipids binding with negatively charged phosphate group in nucleic acids. Transfection efficiency depends on overall geometric shape, number of charged group per molecules, nature of lipid anchor and linker bondage. **Figure 2** shows N[1-(2,3-dioleyloxy)propyl]-N,N,N,trimethylammonium (DOTMA) and this was the first non-natural cationic lipid employed for gene transfer. Neutral lipids, such as the fusogenic phospholipid dioleylphosphatidylethanolamine (DOPE) or the membrane component cholesterol, were included in liposomal formulations as "helper lipids" to enhance transfection activity. Cholesterol provides structural stability, whereas DOPE can fuse with other lipids when exposed to a low pH, such as in endosomes, facilitating the release of the associated DNA into the cytosol. Since then, many different lipids were developed to form self-assembling nano-sized DNA delivery systems (lipoplexes) **Figure 3**.

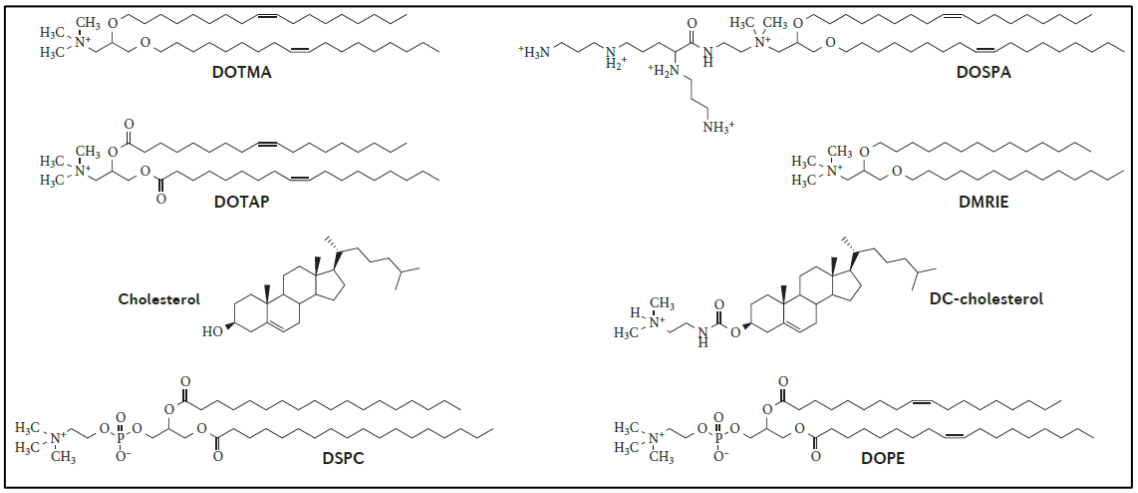

Figure 3 Chemical structures of cationic and neutral lipids are shown. Liposomal formulations used for DNA delivery typically include a mixture of a neutral lipid and a cationic lipid. Cationic lipids (such as DOTMA, DOSPA, DOTAP, DMRIE and DC-Cholesterol) have an active role in DNA binding and transfection. They are characterized by a cationic head group, a hydrophobic tail and a linker region. Neutral lipids (such as the phospholipids DSPC and DOPE, and the membrane component cholesterol) function as "helper lipids" to further enhance nanoparticle stability and overall transfection efficacy.[5]

The major problem behind the use of lipoplexes *in vivo*, besides poor efficiency, is cytotoxicity resulting from the lipoplex-positive charge interaction with negatively charged serum proteins and reduced half-life in blood.[2,5]

• Polyplexes: A cationic polymer (at physiological pH) is used to condense anionic nucleic acid into a nano-sized complex called "polyplex" by self-assembly via electrostatic interactions. It can compress DNA molecules to relatively small size which facilitates cellular internalization and thus improves transfection efficacy. Moreover cationic polymers are attractive because of their immense chemical diversity and their potential for functionalization. Cationic polymers used for polyplexes are generally divided into natural (proteins, peptides, polysaccharides) and synthetic (poly ethylenimine, dendrimers,…) polymers. Unfortunately, the use of polyplexes as gene-transfer systems *in vivo* must overcome many obstacles, such as their toxicity, poor efficiency, polymer polydispersity, and the lack of information about the gene transfer mechanism involved in these methods. Poly-L-lysine (PLL) is considered as one of the first polymers to be used for gene transfer *in vivo*. Unlike lipoplexes, polyplexes formed with PLL usually use ligands to facilitate their cellular uptake, and endosomolytic reagents are usually used to facilitate endosomal escape. Many cationic polymers have been also evaluated as gene carriers both *in vitro* and *in vivo*, such as poly ethylenimine (PEI) and poly amido amine (PAA) and others **Figure 4**.[2,5] PEI-based polyplexes are more efficient and do not require agents for endosomal escape.[6]

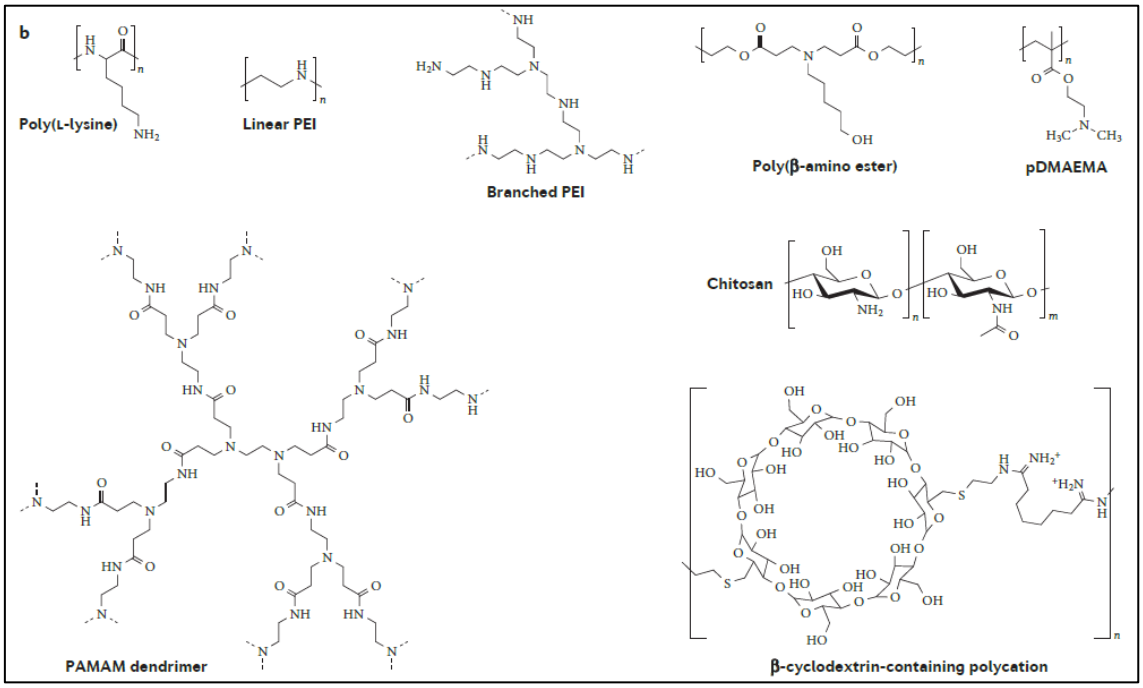

Figure 4 Chemical structures of selected polymeric DNA vectors that are commonly used in gene delivery studies and clinical trials. Poly(L-lysine) and poly ethylenimine (PEI) are among the oldest and most commonly used polymeric gene vectors. To improve safety and efficacy, numerous other polymers have been studied for gene delivery, including methacrylate-based polymers such as poly[(2-dimethylamino)ethyl methacrylate] (pDMAEMA), carbohydrate-based polymers such as chitosan and β-cyclodextrin-containing polycations, polyamidoamine (PAMAM) dendrimers and degradable poly(β-amino ester) polymers.[5]

The main purpose of all these developments and methods in gene therapy is to increase the desired medical impact of a drug, and to decrease the side effects related to its use. Nowadays a lot of effort is being made to improve the efficiency of non-viral vectors and this Master's thesis work actually provides a series of biophysical techniques useful to give insights into the cellular mechanisms involved during transfection. This kind of studies are crucial to help understanding which are the key rate-determining steps that limit the transfection efficacy of non-viral gene delivery methods.

2.2 Cellular transfection barriers involved in gene delivery

The successful delivery of therapeutic genes to specific target cells and their availability at the intracellular site of action are fundamental requirements for successful gene therapy. By hijacking a variety of cellular mechanisms, viruses have evolved over millions of years strategies to bypass multiple cellular barriers and carry their genomic material into the nucleus. Despite their immunogenicity, they present a high transfection efficiency. Non-viral vectors, on the other hand, represent a more recent promising approach for the delivery of the DNA but they are limited by a low transfection efficiency. As can be seen in **Figure 5** lipoplexes (in this case Lipofectamine plus) requires 3 orders of magnitude more gene copies than the Adenovirus vector to achieve comparable gene expression.[7] It has been established that numerous cellular obstacles account for this low level of transgene expression by non-viral vector-mediated gene delivery. Apart from extracellular barriers like interaction with blood components, accessibility and specificity of target tissue/organ, as well as rapid pDNA clearance from the extracellular milieu, here we will concentrate on the major obstacles encountered by a plasmidic DNA at a cellular level during its nucleocytoplasmic trafficking. These barriers include binding to the cell surface, traversing the plasma membrane, escaping lysosomal degradation, and overcoming the nuclear envelope **Figure 6**.[8,9,10,11,12,13]

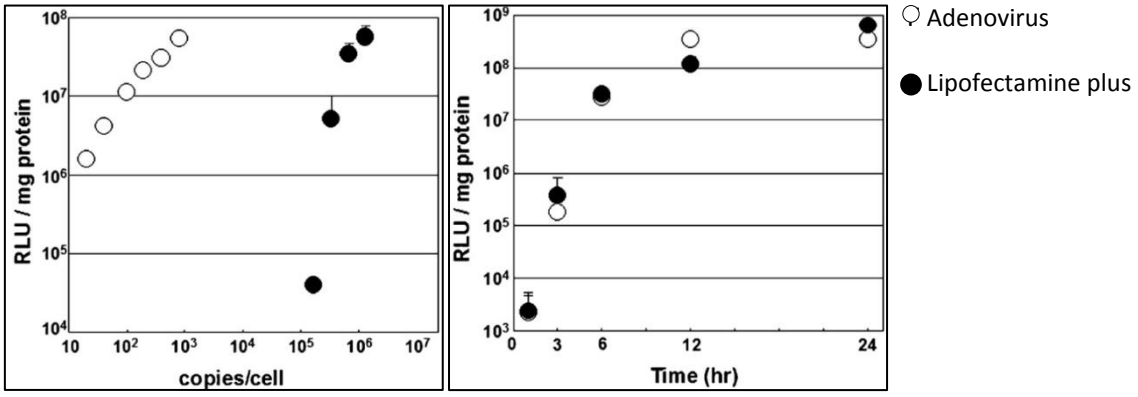

Figure 5 Dose-response curve and time course of luciferase gene expression in A549 cells transfected by Adenovirus or Lipofectamine plus. (Left) Luciferase gene expression in cells transfected by Adenovirus or Lipofectamine Plus was measured 6 h after incubation at the indicated dose. (Right) Transfection activities were measured at indicated times after incubation with a dose of 200 copies/cell using Adenovirus and 6.7 x 10^5 copies/cell (5 pg/cell) with Lipofectamine plus. These data represent the mean values and standard deviation of three experiments.[7]

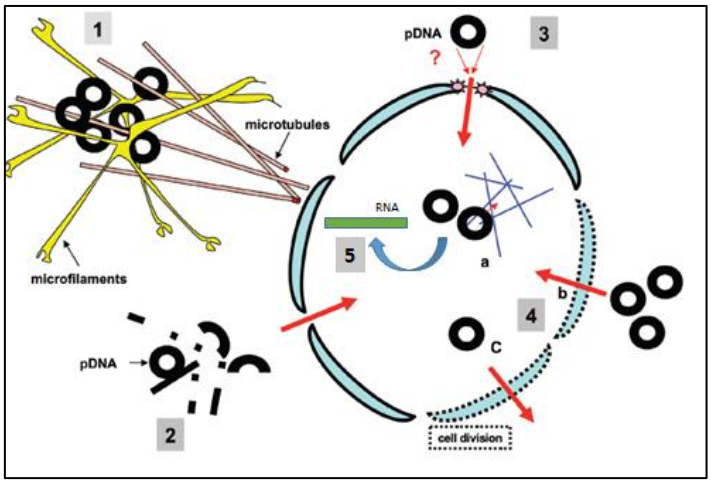

Figure 6 Schematic representation of the cellular barriers to nucleocytoplasmic traffic of plasmid DNA (pDNA). Cellular barriers that are implicated in the low efficiency of pDNA uptake: 1) the cytoskeleton and molecular crowding restrict the diffusional mobility of pDNA in the cytoplasm, 2) degradation of pDNA by constitutively active cytosolic nuclease(s), 3) restricted translocation efficiency of pDNA in the nucleus, and 4) upon the disassembly of the nuclear envelope both nuclear entry (b) and escape (c) of pDNA may occur, 5) limited transcriptional activity of pDNA in the nucleus which is conceivably influenced by interactions with the nuclear matrix components (a).[8]

2.2.1 Uptake pathways for non-viral Gene Delivery

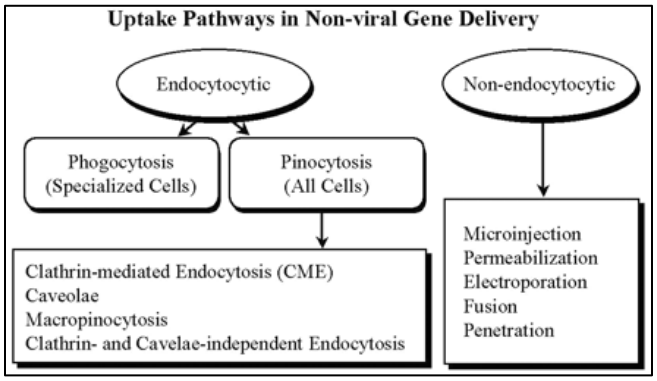

Figure 7

DNA is a large and charged molecule that needs to cross the plasma membrane in order to reach its target (i.e. the nucleus). The plasma membrane of living cells is a dynamic structure that is relatively lipophilic and, as a result, it restricts the entry of large, hydrophilic, or charged molecules. An appropriate gene delivery system is therefore required for the efficient cellular uptake and it is necessary a complete understanding of both the characteristics of the vectors as well as the mechanisms by which they interact with the targeted cells. Several internalization mechanisms have been proposed to explain the uptake of different synthetic vectors. The uptake mechanisms are, in general, closely linked with the intracellular trafficking and the fate of the vectors. The main different endocytotic as well as non-endocytotic uptake pathways used in gene delivery can be seen in **Figure 7**.

Unless a specific targeting ligand is incorporated in the system, the binding of lipoplexes and polyplexes to the cell surface is the result of a nonspecific ionic interaction between the positive charge of the complexes and the negative charge of the cell surface. Negatively charged cell surface constituents, such as heparin sulfate proteoglycans and integrins play a role in the cellular binding of positively charged lipoplexes, polyplexes, or even cationic peptides, such as TAT.

The internalization mechanism of lipoplexes is not well understood. In general, following some experimental evidences, it is currently believed that membrane fusion is important for transfection but that most of the uptake occurs through **endocytosis** (**Figure 8**). The current question is then, which pathway of endocytosis is responsible for the uptake? Data have shown that uptake may occur by clathrin-mediated endocytosis, cholesterol-dependent clathrin-mediated endocytosis, clathrin-independent endocytosis like claveolae or macropinocytosis. The variability of reported results suggests that a variety of factors may affect the actual mechanism.[6,14]

2.2.2 Endosomal Escape

After internalization via endocytosis, lipoplexes and polyplexes exist in endosomes and have no access to the cytosol or the nucleus. The destiny of these endosomes is the fusion with lysosomes for degradation or the recycle of their contents back to the cell surface. That is the reason why **endosomal escape** is essential for efficient transfection **Figure 8**. Lipoplexes containing the pH-sensitive fusogenic lipid DOPE can release the associated DNA into the cytosol. DOPE forms a stable lipid bilayer at physiological pH ≈ 7; however, at an acidic pH 5 to

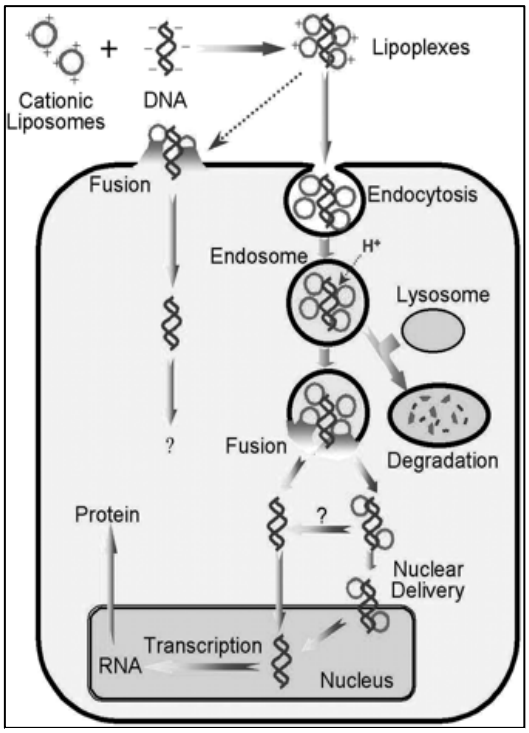

Figure 8

6, it undergoes a transition from a bilayer to an inverted hexagonal structure, which fuses and destabilizes the endosomal membrane, releasing its contents to the cytosol. It is possible that only DNA or the lipoplex as a whole will be released to the cytosol after fusion. If lipoplexes are released, the dissociation of DNA must occur in the cytosol or even at the nuclear membrane to achieve transfection. PEI has the same ability, although through a different mechanism. PEI becomes more protonated at low pH as in endosomes. This protonation triggers an influx of Cl^- ions with protons leading to a water influx and finally the swelling and rupturing of the endosomes.

Lipoplexes lacking fusogenic lipids and polyplexes without proton sponge ability are not released efficiently into the cytosol unless additional functional devices for endosomal release are used. An example is the use of peptides that undergo conformational changes at the low pH in the endosomes to interact with and perturb the endosomal membrane. Another approach is the use of lysosomotropic reagents such as chloroquine, a weak hydrophobic base, which enters the lysosomes and becomes protonated in its acidic environment. This triggers a swelling of lysosomes and destabilization of their membranes. Chloroquine also inhibits the acidification and maturation of endosomes, thus retarding the lysosomal degradation of genes. It is worth mentioning, that the use of chloroquine and similar lysosomotropic reagents is usually associated with toxicity, which limits their use in actual applications.[6]

2.2.3 Fate of plasmidic DNA in the cytoplasm

Another obstacle that DNA may encounter, after endosomal escape, is cytoplasmic **molecular crowding**. On the basis of the observation that plasmidic DNA (pDNA) remained at the site of microinjection, it was proposed that diffusional freedom of pDNA in the cytoplasm of myotubes is severely impeded[15], whereas oligonucleotides up to 250 bp rapidly enter the nucleus after cytoplasmic delivery[16]. Consistently, microinjection of pDNA in the proximity of the nucleus, or decreasing the expression cassette size, could significantly enhance transgene expression. Direct determination of the diffusional mobility of fluorescein-conjugated pDNA was accomplished by fluorescence recovery after photobleaching (FRAP). Microinjected nucleic acids > 2 kbp are virtually immobile during the course of the measurements (a few minutes). Diffusion of 250- and 2000-bp DNA fragments is 17- and > 100-fold slower, respectively in the cytoplasm than in water[16]. Presumably the mesh-like structure of the cytoskeleton accounts for the anomalous mobility of pDNA in the cytoplasm, because diffusion was significantly increased after disruption or reorganization of the actin cytoskeleton[17,18,19].

This may overall bring to hypothesize that cytoplasm imposes a diffusional barrier to nucleocytoplasmic transport of pDNA.

Restricted diffusion increases the residence time of pDNA in the cytoplasm, which in turn favors the metabolic degradation of pDNA. Some observations, like potentiation of transgene expression by nuclease inhibitors, are in support of the conclusion that metabolic instability of pDNA may contribute to the low gene transfer efficiency of non-viral gene delivery vectors. Actually, a subset of nucleases plays a central role in the fragmentation of chromosomal DNA and may transiently appear in the cytoplasm.[8]

2.2.4 Nuclear delivery

The **nuclear envelope** contains nuclear pores with a passive transport limit of 70 kDa molecular mass or ≈ 10 nm diameter[20]. This is much smaller than the size of DNA, even when condensed in lipoplexes or polyplexes. Data show that microinjections of plasmid DNA into the nucleus produce a much higher gene expression than when the same plasmid is microinjected into the cytosol. For instance, the measure of luciferase activity in growth-arrested COS-7 cells after the injection of known amounts of reporter gene into the cytosol or the nucleus showed that only 1 of 1000-1500 cytosolic pDNA molecules is successfully transcribed in the nucleus **Figure 9**. This suggests the overall inefficiency of pDNA nucleocytoplasmic trafficking and that the nuclear envelope is a significant barrier against transfection.[8]

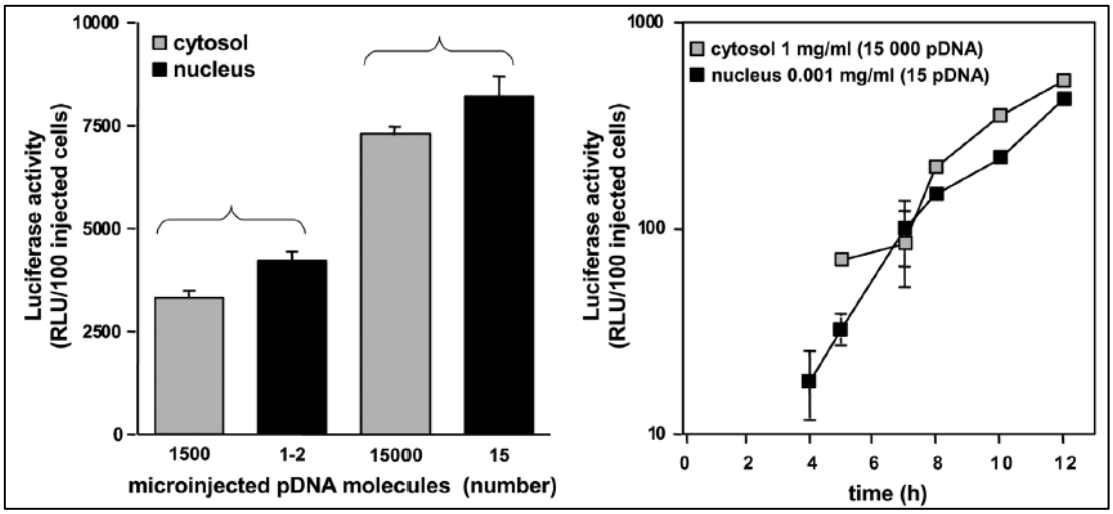

Figure 9 Nuclear uptake efficiency of pDNA microinjected from the cytoplasm. Nuclear uptake efficiency of luciferase expression cassettes was inferred from the relative expression level of known amount of microinjected pDNA in the cytoplasm and the nucleus. (Left) The indicated amount of pGL2 plasmids, encoding the luciferase reporter gene, was injected into the cytoplasm of the nucleus of 300-400 COS-7 cells. Cells were growth-arrested by serum depletion and luciferase activity was measured after 8 hr of injection. Cell viability was determined by co-injection of fluorescein-labeled dextran. The amount of pDNA copies injected was calculated from the pDNA concentration and the microinjected volume, determined by radioactive dextran in parallel measurements. (Right) Time course of luciferase expression was monitored following cytoplasmic or nuclear microinjection of pGL2 using the indicated number of pDNA in COS-7 cells. Based on these experiments it is estimated that only 1 out of 1000 cytosolic pDNA molecules reached the nucleosol. Data are means (± SEM, n = 3).[8]

2.2.5 Transcription efficiency

Although the efficiency of plasmid nuclear delivery is a critical determinant of the level of transgene expression, intranuclear events also influence the transcriptional activity of the transgene, and should be taken into consideration when attempting to maximize the efficiency of non-viral vectors.[21]

Hama *et al.*[7] describe a systematic and quantitative comparison of the cellular uptake and subsequent intracellular distribution of exogenous DNA transfected by viral and non-viral vectors in living cells, using a combination of TaqMan PCR and a confocal image-assisted three-dimensionally integrated quantification method (CIDIQ). They use adenovirus (Ad) and Lipofectamine Plus (LFN) as models for comparison, since they are highly potent and widely used viral and non-viral vectors, respectively. Their findings show that efficiency of cellular uptake of LFN is significantly higher than that for Ad. Once taken up by a cell, Ad exhibits comparable endosomal escape and slightly higher nuclear transfer efficiency compared with LFN. In contrast, LFN requires 3 orders of magnitude more intranuclear gene copies to exhibit a transgene expression comparable to that of the Ad, suggesting that the difference in transfection efficiency may principally arise from differences in nuclear transcription efficiency and not from a difference in intracellular trafficking between Ad and LFN **Figure 10**.

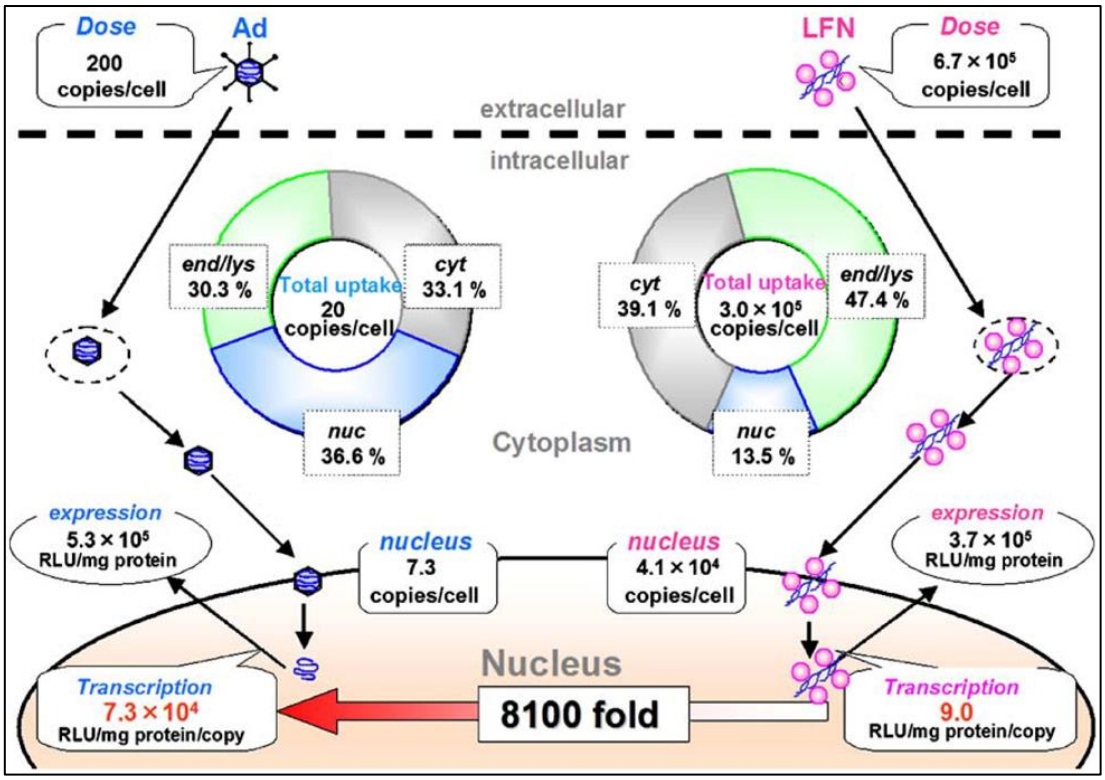

Figure 10 Summary of the quantitative comparison of intracellular trafficking in A549 cells between Ad and LFN. These values were quantified by TaqMan PCR and CIDIQ analysis.

It is difficult to find an explanation to this observation. A plausible hypothesis could be a difference in decondensation in the nucleus: the nuclear DNA introduced by the LFN could be so well condensed that the transcription process is inhibited. Another possibility is that the Ad genome structure and/or proteins coded in the Ad genome affect transgene expression

though some of the regions of Ad genome were deleted. The take-home message is that transcriptional activity should not be excluded as a rate-limiting process during transfection and it might be worthy to be considered for the optimization protocol of non-viral vectors.

2.3 Focusing on the nucleus as a barrier for non-viral gene delivery

In eukaryotic cells, the DNA is segregated away from the cytoplasm by the nuclear envelope (NE). Unlike other cellular membranes, the NE is a double lipid bilayer composed of an outer (ONM) and inner membrane (INM) separated by a perinuclear space. The ONM is contiguous with the ER and is thought to contain many of the same proteins and lipids in contrast with the INM that has a distinct composition and interacts with chromosomes and/or the nuclear lamina **Figure 11**[22]. The NE is generally considered as a hydrophobic barrier: transport of macromolecules into and out of the nucleus occurs through **nuclear pore complexes** (NPCs) that are embedded in the NE at sites where the ONM and INM are contiguous **Figure 11**[23]. The NPC has often been considered to be the sole route for crossing the NE; however, Speese *et al*.[24] found that large ribonucleoproteins particles cross the NE by vesicle budding and fusion pathway through a NPC-independent mechanism, very similar to the nuclear egress of herpes virus. This poses interesting questions as to whether this could be a widespread export, or even possibly import, mechanism.[22]

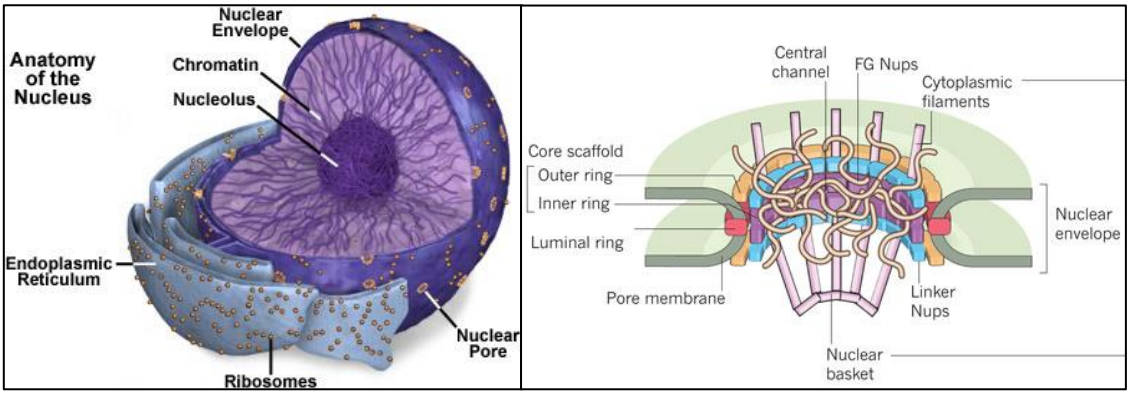

Figure 11 Eukaryotic cell nucleus (taken from http://micro.magnet.fsu.edu/cells/nucleus/nucleus.html) and nuclear pore complex (NPC)[23]

Anyway, molecules smaller than about 40 kDa diffuse passively through the NPC, whereas proteins > 60 kDa are taken up by energy-dependent transport. Active nuclear accumulation requires the presence of nuclear localization sequence (NLS) in the cargo. A NLS is an amino acid sequence that 'tags' a protein for import into the cell. Generally, this signal consists of one or more short sequences of positively charged lysines or arginines exposed on the protein surface. Docking of NLS provokes considerable conformational change in the NPC, leading to opening of the channel diameter from 9 to 40 nm. This conformational change provides a plausible explanation for the ability of the NPC to translocate substrates as large as 25-50 MDa. The size-dependent diffusional barrier of the NPC can be visualized by the cytoplasmic microinjection of fluorescent nucleic acids: DNA fragments smaller than 250 bp are able to diffuse into the nucleus, whereas nucleic acids larger than 250 bp are excluded from the nucleus.[16,25]

Cargo proteins bearing NLSs are bound and imported by a class of proteins known as karyopherins (importins) that are soluble in the NPC. In the case of the classical NLS system (from SV40 Large T-antigen PKKKRKV), the NLS of the cargo protein is recognized in the cytoplasm by importin-α, an NLS receptor, which then dimerizes with importin-β to form a

nuclear pore targeting complex. The interaction between the importins and a series of phenylalanine-glycine (FG)-repeat proteins that make up the NPC facilitates translocation across the pore **Figure 11**. Once inside the nucleus, the small guanosine-triphosphate (GTP)-binding protein RAN, in its GTP-bound state, recognizes the importing-cargo complex at the nuclear face of the NPC, binds to importin and induces conformational change in the protein that releases the cargo. After inducing release of the cargo within the nucleus, the RAN-GTP-importin-β complex is transported back into the cytoplasm where the Ran GTPase-activating protein (RanGAP) regenerates RAN-GDP to maintain the RAN gradients. RAN is maintained in its GTP-bound state in the nucleus by the guanine nucleotide exchange factor RCC1 which is bound to chromatin. To maintain relative levels of RAN across the nuclear envelope, RAN-GDP is transported into the nucleus by the small protein NTF2 where it is reconverted to the GTP-bound state **Figure 12**.[26]

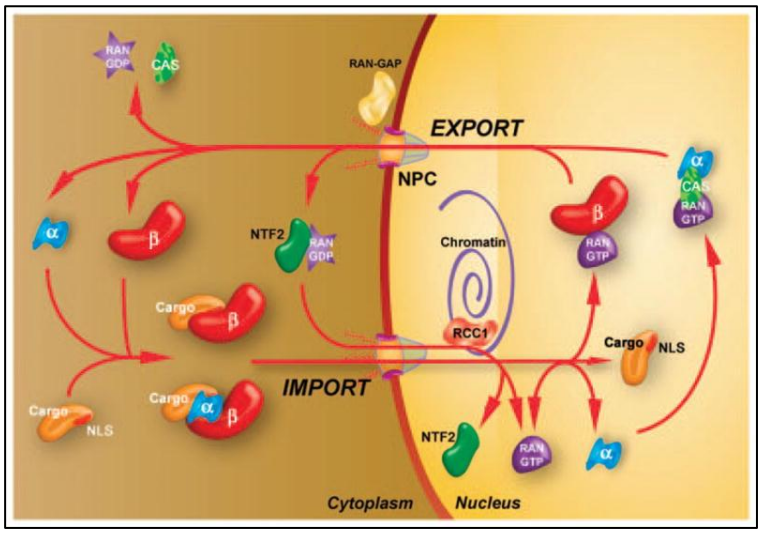

Figure 12 Mechanisms of protein nuclear import

2.3.1 Nuclear entry of viruses

Viruses had millions of years to develop strategies to circumvent cellular barriers in order to ensure infection of their target cells. Most of these mechanisms involve designing and incorporating proteins into the virus that help stabilizing virus-cell interactions and increasing internalization, enhancing endosomal escape, promoting movement through the cytoplasm to the nuclear envelope, improving nuclear entry in dividing and non-dividing cells (often by promoting mitosis) and finally increasing transcription. Non-viral vectors have not had the luxury of evolution to aid the delivery and are thus confronted by each of these barriers. It has long been appreciated that the nuclear envelope represents a barrier to efficient gene delivery. Most successful laboratory transfections occur in actively dividing cells. As one of the hallmarks of mitosis is nuclear envelope breakdown, any DNA that has entered the cytoplasm before mitosis would gain access to the nuclear compartment once cells initiates division.

As indicated in **Figure 13**, five general strategies have been identified, ordered according to where in the cell uncoating of the viral genome occurs:
1) some viruses, such as the retrovirus murine leukemia virus (MLV), gain access to the nucleus during mitosis, when the NE is temporarily disassembled;

2) some viruses, such as human immunodeficiency virus 1 (HIV-1) and influenza A virus, undergo extensive disassembly in the cytoplasm. The cytoplasmic released components contain NLSs and are thereby able to cross the NPC using the host transport machinery;
3) some viral capsids use importins or viral proteins to attach to the cytoplasmic side of the NPC. Interaction with the NPC is then used as a cue for disassembly, and the viral genome crosses the NPC and is released into the nucleus, often as a complex with viral proteins. Viruses that use this strategy include herpesviruses (which bind to the NPC via importins) and adenoviruses (which bind directly to the NPC);
4) some viral capsids, such as those of hepatitis B virus (HBV) and some baculoviruses, are small enough to cross the NPC intact. Genome release then occurs at the nuclear side of the NPC or inside the nucleus;
5) some viruses, such as parvoviruses, do not use the NPC to deliver their genome into the nucleus; rather, they transiently disrupt the NE and nuclear lamina, and enter the nucleus through the resulting gaps.[27]

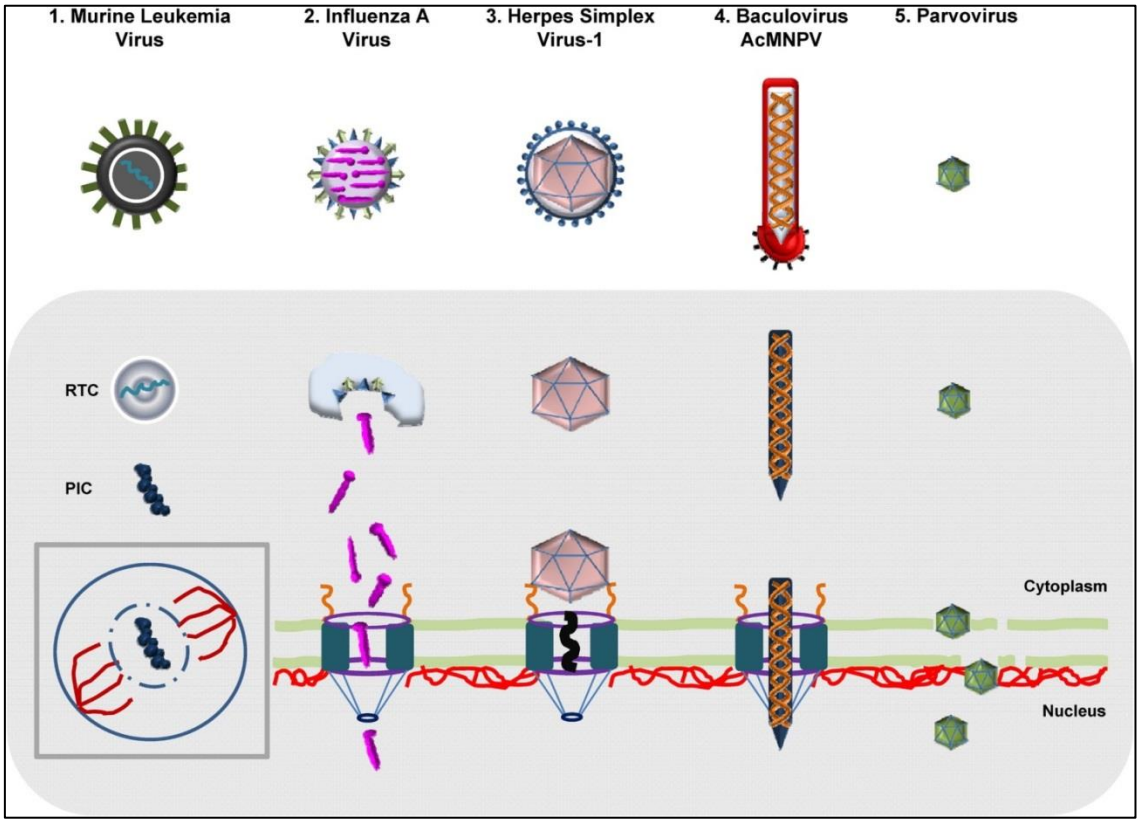

Figure 13 Schematic representation of different strategies for nuclear entry of viral genomes.[27]

2.3.2 Transcription factor-binding sites promote DNA nuclear translocation

Certain DNA sequences can increase the nuclear targeting of plasmids. Miller *et al.*[28] showed that the nuclear import of plasmid DNA through the NPC is a sequence-specific process, mediated by specific eukaryotic sequence elements. When delivered side by side by

microinjection into the cytoplasm, plasmids containing as little as 72 bp of the SV40 enhancer target to the nucleus of most cells within several hours, whereas an identical plasmid lacking this 72-bp sequence remains cytoplasmic until cell division (or indefinitely if the cell is non-dividing). This sequence, termed the "SV40 DNA nuclear targeting sequence (DTS)", has been shown to mediate plasmid nuclear import in several cell lines.

The distinguishing feature of the SV40 DTS is that it contains binding sites for a number of ubiquitously expressed mammalian transcription factors (such as AP1, AP2, nuclear factor (NF)-κB, Oct1, TEF-1). As transcription factors function in the nucleus, they contain NLSs for their nuclear importation. Under normal conditions, these factors would be transported into the nucleus after translation or in a regulated manner when signals activate transcription. In either case, a significant cytoplasmic pool of these factors exists at any given time. When plasmids carrying the SV40 DTS are delivered into the cytoplasm by any method, some of these transcription factors can bind to the DTS, thereby coating a region of the plasmid with NLSs, at least some of which are oriented away from DNA itself. These DNA-bound NLSs can be recognized by importin-β and/or transportin and transported into the nucleus through the NPC. Apart from the requirement for the NLS to be spatially accessible to the importins when the transcription factor is bound to the DNA, the binding sites for the transcription factors must also be accessible to the transcription factors for any complex to assemble.[26,29]

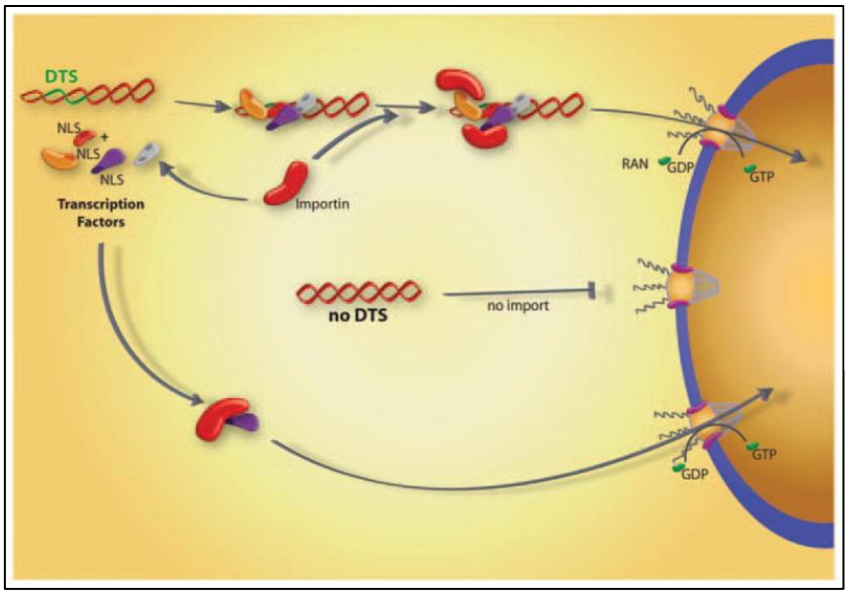

Figure 14 Protein-mediated plasmid nuclear import.

This finding could be extended also to eukaryotic promoters or enhancers with the important premise that the transcription factors binding to these promoters/enhancers would keep presenting their NLSs in an orientation that is accessible to the importins. Miller *et al*.[30] managed then to exploit cell-specific transcription factors to drive cell-specific DNA nuclear entry. They studied a smooth muscle-specific DTS (containing a 176 bp sequence of the smooth muscle γ-actin (SMGA) promoter) to drive nuclear import of plasmids in airway or vascular smooth muscle cells but not in other cell types, both in cultures cells and *in vivo*.

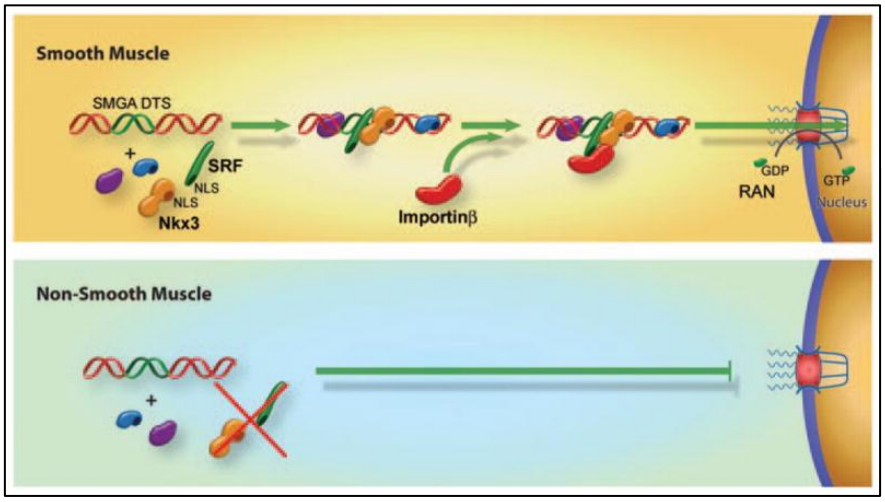

Figure 15 Cell-specific plasmid nuclear import

The importance of sequences brought to develop methods that enhance plasmids nuclear import. A number of different approaches have been created to promote recognition of plasmid by importin family members to increase nuclear import like: peptide-nucleic acid clamp-conjugated NLS peptides bound to DNA, sequence specific DNA binding proteins bound to DNA, NLS-peptides covalently attached to DNA and NLS peptides electrostatically bound to DNA.[26,31,32,33,34]

2.3.3 Cell division and nuclear uptake of plasmidic DNA

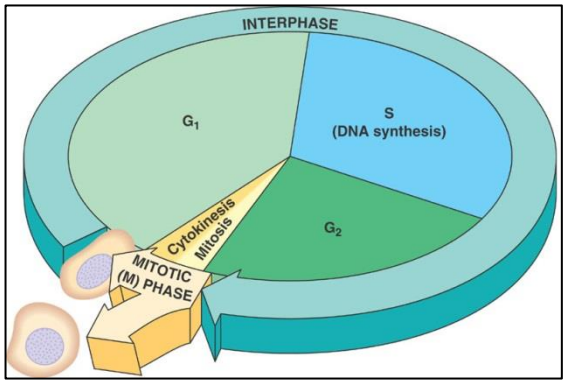

Figure 16 Schema of the cell cycle (Taken from http://kvhs.nbed.nb.ca/gallant/biology/cycle.jpg)

The **cell cycle** is divided into two basic parts: mitosis and interphase. Mitosis (nuclear division) is the most dramatic stage of the cell cycle, corresponding to the separation of daughter chromosomes and usually ending with cell division (cytokinesis). Interphase is the time during which both cell growth and DNA replication occur in an orderly manner in preparation for cell division.

The M phase of the cycle corresponds to mitosis, which is usually followed by cytokinesis. This phase is followed by the G_1 phase (gap 1), which corresponds to the interval (gap) between mitosis and initiation of DNA replication. During G_1, the cell is metabolically active and continuously grows but does not replicate its DNA. G_1 is followed by S phase (synthesis), during which DNA replication takes place. The completion of DNA synthesis is followed by the G_2 phase (gap 2), during which cell growth continues and proteins are synthesized in preparation for mitosis **Figure 16**. The duration of these cell cycle phases varies considerably in different kinds of cells. For a typical rapidly proliferating human cell with a total cycle time of 24 hours, the G_1 phase might last about 11 hours, S phase about 8 hours, G_2 about 4 hours, and M about 1 hour. Other types of cells, however, can divide much more

rapidly. Budding yeasts, for example, can progress through all four stages of the cell cycle in only about 90 minutes. Even shorter cell cycles (30 minutes or less) occur in early embryo cells shortly after fertilization of the egg.[35]

The higher transfectability of dividing over quiescent cells appears to be compatible with the hypothesis that disassembly of the nuclear envelope during the M phase enhances plasmidic DNA (pDNA) uptake. Grosjean and *et al*.[36] used cell synchronization with mimosine (a drug that blocks cells at the border between G1 and S-phase) to evaluate transfection efficiency at different phases of the cell cycle using calcium-phosphate (CaPi) method. They showed that transfection of a GFP-codifying plasmid using CaPi-DNA co-precipitation method, at different phases of the cell cycle, yields variable expression levels of GFP: highest GFP expression levels are seen when transfecting cell populations with a dominant representation of S-phase cells **Figure 17**. They suggest this is due to the imminent nuclear membrane disintegration at mitosis. Tseng *et al*.[37] used a liposomal vector containing DOTAP and DOPE and observed transfection with a GFP-codifying plasmid in Hela G1-synchronized cells with a standard double thymidine blocking procedure. Cell samples were transfected and subsequently maintained in G1 phase for various durations to modulate the time between plasmid entry and mitosis. The percentage of cells expressing GFP increase sharply as the synchronized cell population passes through M phase, suggesting that an event associated with mitosis is essential for transgene expression. Brunner *et al*.[38] also investigated the influence of cell cycle on transfection efficiency. They fractionated, by means of size and density, fractions of cells corresponding to discrete cell cycle phase-specific populations and transfected them with various non-viral methods and viral methods. Transfection efficiency is found to be strongly dependent on the cell cycle stage at the time of transfection. Luciferase activity in cells transfected with non-viral vectors is from 30- to more than 500-fold higher when transfection is performed during S or G2 phase compared with cells in G1 phase which had the lowest expression levels. In contrast, this effect is not observed with recombinant adenovirus which varied only four-fold. Although it has been shown that mitosis-associated nuclear envelope breakdown greatly enhances nuclear localization of plasmids and transfection efficiency, this is not a prerequisite.

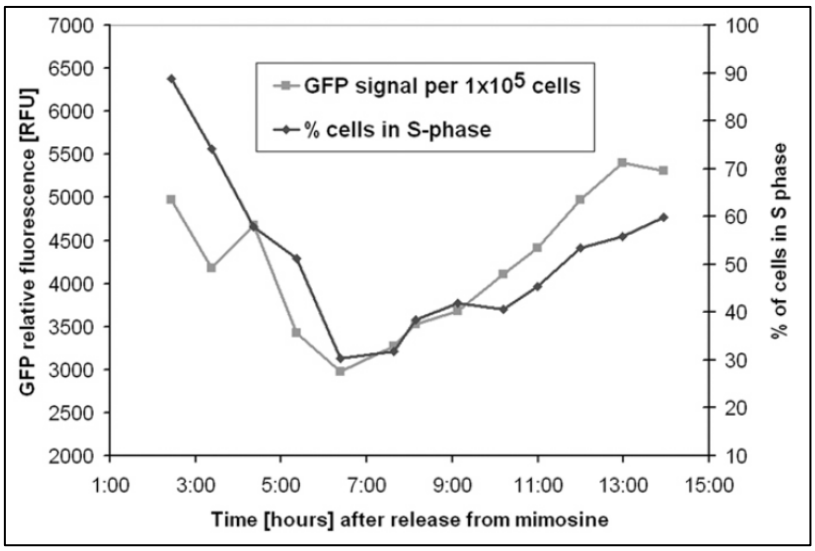

Figure 17 Levels of GFP expression per 1 x 10^5 cells correlate with percentage of cells in the S-phase. Transfections were done every hour after release from synchronization and cell cycle distribution was measured for every cell population being transfected.[36]

Several groups have shown that plasmids can enter the nuclei in the absence of cell division, although the efficiency of such transfection is usually much lower than in dividing cells. Dowty

et al.[15] showed that pDNA injected into the cytoplasm could be expressed with relatively high efficiency in myotubes providing irrefutable evidence that pDNA can enter the karyoplasm of a post-mitotic nucleus with intact membranes. Akita *et al*.[39] showed that DNA transfected with Lipofectamine Plus could be detected in the nucleus in time intervals as low as 1 h after lipoplex-mediated transfection, which suggests that a different mechanism is involved in this early nuclear delivery. Also Kamiya *et al*.[40] observed exogenous DNA within the nucleus after 0.5- to 1-h incubations, and some molecules that extended through the nuclear membrane. These results may provide evidence for a possible nuclear entry in the presence of the nuclear membrane

2.4 Lipid-polymer hybrid system as an additional non-viral gene delivery vector

Although substantial progress has been made in the field of non-viral gene therapy over the past three decades there is still the need of additional biological insights into the key rate-determining steps that limit effective delivery and transfection efficacy of non-viral gene delivery methods. The main drawback of these methods – that is low transfection efficiency – has brought to developments in material sciences, which have yielded new polymers and lipids as delivery vectors. At the same time the rapid progress of nanotechnology is enabling a better understanding of nanosized materials for gene delivery.

Hybrid systems made of lipids and polymers (lipopolyplexes) have been explored to improve gene delivery. In these systems, DNA is pre-condensed with either poly-L-lysine, protamine, histone or several synthetic polypeptides, followed by lipid wrapping using either cationic liposomes, anionic liposomes or amphiphilic polymers. It combines the high compaction of polyplexes and the facilitated endosomal escape of the lipoplexes. In addition, they provide more protection to DNA. Additional efforts are needed to prove that the lipid/polymer hybrid system is superior to that of lipoplexes or polyplexes for *in vivo* gene delivery.[41]

2.4.1 Protamine as an enhancer of lipid-mediated gene transfer

Protamines are small peptides (MW 4000-4250) which are very basic due to their high arginine content. They are naturally occurring substances found only in sperm and purified from the mature testes of fish, usually salmon. Protamine's role in sperm is to bind with DNA, assist in forming a compact structure, and deliver the DNA to the nucleus of the egg after fertilization. This unique role overcomes a major obstacle in gene therapy by non-viral vectors, the efficient delivery of DNA from the cytoplasm into the nucleus. Furthermore, protamine is a FDA-approved substance with a documented safety profile and could be readily used as an adjuvant to a human gene therapy protocol.

Sorgi *et al*. showed that condensation of plasmidic DNA with protamine before complexation with cationic liposomal formulations (DC-Chol and lipofectin) exhibited increased transfection activities in CHO cells comparable to that seen with the multivalent cationic liposome formulation, lipofectamine. They hypothesize this is probably due to the spermine head group of DOSPA of Lipofectamine that can effectively condense DNA into a compact structure. This condensed structure, due to its diminished size, may be more readily endocytosed by the cell, resulting in the increased levels of transgene expression. Protamine could apparently do the same, thus improving the transfection activities of other lipids.[42,43]

Salmon sperm protamine is a protamine which has been sequenced and shown to contain the following 32-amino acid sequence: PRRRRSSSRPVRRRRRPRVSRRRRRRGGRRRR (PRO ARG ARG ARG ARG SER SER SER ARG PRO VAL ARG ARG ARG ARG ARG PRO ARG VAL SER ARG ARG ARG ARG ARG ARG GLY GLY ARG ARG ARG ARG). Nearly two-thirds of this sequence (21 of 32 residues) is composed of arginine, found clustered in four distinct regions, containing four to

six arginine repeats. The protamine molecule has the ability to change its structure from a random coil in solution to a structure containing four α-helical regions in the presence of nucleic acids. These four α-helical regions are well known helix breakers and this confirms that protamine can align with the major groove of double helical DNA of the B form **Figure 18**.[44,45] Further, protamine may wind around a single double-strand or may cross-link with adjacent strands, resulting in cross-linking, condensation, and stabilization of the DNA into a highly compact structure.[46,47]

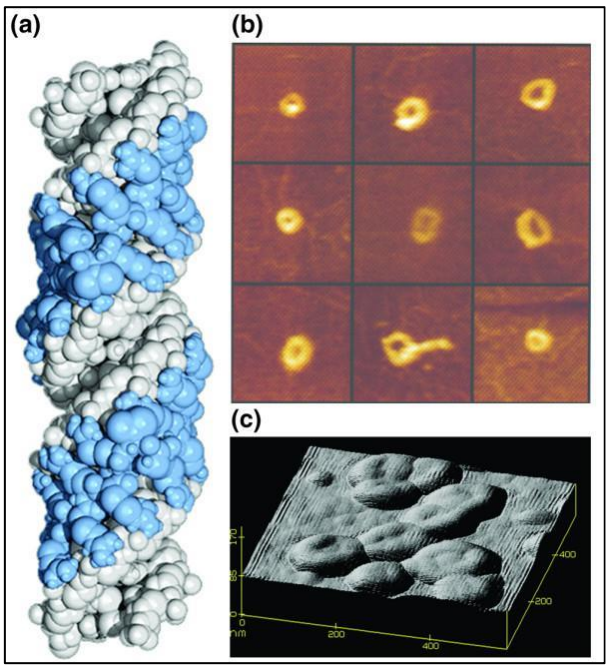

Figure 18 Protamine molecules bind in the major groove of DNA, neutralizing the phosphodiester backbone of DNA and causing the DNA molecules to coil into toroidal structures.

(a) Model showing how two adjacent salmon protamine molecules (blue atoms) wrap around the DNA helix (white atoms) and bind within the major groove of DNA.

(b) Scanning-probe images of toroidal DNA-protamine complexes prepared *in vitro* on a graphite surface by adding protamine to DNA attached loosely to the surface. The toroids formed *in vitro* are similar in size and shape to those isolated from human sperm chromatin (c).

(c) Scanning-probe microscope images of native DNA-protamine toroids obtained from human sperm chromatin. These toroids, which comprise the basic subunit structure of protamine-bound DNA, contain approximately 50,000 bp of DNA coiled into each donut-shaped structure.[44]

Sorgi *et al*. also found protamine to be superior to poly-L-lysine as well as to various other types of protamine (with more lysine residues). The data seem to suggest that the lysine residues are the cause of the loss of activity. The appearance of lysine is at the expense of arginine, with the amount of lysine and arginine within each protamine molecule remaining constant. As both lysine and arginine are cationic, the net charge of the various protamines remain constant and should produce similar condensed structures, assuming that this effect is due solely to charge, rather than structural composition. There are two possible explanations for the above observations:

1) the exchange of one or several arginine residues for lysine interferes with the binding or affinity of protamine to DNA because of interruption of the α-helical structures. This hypothesis is strongly supported by the amino acid analysis, transfection and binding assays which all indicate a loss in activity/binding correlating with the appearance of lysine residues within the protamine molecule;
2) protamine contains a nuclear localization signal (NLS) which specifically directs the complex to the nucleus. From the general properties found among NLSs – generally characterized as containing short runs of basic amino acids – there exist four potential regions within the 32-mer protamine which could potentially serve as a nuclear localization signal (amino acids 2-5, 12-16, 21-26 and 29-32). The existence of a NLS within protamine could account for the increased activity in comparison to other cationic polymers (such as poly-L-lysine) and the disruption of the NLS by the

incorporation of a lysine residue could lead to its loss of activity since a single point mutation is often sufficient to result in complete loss of nuclear targeting.[42]

2.4.2 Comparison between Lipoplexes and Lipid/Protamine/DNA Nanoparticles

Nanostructure of Lipoplexes

Cationic lipid-DNA complexes are denoted as lipoplexes. Cationic lipids are typically used in the form of cationic liposomes which can be identified as artificial vesicles consisting of one or more bilayers of amphipathic lipids that trap an equal number of internal aqueous compartments. These structures are formed spontaneously when certain lipids are placed in aqueous phase, through the self-assembly of these lipids in such a way as to orient their hydrophobic parts away from the water, while the hydrophilic parts are oriented towards the aqueous phase surrounding the hydrophobic ones. Due to the structure of liposome, it can encapsulate a wide range of hydrophilic and hydrophobic drugs, in the phospholipid bilayer, in the internal aqueous compartments or at the bilayer interface **Figure 19**.[2]

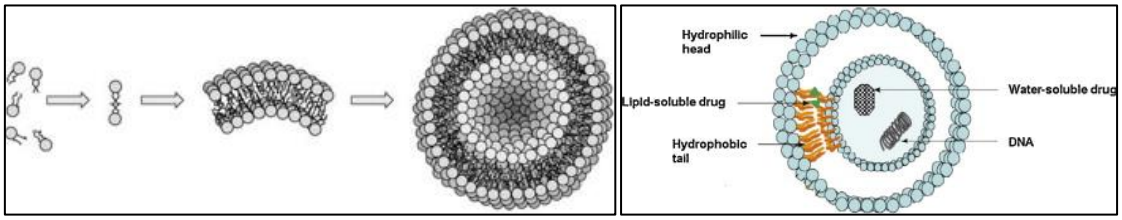

Figure 19 Formation of liposome by the self-assembly of amphiphilic lipids placed in aqueous phase (left) and schematic illustration representing the structure of liposome and the potential position of lipophilic and hydrophilic drugs (right).[2]

Other properties that made liposomes attractive are:

- biocompatibility;
- liposome-incorporated pharmaceuticals are protected from the inactivating effect of external conditions, yet do not cause undesirable side reactions;
- size, charge and surface properties of liposomes can be easily changed simply by adding new ingredients to the lipid mixture before liposome preparation and/or by variation of preparation methods;
- unique opportunity to deliver pharmaceuticals into cells or even inside individual cellular compartments.[48]

The formation of lipoplexes is generally difficult to control, and different structures are produced in the same lipoplex preparation. The proposed model for describing the interaction between cationic liposomes and DNA involves the following: (i) liposomes cause a compaction of the DNA molecules and charge neutralization; (ii) neutralization may induce aggregation, resulting in the formation of a heterogeneous group of multilamellar structures of different shapes and consisting of DNA sandwiched between lipid bilayers; (iii) it is proposed that DNA affects the liposomes, inducing lipid mixing and rearrangement resulting in fusion of the multilamellar structures to form large DNA-lipid complexes.[49] Lipoplexes are classified into three types, small unilamellar vesicles (SUV), with a diameter less than 50 nm, large unilamellar vesicles (LUV) with a diameter of 50-500 nm, and multilamellar liposomes (MLV) with a large diameter up to 10,000 nm **Figure 20**.[2]

SUV can condense DNA on its surface, making it vulnerable to the enzymes in the medium. This ineffective protection, in addition to the short half-life of the DNA-SUV complex in the blood circulation, limits its use as a DNA delivery system. The large size of multilamellar liposomes (MLV) hinder their use for systematic administration or transport of DNA into cells.[2] Once inside the cell, such multilamellar structure offers protection from DNA degradation but do not often allow for an adequate DNA release from endosomal compartments. If gene payload is not released from endosomes, it is shuttled to the lysosomes, where it is degraded by nucleases and transfection may fail.[50]

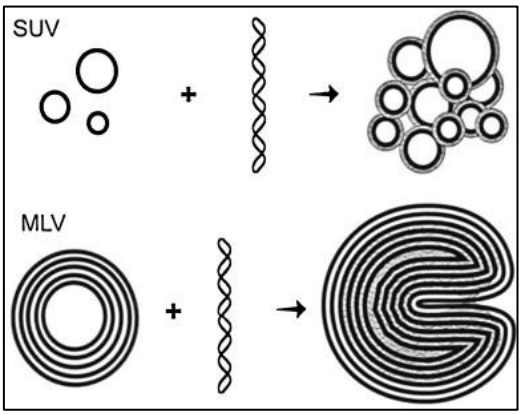

Figure 20 Liposome formulations used as DNA delivery systems.[2]

Nanostructures of Lipid/Protamine/DNA (LPD) Nanoparticles

As briefly described before, to overcome the problem of efficient release from endosomal compartments, lipid/polycation/DNA (LPD) complexes, in which plasmidic DNA condensed with a polycation is encapsulated by a lipid envelope, have recently been developed. Over the past few years several efforts to improve the delivery efficiency of LPD systems have been made: the composition of the lipid envelope has been modified with novel chemical compounds and the surface has been functionalized with several polymers and ligands. One of the most challenging issues in the drug delivery field is systemic tumour-targeted delivery and LPD nanoparticles may represent a potential vector. Caracciolo *et al.*[50], based on the concept of core-shell-type lipid nanoparticles[51], showed that the transfection efficiency of protamine/DNA complexes coated with a lipid envelope made of cationic 1,2-dioleyl-3-trimethylammonium propane (DOTAP) is from 3 to 20 times higher than that of DOTAP/DNA lipoplexes. They showed that the superior efficiency of LPD complexes over lipoplexes does correlate with their distinctive physical-chemical properties. They investigated complex formation, DNA protection, surface properties, nanostructure, ability to release DNA upon interaction with cellular lipids, and intracellular trafficking.

Complexes formation of LPD nanoparticles was studied with gel retardation assay and by determining the average dimensions and the ζ-potential of P/DNA. Gel retardation assay showed substantial retardation of the binary P/DNA complex when P/DNA weight ratio, R_w, was above 0.5. Starting from R_w= 0.75, the molar fraction of plasmid DNA completely protected by protamine, X_{DNA} was maximum (i.e., X_{DNA}= 1) **Figure 21**. The ζ-potential evaluation of P/DNA particles led to choose R_w= 0.75 because it guaranteed complete DNA protection, exhibited negative charge (-20 mV), and had appropriate dimensions (260 nm) with the

minimum P content **Figure 21**. Then the preassembled negatively-charged P/DNA core was coated with a lipid envelope through membrane fusion of positively charged DOTAP small unilamellar vesicles (SUVs), triggered by the electrostatic attraction around the negatively charged core. ζ-potential and dimensions of complete LPD were determined again giving rise to a final chosen LPD nanoparticle (R_V= 2, R_V being lipid/DNA volume ratio) with dimensions of approximately 220 nm, positive charge of 47.8 mV **Figure 21**. The charge of nanocarriers must be positive to let them associate with proteoglycans that are a major constituent of the extracellular cell matrix and are negatively charged under physiological conditions, due to the occurrence of sulfate and uronic acid groups.

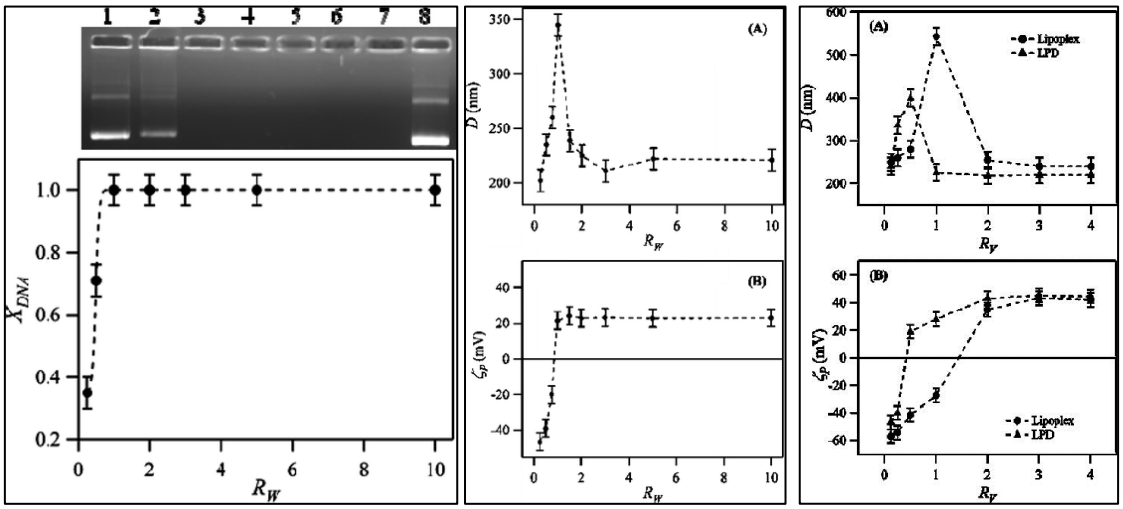

Figure 21 (Top left) Digital photograph of protamine/DNA complexes (P/DNA) with increasing P/DNA weight-ratio R_w= 0.1 (lane 1), R_w= 0.5 (lane 2), R_w= 1 (lane 3), R_w= 2 (lane 4), R_w= 3 (lane 5), R_w= 5 (lane 6), R_w= 10 (lane 7), and control DNA (lane 8). The high mobility band was attributed to the most compact (supercoiled) form, and the less-intense one was considered to be the non-super coil content in the plasmid preparation. (Bottom left) Molar fraction of plasmid DNA protected by protamine, X_{DNA}, against the P/DNA weight ratio, R_w. (Top centre) Diameter of P/DNA complexes, D_H, as a function of the P/DNA weight ratio, R_w. This behavior is typical of the reentrant condensation effect. (Bottom centre) ζ-potential of P/DNA complexes as a function of R_w. The charge inversion effect occurring for $0.5<R_w<1$ changes the overall charge of the aggregates from negative (DNA excess) to positive (protamine excess).[50] (Top right) Diameter of LPD complexes (triangles) and lipoplexes (circles) as a function of the lipid/DNA volume ratio, R_V. (Bottom right) ζ-Potential of LPD complexes (triangles) and lipoplexes (circles) as a function of R_V.

Studies on the nanostructure of LPD complexes and lipoplexes with synchrotron showed that LPD complexes are made of about 10 lipid layers in a highly swollen state, while lipoplexes are well ordered multilamellar structures made of more than 30 alternating lipid/DNA layers **Figure 22**.[50]

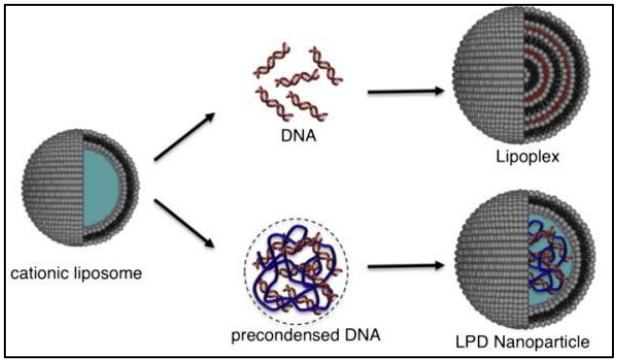

Figure 22 (Cartoon) Mechanism of formation of lipoplexes and lipid nanoparticles: lipoplexes are typically formed by bulk mixing between cationic liposomes and DNA solutions and are arranged as multilayer structures in which DNA is intercalated between alternating lipid bilayers. Lipid NPs are composed are composed of a core of DNA complexed with protamine and covered by a lipid shell that protects DNA from degradation, imparts biocompatibility and improves stability in biological fluids.[50]

Differences in transfection efficiency, interaction with cellular lipids and cell imaging

To compare the ability of LPD nanoparticles and lipoplexes to deliver plasmid DNA, Caracciolo *et al.* performed experiments of Transfection Efficiency (TE) in NIH 3T3, CHO, Hek293, and A17 cells. As shows **Figure 23**, LPD nanoparticles exhibit superior performance over lipoplexes in all the tested cell lines. (As previously described before, these two formulations were coated with the same cationic lipid (DOTAP). The only difference is the pre-condensation step of DNA with protamine in LPD nanoparticles).[50]

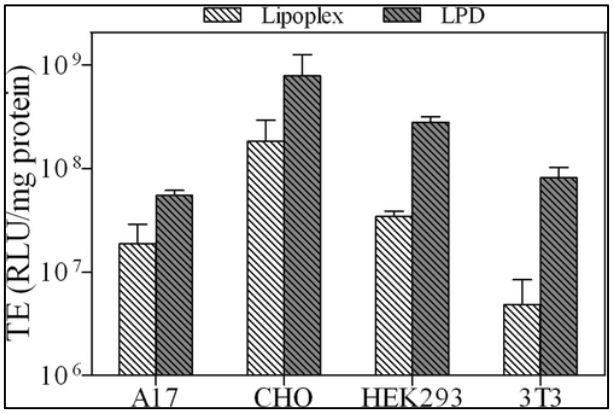

Figure 23 Transfection efficiency of LPD complexes and lipoplexes at the same lipid/DNA ratio (R_V = 2). Luciferase activity is expressed as relative light units/mg of protein in the cell lysate. TE was found to increase by a factor ~3 in A17, ~4 in CHO, ~8 in Hek293, and ~20 in NH 3T3 cells.[50]

The structural evolution of lipoplexes upon interaction and mixing with anionic cellular lipids plays a central role in the DNA escape process, i.e., in how DNA dissociates from lipoplexes and is released into the cytoplasm and eventually into the nucleus. Caracciolo *et al*. performed electrophoretic experiments that allow to quantify the molar fraction of DNA that is no longer electrostatically associated with cationic lipids, 1- X_{DNA}, as a function of the anionic/cationic charge ratio R upon interaction with 1,2-dioleoyl-*sn*-glycero-3-[phospho-*rac*-(1-glycerol)] (DOPG) and 1,2-dioleoyl-*sn*-glycero-3-phosphate (DOPA) anionic cellular lipids. As shows **Figure 24**, at the lowest *R* (*R*= 0.5), DNA is almost completely dissociated from LPD complexes (1 – X_{DNA} ≈ 1), while a large fraction of DNA is still protected by lipoplexes (1 – XDNA of ~ 0.35 and ~ 0.45 for DOPG and DOPA, respectively). **Figure 24** also shows that DNA released from lipoplexes, 1 – X_{DNA}, increases with increasing *R* and reaches 1 at *R* ≈ 10. These findings suggest that a much lower amount of anionic lipids is needed to promote complete DNA dissociation from LPD complexes.[50]

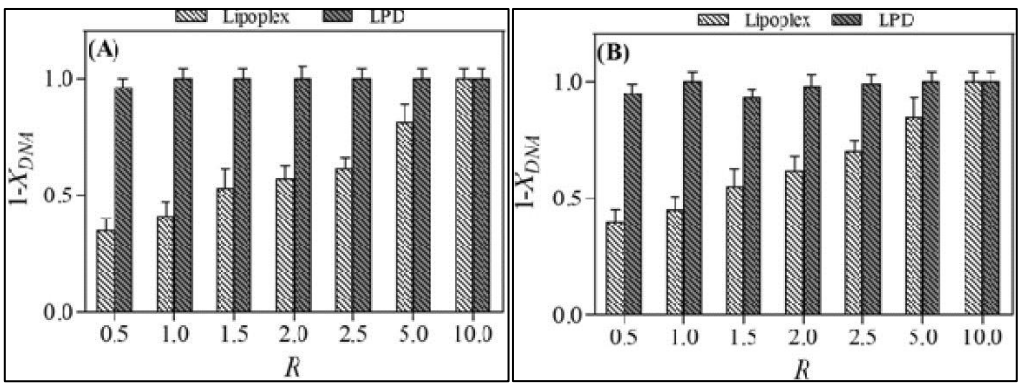

Figure 24 Molar fraction of DNA, 1 – X_{DNA}, that is no longer electrostatically associated with LPD complexes and lipoplexes after interaction with DOPG (A) and DOPA (B) cellular lipids of as a function of the anionic/cationic charge ratio, *R*.[50]

These results show that for R < 0.5 DNA is almost completely released from LPD systems, while it is still largely protected by lipoplexes. The DNA release ability may be connected with the membrane fusion rate of complexes with cellular membranes that is, in turn, inversely related to the multilamellarity of lipid aggregates. Such suggestion is in good agreement with synchrotron experiments showing that lipoplexes are multilamellar systems, while LPD nanoparticles are made of a few membranes and are therefore more disposed to fuse with anionic lipids mimicking cellular membranes and to release their gene cargo.

Confocal images of CHO-K1 cells 4 h after incubation with LPD complexes and DOTAP/DNA lipoplexes are shown in **Figure 26**. Caracciolo *et al*. observed that green fluorescence from lipids forming LPD nanoparticles is clearly localized, while DNA (red fluorescence) has visibly spread into the cytoplasm. This may be plasmid DNA exiting from the endosomal of lysosomal stage into the cytoplasm. Over the same time scale, cells incubated with DOTAP/DNA lipoplexes are mainly distributed throughout the cytoplasm and to some extent at the cell periphery. Complexes do not appear to be spread in the cytoplasm and this could suggest that such binary formulation is defective in facilitating endosomal escape of nucleic acids, resulting in entrapment of plasmid DNA in endosomes.[50]

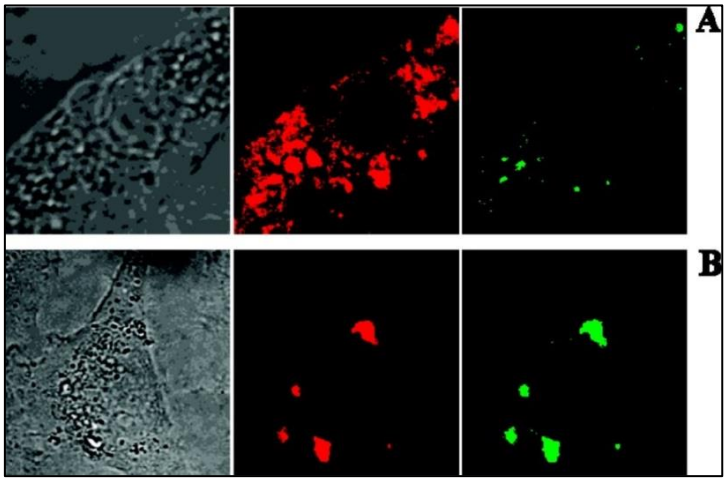

Figure 25 Confocal microscopy of CHO-K1 cells 4 h after treatment with LPD complexes (A) and lipoplexes (B). Green fluorescence from NBD lipids forming LPD complexes was clearly localized, while DNA (red fluorescence) had visibly spread into the cytoplasm. DOTAP/DNA lipoplexes were distributed throughout the cytoplasm and to some extent at the cell periphery. Colocalization of green and red fluorescence signals suggests that lipoplexes are intact with DNA trapped within.[50]

Here in **Table 3** can be found the main characteristics and properties that Caracciolo *et al*. discovered in their work[50] and it is useful to understand the possible different mechanism occurring upon complex-cell interaction between lipoplex and LPD nanoparticle. Because of comparable size and ζ-potential, as well as identical lipid composition, it is reasonable to judge that LPD complexes and lipoplexes enter the cell using similar internalization mechanisms. However, after complex internalization, both LPD complexes and lipoplexes fuse with the negatively charged endosomal membrane. LPD complexes are more fusogenic than lipoplexes, a phenomenon that is presumably related to higher interaction between cationic and anionic cellular lipids due to the absence of competing DNA in the lipid envelope and to the lower number of lipid layers to be peeled off. DNA release from endosomes is not a relevant barrier for LPD complexes, while DOTAP/DNA lipoplexes remained largely intact and accumulated at the nuclear membrane without releasing DNA abundantly **Figure 27**.[50]

	Lipoplexes	LPD Nanoparticles
Composition	DNA + DOTAP	DNA + Protamine + DOTAP
ζ-potential	44.4 mV	47.5 mV
Size	> 200 nm	> 200 nm
Encapsulation/Toxicity	A larger amount of cationic lipids are required to condense the same amount of DNA. More toxic.	A smaller amount of cationic lipids are required to condense the same amount of DNA. Less toxic.
Surface	Adsorption of DNA molecules. Detrimental effect for *in vivo* application because of interactions between negative charged DNA and positively charged serum components that may form aggregates and undesirable lung accumulation	Resembles that of pure DOTAP cationic lipids complexes
Nanostructure	Well-ordered multilamellarity (more than 30 alternating lipid/DNA bilayers)	About 10 lipid layers in a highly swollen state
Transfection efficiency	Lower	Higher
Interaction with anionic cellular lipids	Less disposed to fusion	More disposed to fusion
Cell imaging	Larger entrapment of plasmidic DNA in endosomes/lysosomes	Higher cytoplasmic spread of plasmidic DNA

Table 3

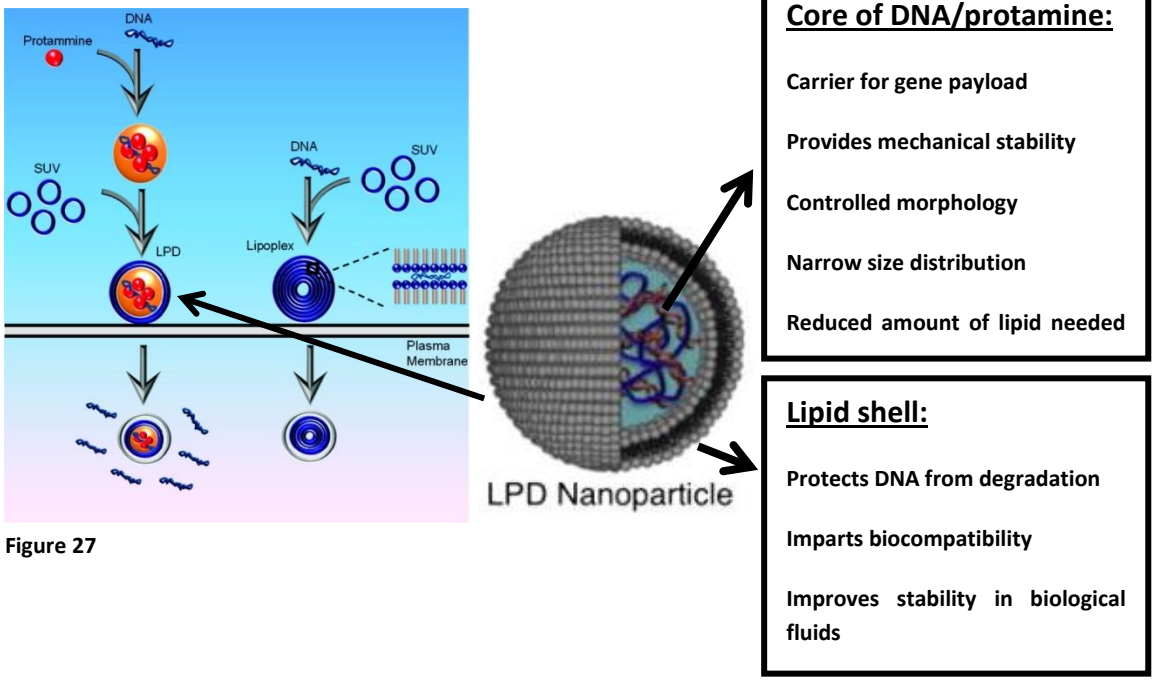

Figure 27

Evaluation of the transfection barriers involved in lipid-mediated gene delivery

Pozzi *et al.*[52] used two lipid formulations to compare cell uptake, intracellular trafficking, endosomal escape and final fate of lipoplexes and lipid-protamine/DNA (LPD) nanoparticles in living Chinese Hamster Ovary (CHO) cells. The first formulation is made of the cationic lipids DOTAP and DOPC, while the second mixture is made of DC-Chol and DOPE. As shows **Figure 28**, DC-Chol-DOPE/P-DNA nanoparticles and DC-Chol-DOPE/DNA lipoplexes are about three orders of magnitude more efficient (using the luciferase expression assay) than their DOTAP-DOPC counterpart. At the same time, transfection efficiency (TE) of DC-Chol-DOPE/P-DNA nanoparticles is about 2-fold times higher than that of DC-Chol-DOPE/DNA lipoplexes. It then looks like LPD nanoparticles show potential superior efficacy compared with lipoplexes. To understand which intracellular barriers are responsible for the different transgene expression, they performed a quantitative mechanism-based investigation comparing cell uptake, intracellular trafficking, endosomal escape and final fate of the four formulations in the selected cell line.

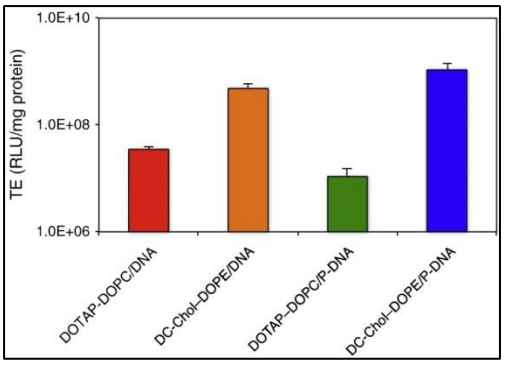

Figure 28

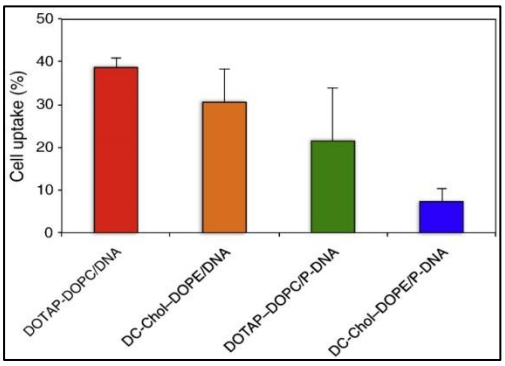

Figure 29

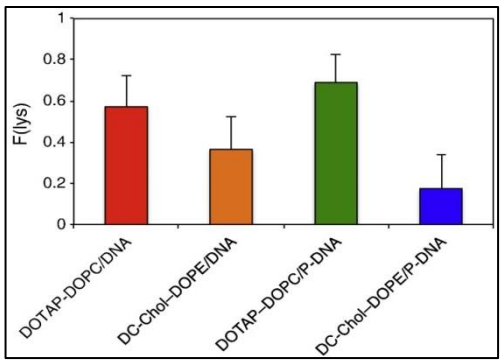

Figure 30 F(lys): fraction of DNA in the lysosomes

In **Figure 29** it is reported the amount of fluorescence positive cells after 3 h of incubation with lipoplexes and LPD nanoparticles prepared with Cy3-labeled DNA at 37 °C, measured by flow cytometry. It shows that cellular uptake of lipoplexes is higher than that of their LPD nanoparticles counterparts. Moreover, it is remarkable that, upon CHO treatment with the less efficient formulation of DOTAP-DOPC/DNA lipoplexes, cell uptake reached a level as high as ≈40 %, anyhow superior to the most efficient formulation of DC-Chol-DOPE/P-DNA nanoparticles (less than 10 %). They conclude that cellular uptake does not correlate with the measured transgene expression. To define the endocytotic route of lipid-mediated DNA delivery, CHO cells were treated with Cy3-DNA (red) and co-labeled with specific markers of endocytic pathways (green): clathrin-mediated endocytosis (Alexa488-labeled transferrin), caveolae-mediated endocytosis (caveolin-E1GFP) and micropinocytosis (70 kDa dextran). Colocalization of red and green fluorescence gave rise to visible yellow/orange punctate structures and they performed, in addition to a qualitative inspection of confocal images, a quantitative analysis of the fluorescence signal distribution. Their findings indicate that fluid-phase micropinocytosis is the main internalization pathway of lipoplexes, while the uptake of LPD nanoparticles occur equally through micropinocytosis and the classical clathrin-associated endocytosis. By using correlation techniques, they found that inside the cell both lipoplexes

and LPD nanoparticles are actively transported towards the cell nucleus. For each lipid formulation, by analyzing colocalization with the lysosome marker Lysosensor, **Figure 30**, it was observed that LPD nanoparticles escaped from endosomes more efficiently than lipoplexes, most likely due to their distinctive core-shell-type nanostructure. The largest fraction of DOTAP-DOPC-containing systems reaches the lysosome compartment, suggesting that poor endosomal escape and extensive lysosomal degradation are the most relevant barriers in DOTAP-DOPC mediated transfection. On the other side, escape from endosome is large in DC-Chol-DOPE-containing systems most likely due to the use of DOPE and cholesterol-like molecules, which can cause rupture of endosomes. **Figure 31** shows a schematic summary and a comparison of the barriers encountered by lipoplexes and LPD nanoparticles analyzed by Pozzi *et al*.[52] Nuclear and post-nuclear processes represent the last steps towards a full identification of intracellular barriers accountable for transfection efficiency dissimilarities between selected formulations. Therefore, future experiments are needed to further investigate what happens during the last phases of DNA intracellular delivery after transfection.

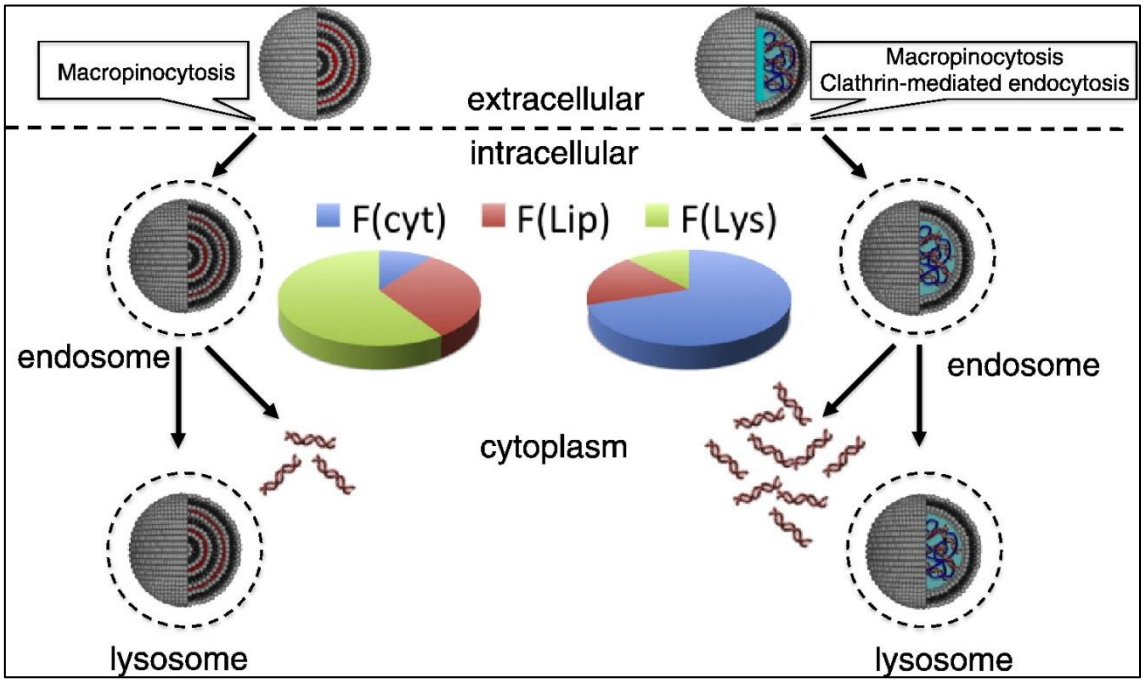

Figure 31 Schematic summary and comparison of the barriers encountered by lipoplexes and LPD nanoparticles.

Overall, these last data indicate that condensation of DNA with protamine before complexation with liposomes increases the transfection efficiency measured with the luciferase assay. Thus protamine represents a potential efficient candidate capable of overcoming the main limit of non-viral methods, i.e. the low transfection efficiency. In this Master's thesis project fluorescence-based state-of-the-art techniques, such as confocal microscopy and flow cytometry, are used to better elucidate the cellular processes involved in protamine-mediated transfection. Indeed, a special focus is given on the nuclear envelope barrier and on the correlation between transfection and cell cycle. In order to have a deeper understanding of these phenomena, the gold standard transfection formulation Lipofectamine is used in comparison with lipid-protamine nanoparticles to elucidate, through live cell imaging and large cell population analysis, the mechanisms involved in the different transfection efficiency between these two nanoformulations. The methods and results described in this work offer a powerful and additional protocol to evaluate, compare and analyze further non-

viral approaches with the expectation of a better comprehension of intracellular mechanisms and improvement of gene delivery methods.

3 Materials and methods

3.1 Cell culture

CHO-K1 cells (purchased from American Type Culture Collection CCL-61 ATCC) were grown in Ham's F12K medium supplemented with 10% of fetal bovine serum and 1% of penicillin/streptomycin at 37°C and in 5% CO_2. The sub-culturing protocol was:

1. cells were maintained in 100 mm X 15 mm Petri dishes (≈ 78,5 cm^2) with 10 mL complete growth medium;
2. every 2-3 days, when cells reached confluence (≈ 1-2 x 10^6), they were washed with Phosphate-Buffer Saline (PBS) to remove all traces of serum that may inhibit trypsin and trypsinized by adding 1 mL of 0.25% (w/v) Trypsin - 0.53 mM EDTA solution and left at 37 °C for 5 minutes;
3. cells were observed under the microscope to ensure the cell layer detached and avoid clumpings of cells;
4. add 9 mL of complete growth medium and aspirate cells by gently pipetting;
5. add appropriate aliquots of cell suspension to a new culture vessel (sub-cultivation volume dilution 1:10 – 1:20).

CHO cell line was chosen due to its common use in research, especially for expression, transfection, and recombinant protein production.

3.2 Transfection with Lipofectamine® Reagent

The following quantities were used depending on the plate format.

Culture vessel	Growth area / well (cm^2)	Vol. plating growth medium (mL)	Vol. Serum-Free Medium (µL)	DNA (µg)	Lipofectamine (µg)
12-well	4,01	1	2 x 50	1	10
6-well	9,62	2	2 x 100	2	20

Cells were transfected according to the following protocol:

1. seed cells to be 70-90% confluent at transfection;
2. dilute DNA with serum-free medium for 5 minutes at room temperature (RT);
3. dilute Lipofectamine (Life Technologies) with serum free-medium for 5 minutes at RT;
4. add diluted DNA to diluted Lipofectamine® Reagent (1:1 volume ratio) and incubate for 20 minutes at RT;
5. add DNA-lipid complexes to cells in serum-free medium for 3 hours at 37°C;
6. wash the cells with PBS and add with complete growth medium and incubate at 37 °C.

3.3 Transfection with Lipid/Protamine/DNA nanoparticles

The following quantities were used depending on the plate format.

Culture vessel	Growth area / well (cm^2)	Vol. plating growth medium (mL)	Protamine (µg)	DNA (µg)	Lipids DC-Chol/DOPE (µg)	Protamine / DNA mass ratio	Protamine / DNA charge ratio
12-well	4,01	1	0.5	1	10	1:2	0,64
6-well	9,62	2	1	2	20	1:2	0,64
6-well	9,62	2	4	2	20	2:1	2,54
6-well	9,62	2	8	2	20	4:1	5,08
6-well	9,62	2	16	2	20	8:1	10,16

First of all dissolve protamine sulfate salt (MW = 5.1 kDa) from salmon (Sigma-Aldrich St. Louis, MO, USA) in distilled water at a final concentration of 0.5 mg/mL and incubate for 24 h at 4 °C. Cells were transfected according to the following protocol:

1. seed cells to be 70-90% confluent at transfection;
2. mix DNA with protamine and incubate for 30 min at RT;
3. add lipids to protamine/DNA complexes and incubate for 30 min at RT;
4. add lipid/protamine/DNA complexes to cells in serum-free medium for 3 hours at 37°C;
5. wash the cells with PBS and add with complete growth medium and incubate at 37 °C.

Protamine/DNA charge ratio was calculated as follows:

$$Charge\ Ratio = \frac{n\,(+)}{n\,(-)}$$

where $n\,(+)$ is the total number of positive moles derived from protamine and $n\,(-)$ is the total number of negative moles derived from the DNA. The equation can also be written in another way:

$$Charge\ Ratio = \frac{n\,(+)}{n\,(-)} = \frac{n_{prot} \times n^{+}}{n_{DNA} \times n^{-}} = \frac{\frac{m_{prot}}{MW_{prot}} \times n^{+}}{\frac{m_{DNA}}{MW_{DNA}} \times n^{-}} = \frac{\frac{m_{prot}}{5100} \times 21}{\frac{m_{DNA}}{MW_{nt} \times 2 \times \mathrm{bp}} \times 2 \times \mathrm{bp}}$$

$$= \frac{\frac{m_{prot}}{5100} \times 21}{\frac{m_{DNA}}{308}} \cong \frac{m_{prot}}{m_{DNA}} \times 1{,}27$$

where n^{+} is the total number of positive residues in protamine (21), n^{-} is the total number of negative residues in DNA, m_{prot} is the mass of protamine, MW_{prot} is the molecular weight of protamine (5100 Da), MW_{DNA} is the molecular wait of DNA, MW_{nt} is the molecular weight of a nucleotide (308), bp is the pair base of DNA.

3.4 Plasmids

A plasmid of 5.5 kbp codifying NLS-SV40 EGFP was used as a protein expression reporter in CHO cells after transfection. This enhanced green fluorescent protein (EGFP) contain at the N-terminal a classical nuclear localization signal (NLS) from SV40 Large T antigen tagging EGFP for import into the cell nucleus by nuclear transport. Since a small amount of plasmid was available in the laboratory, as a first step before utilization, amplification and purification steps were performed. Top10 *E. coli* Competent Cells (Life Technologies) stored at –80 °C were transformed with 100 ng of pcDNA3.1 NLS-SV40 EGFP and left on ice for 30 minutes. Then they received a heat shock for 45 seconds at 42 °C and after 3 minutes on ice again. 250 µL of S.O.C. medium (Life Technologies) were added to bacteria and left to grow for 1 hour at 37 °C. Cells were then plated on LB Agar Ampicillin (100 µg/mL)-100 mm plate and left overnight at 37 °C. A colony was picked and let it grow in LB medium with Ampicillin (1:1000) at 37 °C in the agitator. QIAGEN Plasmid Midi and Maxi Kits was used to purify the plasmidic DNA.

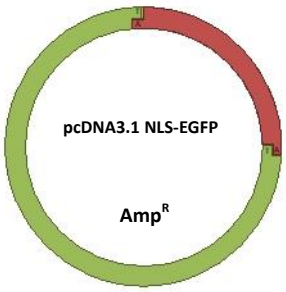

To facilitate visualization of plasmid DNA delivery during transfection with confocal microscopy, the *Label* IT® Plasmid Delivery Control Cy™3 (2.7 kbp, double stranded, circular plasmid, Mirus Bio Corporation, Madison, WI, USA) was used. The excitation wavelength of Cy™3 fluorophore is 549 nm and the emission wavelength is 570 nm **Figure 32**.

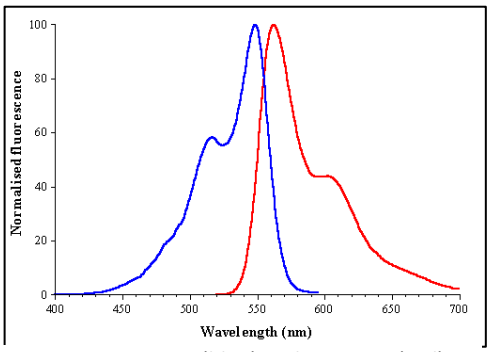

Figure 32 Excitation (blue) and emission (red) spectra of Cy3 fluorophore. (Taken from http://www.bio-ope.com/doc/CyDye.asp)

3.5 Fluorescence phenomenon

Fluorescence is a phenomenon in which a susceptible substance absorbs light and reemits light (photons) from electronically excited states after a given time. Compounds that display fluorescent properties are generally termed as fluorescent probes or dyes or fluorochromes. Fluorochromes include organic molecules, inorganic ions, fluorescent protein (e.g. green fluorescent protein), and atoms. Fluorescence follows a series of discrete steps and the final outcome is the emittance of a photon with a longer wavelength. When a light of particular wavelength hits a fluorescent sample, the atoms, ions or molecules therein absorb a specific quantum of light, which pushes a valence electron from the ground state into a higher energy level, creating an excited state. This process happens in a range of femtoseconds and requires at least the energy between excited and ground state in order for excitation to occur. After excitation to the higher energy level, the electron quickly relaxes to the lowest possible excited sublevel (in some picoseconds). This last process is called internal conversion. When the electron finally returns to the lower energy level it originated from, a quantum of light (photon) is emitted with a longer wavelength because of other phenomena that dissipate energy and

since the wavelength varies inversely with the radiative energy **Figure 33**. This difference between the emission and the excitation maxima is called "Stokes shift". Photon emittance is slow compared with the absorption of photons and the emitted light is collected and transported to detectors. Fluorochromes can enter repetitive cycles of excitation and emission as long as no destruction or covalent modification occurs that irreversibly interrupts this process.[53]

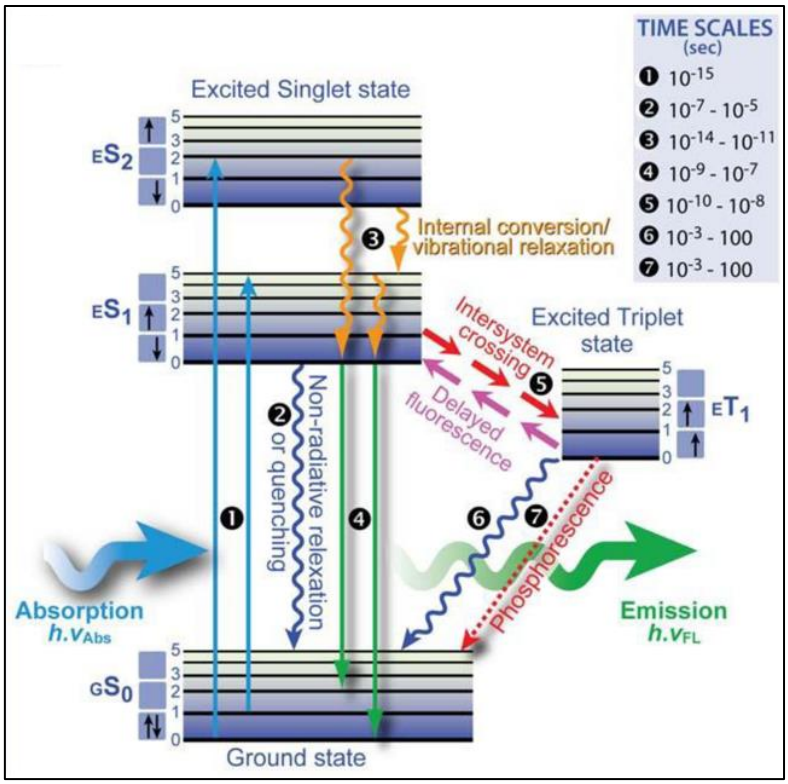

Figure 33 Single photon excitation. Representation of a Jablonski diagram. Singlet (S) and triplet (T) describe the electron spin states. The non-radiative transfer between singlet and triplet states is called intersystem crossing. Emission between triplet and singlet states is called phosphorescence and lasts typically milliseconds to seconds, much slower compared to other molecular events. Internal conversion and vibrational relaxation represent ways to "lose" energy through heat: this can help explain the Stokes shift.

3.6 Green fluorescent proteins as transfection efficiency reporters

The green fluorescent protein (GFP) was first isolated from the bioluminescent jellyfish *Aequorea victoria* and the gene encoding this protein represents today the member of an enormously powerful technology that has revolutionized the way life scientists are carrying out research on living cells. This "genetic code for fluorescence" has the outstanding ability to form an optically active cromophore in the absence of any cofactors, requiring only the presence of oxygen, together with many other advantages **Table 4**. Since its discovery many other novel proteins have been cloned from various marine organisms with different spectral, molecular and chemical properties distinct from GFP, providing cell biologists, medical researchers and biotechnologists with a diverse choice of multicolored fluorescent labels for imaging and screening. Although many suggestions have been made (like photosensing, predator-prey behavior), the biological function of these proteins in marine organisms remains pretty unclear.[54]

GFP-like proteins have the same basic structure made of 11-stranded β-barrel with a threaded α-helix from which, in a solvent-protected environment, the chromophore is suspended. The

original GFP contains 238 amino acids and the N- and C-termini are freely accessible for fusion to other proteins. Three consecutive amino acids (XXG) in the primary sequence give rise, through a series of posttranslational modifications to an optically active cromophore in a process called maturation **Figure 34.**

Advantages and features of fluorescent proteins
Genetically encoded
Optical properties can be readily tuned and optimized using molecular biological techniques
Readily fused to individual proteins
Accessible N- and C-termini for expression fused to target proteins
Can be readily targeted to different locations and compartments of cell
Other than molecular oxygen, no cofactors for chromophore formation required
Non-invasive
Fluorescence emissions covering visible spectrum (460-650 nm)
Variety of different photo-switchable variants available
Instrumentation suitable for fluorescence detection commonly available in molecular cell biology laboratories
Can be configured to sense a wide range of cellular parameters

Table 4

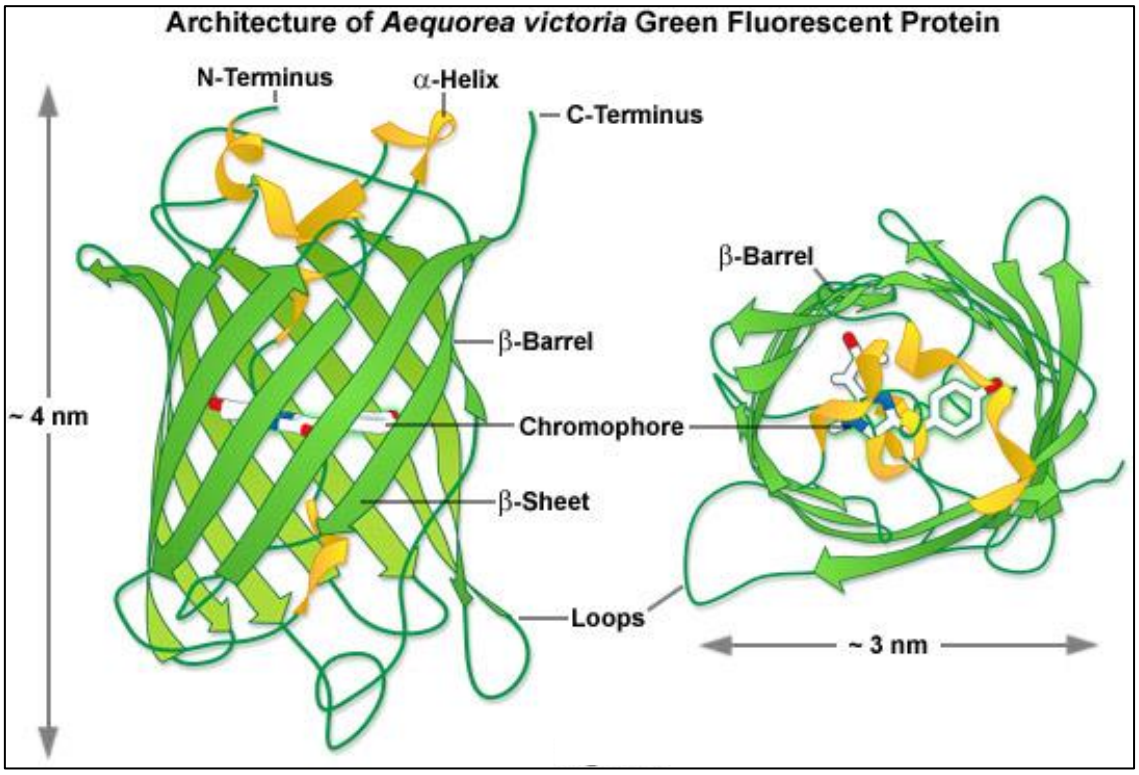

Figure 34 Structure of *A. victoria* GFP
(Taken from http://zeiss-campus.magnet.fsu.edu/articles/probes/jellyfishfps.html)

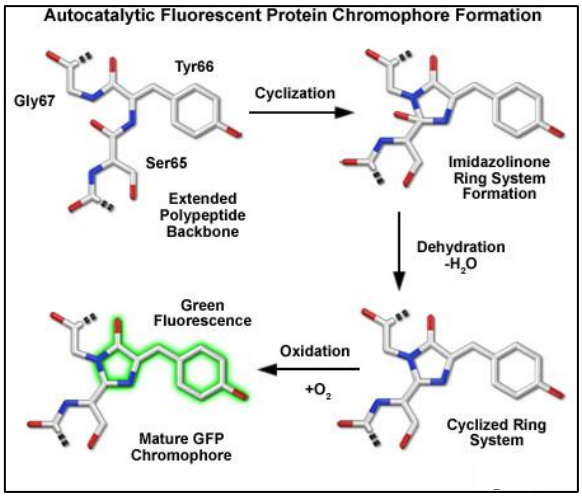

Figure 35 GFP cromophore formation. (Taken from: http://zeiss-campus.magnet.fsu.edu/articles/probes/jellyfishfps.html)

In GFP from *Aequorea victoria* the cromophore amino acids are serine 65, tyrosine 66, and glycine 67. The first step in the maturation is very most likely a series of rearrangements that allow nucleophilic attack of the carboxyl carbon of the serine residue (Ser65) on the amide nitrogen of glycine 67. This is followed by a dehydration step and the formation of an imidazolin-5-one heterocyclic ring system. Oxidation of the tyrosyl-α,β carbon by molecular oxygen extends the imidazolinone conjugation system to include the phenyl ring to form the chromophore characteristic of GFP **Figure 35**. GFP variants containing XWG or XHG give rise to chromophores with cyan or blue emissions, respectively. Amino acids absent in nature or other substitutions in the chromophore motif corresponding to position 66 can lead to proteins with novel properties. The wild type (wt) *Aequorea* GFP displays a complex absorption spectrum, with maximal excitation occurring at 397 nanometers, and a minor secondary peak of residing at 476 nanometers. The complex absorption spectrum featuring a significantly higher extinction coefficient at near-ultraviolet wavelengths, coupled with the low quantum yield of wtGFP, have severely limited its utility for cellular imaging applications. Mutagenesis strategies were initially applied to the sequence encoding the wtGFP in order to determine whether different amino acid substitutions might be used to fine-tune its spectral characteristics. Substitution of Ser65 for threonine produces the "enhanced" green derivative. The S65T mutation stabilized the hydrogen-bonding network in the chromophore, resulting in a permanently ionized form of the fluorophore absorbing at 489 nanometers. The resulting GFP-S65T mutant was a distinct improvement over wtGFP for applications as a fluorescent marker in living cells because it had a well-defined absorption profile with a single peak at 489 nanometers. This enhanced variant features an excitation spectral profile that overlays nicely with the 488-nanometer argon-ion laser line and is similar in profile to fluorescein and related synthetic fluorophores that are readily imaged using commonly available filter sets designed for fluorescein (FITC). Furthermore, EGFP is among the brightest and most photo-stable of the *Aequorea*-based fluorescent proteins. In addition, the GFP-S65T derivative is about five-fold brighter than wtGFP, and it matures more rapidly, allowing fluorescence to be detected at earlier time points after cell transfection. The only drawbacks to the use of EGFP as a fusion tag are a slight sensitivity to pH and a weak tendency to dimerize.

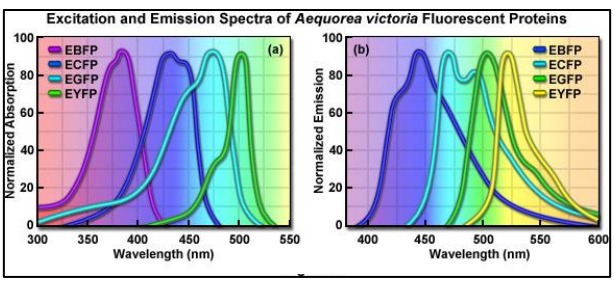

Figure 36 Excitation (right) and emission (left) spectra of EGFP. (Taken from: http://zeiss-campus.magnet.fsu.edu/articles/probes/jellyfishfps.html)

3.7 Other fluorescent dyes used in this work

3.7.1 Hoechst

Hoechst 33342 (2'-[4-ethoxyphenyl]-5-[4-methyl-1-piperazinyl]-2,5'-bi-1H-benzimidazole trihydrochloride trihydrate) is a cell-permeable DNA stain (effective for fixed-cell and live-cell staining) that is excited by ultraviolet light and emits blue fluorescence at 460 to 490 nm. Hoechst 33342 binds preferentially to adenine-thymine (A-T) regions of DNA **Figure 37**. Cells were stained with Hoechst 33342 (2 µg/mL) for 10 min and then examined by confocal microscopy.

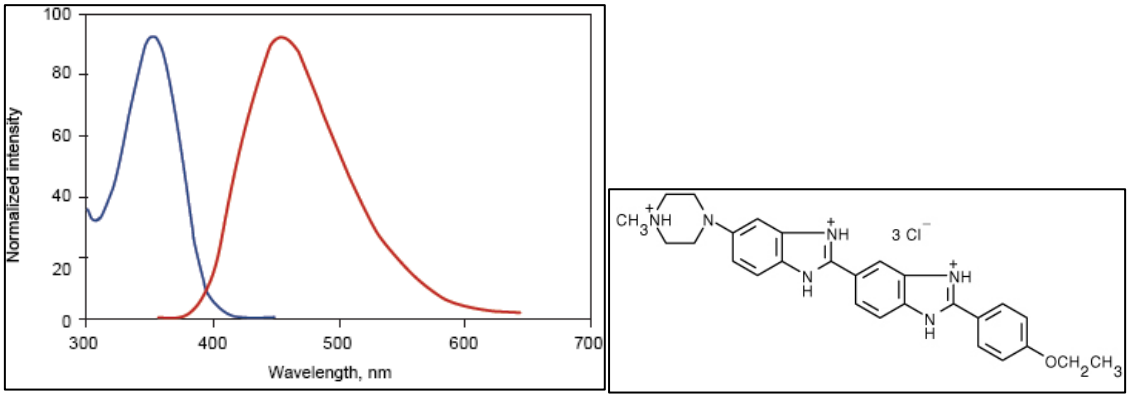

Figure 37 Right: Excitation (blue) and emission (red) spectra of Hoechst. Left: structure of the fluorophore. (Taken from: http://www.sigmaaldrich.com/catalog/product/sigma/p4170?lang=it&region=IT and http://www.olympusconfocal.com/theory/confocalintro.html)

3.7.2 NBD

Various lipid probes have proved to be useful in membrane and cell biology due to their ability to monitor lipid molecules by a variety of physicochemical approaches at increasing spatiotemporal resolution. A widely used fluorophore in biophysical, biochemical, and cell biological studies of membranes is the NBD (7-nitrobenz-2-oxa-1,3-diazol-4-yl) group. NBD-labeled lipids are extensively used as fluorescent analogs of native lipids in biological and model membranes to monitor a variety of processes **Figure 38**[55]. DOPE neutral lipid labeled with NBD was used to localize lipid complexes inside the cell by confocal microscopy. Excitation maximum = 465 nm, emission maximum = 535 nm.

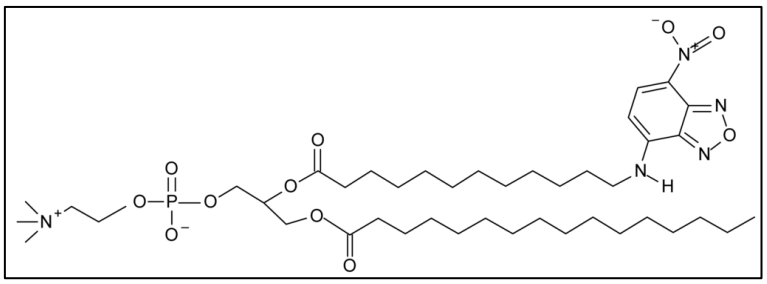

Figure 38[55] Example of a lipid (1-palmitoyl,2-(12-[N-(7-nitrobenz-2-oxa-1,3-diazol-4yl) amino]dodecanoyl)-sn-glycero-3 phosphocholine (C12- NBD-PC)) with the NBD fluorescent dye attached to an aliphatic chain.

3.7.3 FM4-64

Zal *et al*.[56] reported a novel property of the fluorescent dye FM4-64 (N-(3-triethylammonium-propyl)-4-(*p*-diethylaminophenylhexatrienyl)-pyridinium 2Br) to reveal the nuclear envelope (NE) **Figure 39**. The dye readily translocates inside the cells at physiological temperature and, when excited at 620-650 nm, reveals a distinct microenvironment in NE of living cells probably due to a local enrichment of negatively charged lipids. On the other hand, when the dye is excited at 480-520 nm it reveals vesicles in the endocytic pathway and the endoplasmic reticulum. The emission maximum is at 700 nm.

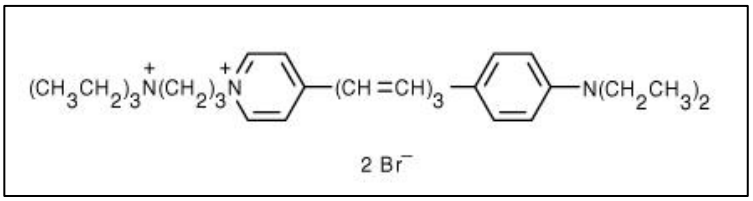

Figure 39 Structure of FM4-64 fluorophore. (Taken from: http://www.lifetechnologies.com/order/catalog/product/T13320)

There was some FM4-64 (T3166 Life Technologies) stored in the laboratory but the concentration was unknown. To determine the concentration of the fluorescent dye, the FM4-64 powder was dissolved in the smallest volume of dimethyl sulfoxide (DMSO) and its concentration was determined by the spectrophotometer by exploiting the known molar absorptivity in chloroform (ε = 51200 $cm^{-1}M^{-1}$) and the maximum of absorption at 560 nm **Figure 40**.

FM4-64 was dissolved in DMSO at 10 mM and added to the cells at 20 µM in complete DMEM medium supplemented with 10% FBS and 1% P/S. The staining was for 30 minutes at 37 °C in a 5% incubator. Cells were washed once with PBS and further incubated for 15 min at 37 °C in complete medium.[56]

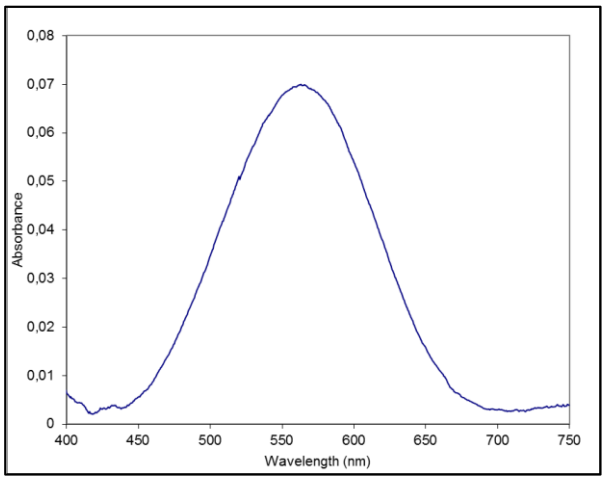

Figure 40 Absorption spectrum of FM4-64 in chloroform obtained to calculate concentration through the law of Lambert-Beer: $\boldsymbol{A = c\varepsilon d}$ where *c* is concentration, ε is molar absorptivity and *d* is the path length.

3.7.4 Propidium iodide

Propidium iodide (PI) is an intercalating agent and a fluorescent molecule that binds to nucleic acids. The fluorescence excitation maximum is 535 nm and the emission maximum is 617 nm **Figure 41**. Propidium iodide is used as a DNA stain for both flow cytometry to quantitatively assess DNA content in cell cycle analysis or to evaluate cell viability because it is membrane impermeant and generally excluded from viable cells. PI also binds to RNA, and thus required previous treatment with RNAse to distinguish between RNA and DNA staining.

In **Table 5** there is a summary of the excitation and emission maxima of the fluorescent dyes used during this master's thesis project.

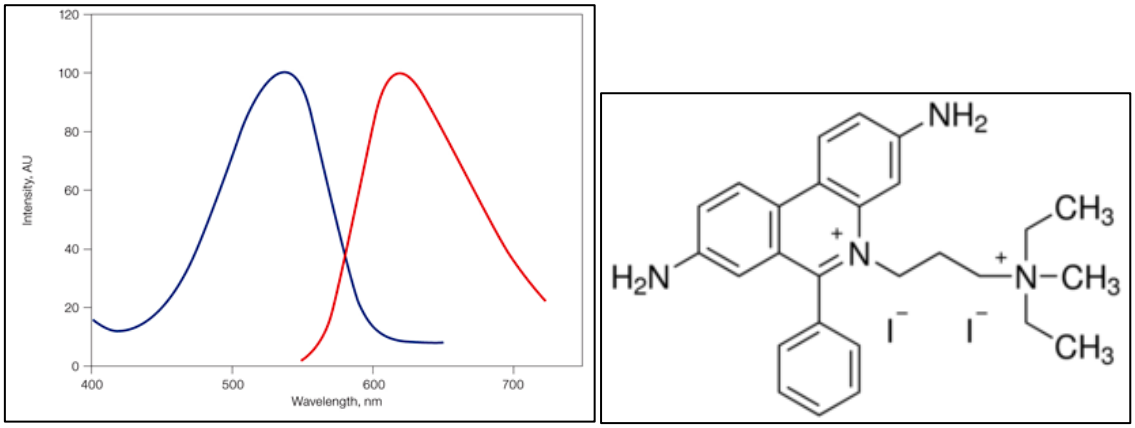

Figure 41 Right: Excitation (blue) and emission (red) spectra of PI. Left: Structure of the PI fluorophore. (Taken from: http://www.bio-rad.com/en-uk/sku/135-1101-readidrop-propidium-iodide and http://www.sigmaaldrich.com/catalog/product/sigma/p4170?lang=it&region=IT)

	Excitation (nm)	Emission (nm)
EGFP	488	507
Cy3	549	570
Hoechst	343	483
NBD	465	535
FM4-64	515	640
PI	535	617

Table 5 Summary of the excitation and emission maxima of the fluorescent dyes.

3.8 Confocal microscopy

Confocal fluorescence microscopy experiments were performed with the Olympus Fluoview 1000 (Olympus, Melville, NY) confocal microscopy. The microscope is equipped with a 405 nm diode laser, a 488 nm Argon laser, and 543 nm Helium-Neon laser. Glass bottom dishes (WillCo-dish GWSt-3522) containing transfected cells were mounted in a temperature-controlled chamber at 37 °C and 5% CO_2.

Confocal microscopy represents one of the most important advances ever achieved in optical microscopy. The reason why it became so popular is the easy with which extremely high-quality images can be obtained from both fixed and living cells/tissues. The main advantages over conventional wide-field optical microscopy are:

- ability to control depth of field;
- elimination or reduction of background information from non-focal plane;
- capability to collect serial optical sections from thick specimens.

In conventional wide-field optical epi-fluorescence microscopy, secondary fluorescence emitted by the sample occurs through the whole excited volume by obscuring resolution of features lying in the objective focal plane. Confocal microscopy provides not such a larger

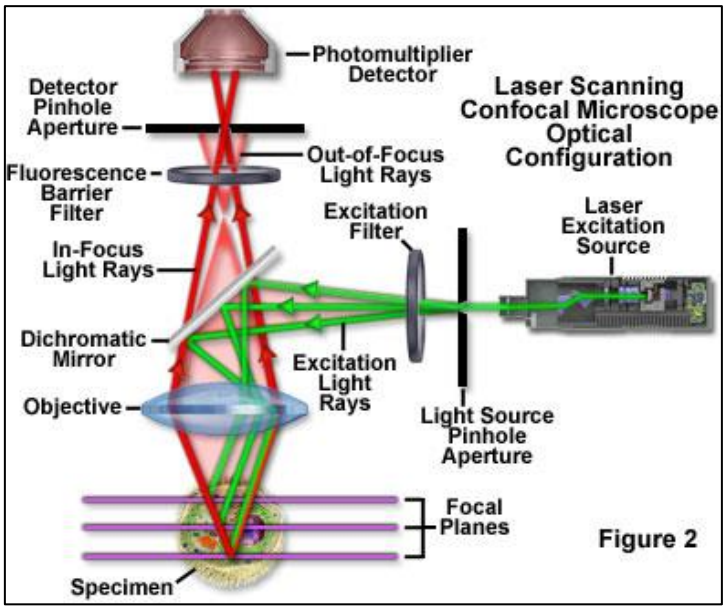

Figure 42 General configuration of a Laser Scanning Confocal Microscope. (Taken from: http://www.olympusconfocal.com/theory/confocalintro.html)

improvement in terms of axial and lateral optical resolution, but is able to exclude secondary fluorescence coming from other planes above and below the focal one.

As in **Figure 42**, coherent light emitted by the laser excitation system passes through a pinhole that is situated in a conjugate plane with a scanning point on the specimen and a second pinhole is positioned in front of the detector. When the laser is reflected by a dichromatic mirror and is scanned across the specimen in a defined focal plane, secondary fluorescence emitted from points on the specimen (in the same focal plane) passes back through the dichromatic mirror and is focused as a confocal point at the detector pinhole aperture. The other significant amount of fluorescence emission coming from points above and below the objective focal plane are not confocal with the pinhole and most of this extraneous light is not detected by the detector (like a photomultiplier) and does not contribute to the resulting image. When the objective is re-focused on a new plane of the specimen, it becomes the new confocal plane whose emission will be selectively detected by the pinhole aperture.

In contrast to wide-field microscopy, the mechanism of image formation in a confocal microscope is fundamentally different. The confocal microscope consists of multiple laser excitation sources (instead of a lamp) and the image of an extended specimen is generated by scanning the focused beam across a defined area in a pattern controlled by two high-speed oscillating mirrors. Traditional wide-field epi-fluorescence microscope objectives focus a wide cone of illumination over a large volume of the specimen, which uniformly and simultaneously illuminated. The majority of the fluorescence emission is gathered by the objective and projected into the eyepieces or detector giving rise to a significant amount of signal due to emitted background light and auto-fluorescence originating from areas above and below the focal plane, which seriously reduce resolution and image contrast. The laser illumination source in confocal microscopy is focused by the lens system to a very small spot at the focal plane. Confocal spot size is determined by the microscope design, wavelength of incident laser light, objective characteristics, scanning unit settings, and the specimen.

3.8.1 Fluorescence Recovery After Photobleaching (FRAP)

Fluorescence Recovery After Photobleaching (FRAP) was originally utilized as a method to measure diffusion in cellular membranes by using organic dyes. However, with the development of both fluorescent protein technology and confocal microscopy, FRAP became a

popular technique to study protein mobility inside the cell like diffusion rates, but also protein dynamics and interactions with other components. This was possible thanks to the large number of fluorescent proteins and by maintaining cellular homeostasis without using microinjection or permeabilization techniques. FRAP has importantly been shown to be a good approach to study nuclear protein dynamics in living cells devoid of disruption of the cell. **Table 6** shows the general aspects that can be investigated through the FRAP method.

Protein/molecule movement and diffusion (diffusional speed)
Compartmentalization and connections between intracellular compartments
Speed of protein/molecule exchange between compartments (exchange speed)
Binding characteristics between proteins
Immobilization of proteins that bind to large structures (e.g. DNA, nuclear envelope, membrane, cytoskeleton, etc.)

Table 6

In a classic FRAP experiment **Figure 43**, fluorescent molecules are irreversibly photobleached in a limited area of the cell by high intensity illumination with a focused laser beam. Subsequently, diffusional exchange of the surrounding non-bleached fluorescent molecules into the bleach area leads to recovery of fluorescence with a particular velocity, which is recorded at low laser power. Photobleaching generally requires excitation to an excited state and the presence of molecular oxygen, that causes irreversible damage to the fluorochrome, thereby permanently interrupting the cycle of repetitive excitation and photon emission.

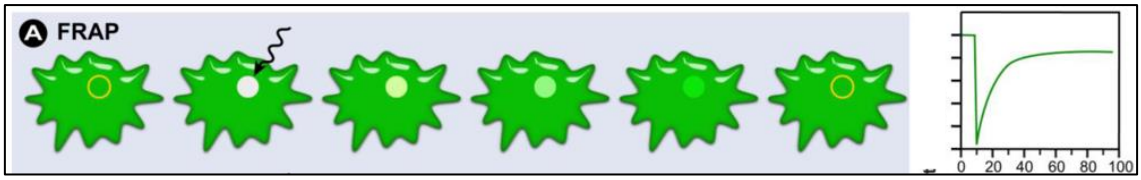

Figure 43[53] Schematic representation of a FRAP experiment. A region of interest (ROI) is selected, bleached with an intense laser beam, and the fluorescence recovery in the ROI is measured over time.

The fraction of fluorescent molecules that can participate in this exchange is called mobile fraction (M_f), whereas the fraction that cannot exchange between bleached and non-bleached regions is called the immobile fraction (I_f). It is then obvious, that FRAP can provide important insights into the properties and interactions of molecules within the cellular environment. In FRAP experiments, images are analyzed and processed to generate a kinetic plot of photobleaching by displaying the temporal fluorescence changes in the bleached region of the cell. From this plot, the mobile and immobile fractions can be determined by calculating the ratios of the final to the initial fluorescence intensity. Conventionally, the speed of recovery to half the plateau intensity (I_∞) is called "half-life" ($\tau_{1/2}$). The shorter the half-life, the faster the fluorescence recovery occurred and the higher the diffusion **Figure 44**.

Changes in the mobile fraction may give clues about various intracellular processes and their temporal outcomes. The mobile fraction can also be markedly affected by cellular membrane barriers and micro-domains within the membrane. These discontinuities can prevent, or temporarily restrict, the free diffusion of molecules through various cellular compartments or within the membrane itself. Conversely, active transport (e.g. via coated vesicles or motor

proteins) can cause a significantly higher mobility compared with diffusion limited processes. Such information can be extracted from FRAP data curves.[53,57]

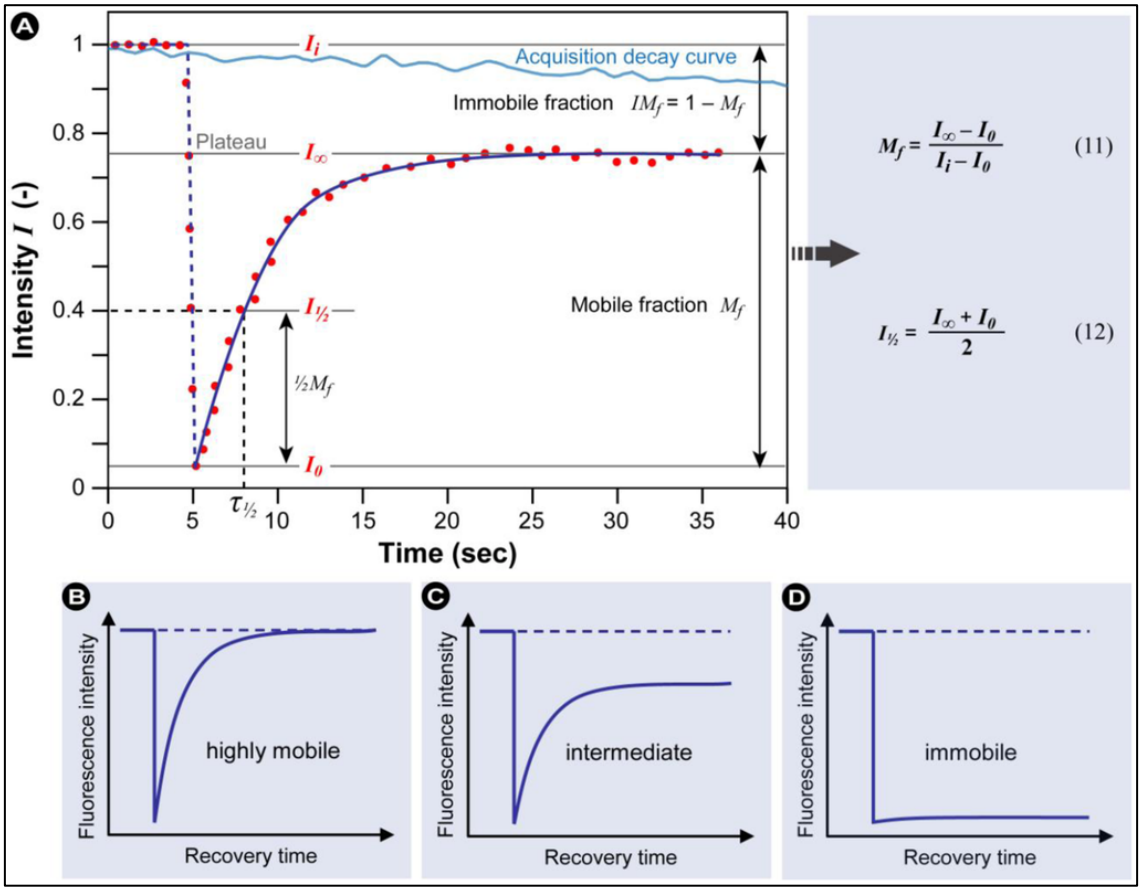

Figure 44 Anatomy of a typical FRAP curve.

3.8.2 Z-stacks of optical sections

With confocal microscopy optical section are not restricted only to x-y plane but also transverse planes can be collected and displayed by software programs. The specimen can appear as if it had been sectioned in a plane perpendicular to the x-y plane, through collecting vertical sections obtained by combining a series of x-y scans taken along the z-axis with the software **Figure 45**. This z-stack of optical sections allows to generate composite and multi-dimensional views and orthogonal views on x-y, y-z, x-z planes can be very useful to determine whether an object is inside or outside another one.

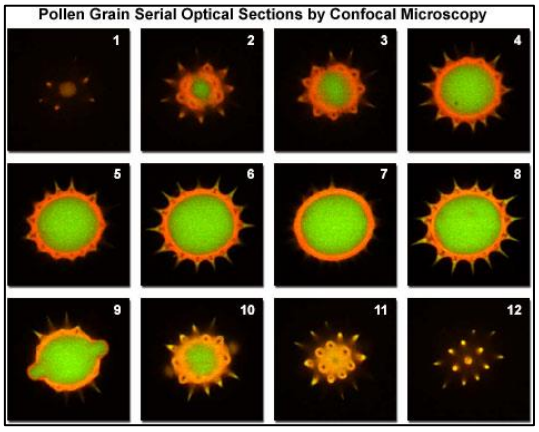

Figure 45 Example of a z-stack of optical sections through a sunflower pollen grain. Optical sections were gathered in 0.5-micrometer steps perpendicular to the x-axis and the picture shows only 12 images collected through this series. It reveals internal variations in auto-fluorescence emission wavelengths using a 488 nm and 543 nm laser system. (Taken from: http://www.olympusconfocal.com/theory/confocalintro.html)

3.8.3 Time lapse

Time-lapse confocal microscopy imaging was performed to observe CHO cells over time after a 3 h transfection in serum-free medium. The time of replacement with regular DMEM F-12 growth medium served as starting point and the incubator was kept at a constant temperature of 37°C and 5% CO_2. Microscope image sequences are recorded at a chosen interval of time (5-10 min) for 24-48 h and then can be viewed at a different speed to make videos, or can be analyzed to investigate further parameters like fluorescence signal over time. As a reporter for successful transfection GFP-NLS is still used with a very weak excitation power of Laser 488 nm, which ameliorates the phototoxic effects that are common to long-term time-lapse measurements. ImageJ software was used for most of the image analysis.

3.9 Flow cytometry

Bio-Rad's S3 Cell Sorter was used to individually analyze cell fluorescence after transfection and it was also utilized for cell cycle analysis of population of cells.

Flow cytometry is a technique which allows rapid analysis of many cells per second by using a fluid stream to transport cells through a narrow region, where they are illuminated by an intense beam of light. The resultant scatter and fluorescence signal is highly correlated with cell physiology. Since a large number of cells are analyzed, accurate statistical data can be achieved on cell populations. The most important feature of flow cytometry is the capability to analyze cell individually, in contrast to other fluorescence methods analysis in which measurements are made for a bulk volume of sample containing a large number of particles. Fluorescence-activated cell sorting (FACS) is a specialized type of flow cytometry that allows sorting of cells: in other words, cell can be accurately separated according to their size, surface characteristics, or fluorescence signatures.

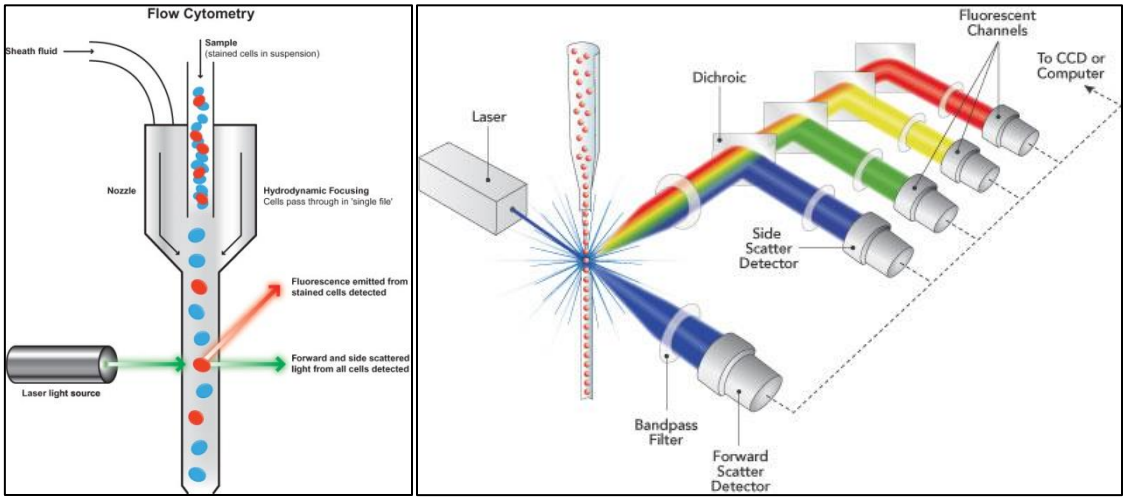

Figure 46 Basic components of a flow cytometer (Taken from: http://flowcytometry.med.ualberta.ca/.)

Figure 46 shows the basic components of a flow cytometer, where a laser is typically used as the light source and detectors are arranged to collect scattered light in the forward direction (forward scatter) and orthogonal to the excitation beam (side scatter). The excitation can also

excite fluorescence either from intrinsic autophluorophores within the cells or from special fluorescent labels attached to their surface or genetically encoded fluorescent proteins. The optical signals are converted to electrical pulses for storage and data are analyzed through a high-speed dedicated computer system. The data are often represented as a two-axis scatter plot for the identification, enumeration, and sorting of unique cell populations **Figure 47**.

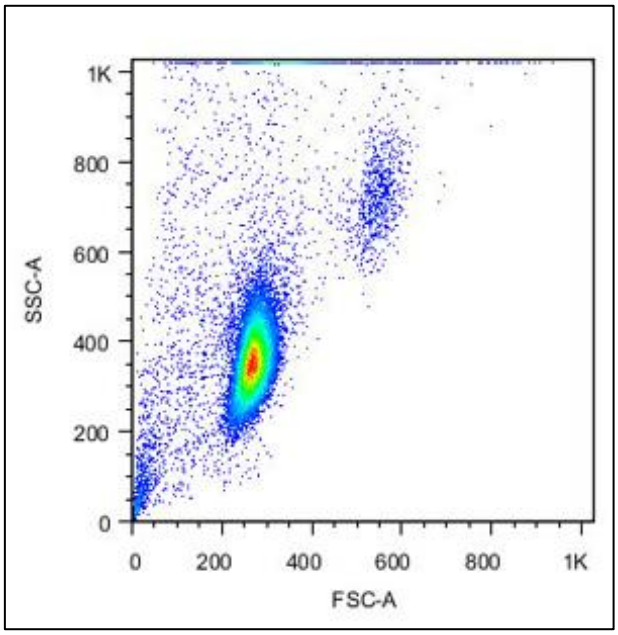

Figure 47 In the x-y scatter plot of FSC vs SSC distribution of cells is based upon size: as the laser passes through the stream, light is deflected and refracted by the cells in the stream. The scattered light is collected by the FSC and SSC photodiodes. The FACS analysis machine and its software present a plot of points that correspond to the morphology of the cells in the stream. FSC light provides indication of cell size; SSC light is strongly influenced by surface roughness and internal granularity of the cells detected. The distribution of the dots is very important because it allows to distinguish one type of cell from another and gate around one particular population of cells for further analysis.

The light collected from the excitation zone can originate from two processes: light scattering, where the beam of light changes its direction, and fluorescence emission, where the excitation light is absorbed and reemitted at a longer wavelength. The scattering and fluorescence characteristics are dependent on the physical features of the cell:

- side scatter signal (SSC) is strongly influenced by refractive components within cells and cell surface topography;
- forward scatter (FSC) is useful to provide indication of particle size and the state of the cells (dead cells refract light differently);
- cellular components (porphyrins, proteins, other fluorescent compound introduced into the cells or fluorescent proteins codified by transfected plasmids, etc.) will fluoresce when excited at appropriate wavelengths.

The side scatter and fluorescence detectors are positioned at right angles to the beam axis **Figure 46**. Fluorescence is typically analyzed in a number of different spectral bands through the use of a network or reflective dichroic filters. Each detector converts photons into electronic signals that are amplified, digitized, and processed.[54]

As the cell passes through the optics and is interrogated by the laser beam, a signal pulse over time (number of photons emitted) is generated, that has a height (or peak), width and an integrated area. It is exactly this pulse that we define as an “event”. The width and peak recorded will give some information about the length of the cell passing through the beam **Figure 48 - Figure 49**. This information is useful to distinguish between single cells or nuclei and doublets.

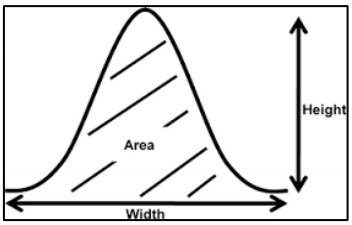

Figure 48[58] Schematic diagram of fluorescence pulse signal (height, width, and area)

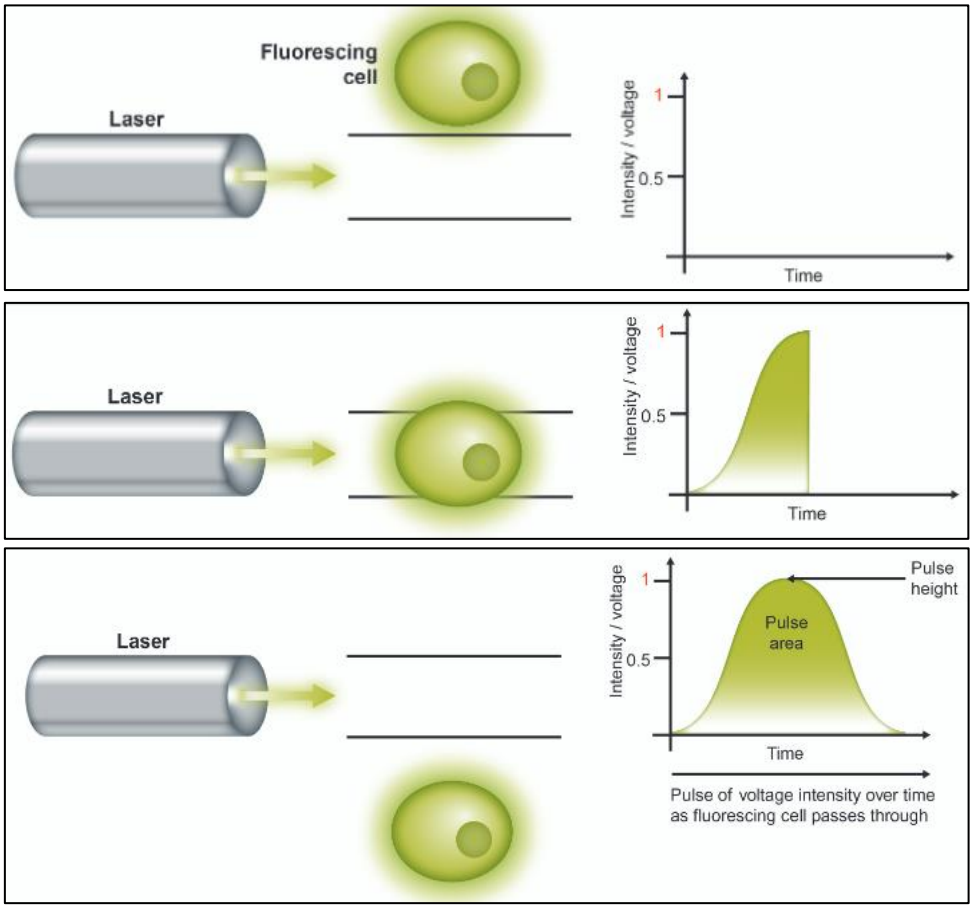

Figure 49 Signal generated when a cell passes through the laser beam. (Taken from http://docs.abcam.com/pdf/protocols/Introduction_to_flow_cytometry_May_10.pdf)

3.9.1 Fluorescence expression analysis of transfected cells as a parameter for transfection efficiency

When a single fluorescent dye is used to label cells, the expression of fluorescence can be easily visualized by using, for example, a plot fluorescence vs SSC. This can be also evaluated with a histogram, but one advantage to looking a dot plot is that one can look at variances in expression as single events, rather than as a collection of events shown as a vertical projection of counts at a particular fluorescence. Another advantage is that events that demonstrate high levels of expression can be hard to visualize in the diminishing tail of a histogram fluorescent frequency diagram. With a dot plot, a second parameter can be used (like SSC) and this gives the operator a clearer picture and allows to see how the levels of fluorescence are, for instance, differentiated by granularity (if SSC is used as a second parameter in the dot plot).

In this case cells were transfected with a GFP-NLS-SV40 codifying plasmid and a dot plot similar to one described above was used to analyze transfection efficiency, where here transfection efficiency means percentage of transfected cells whose fluorescence is above the fluorescence threshold that include more than 99% of not-transfected cells **Figure 50**.

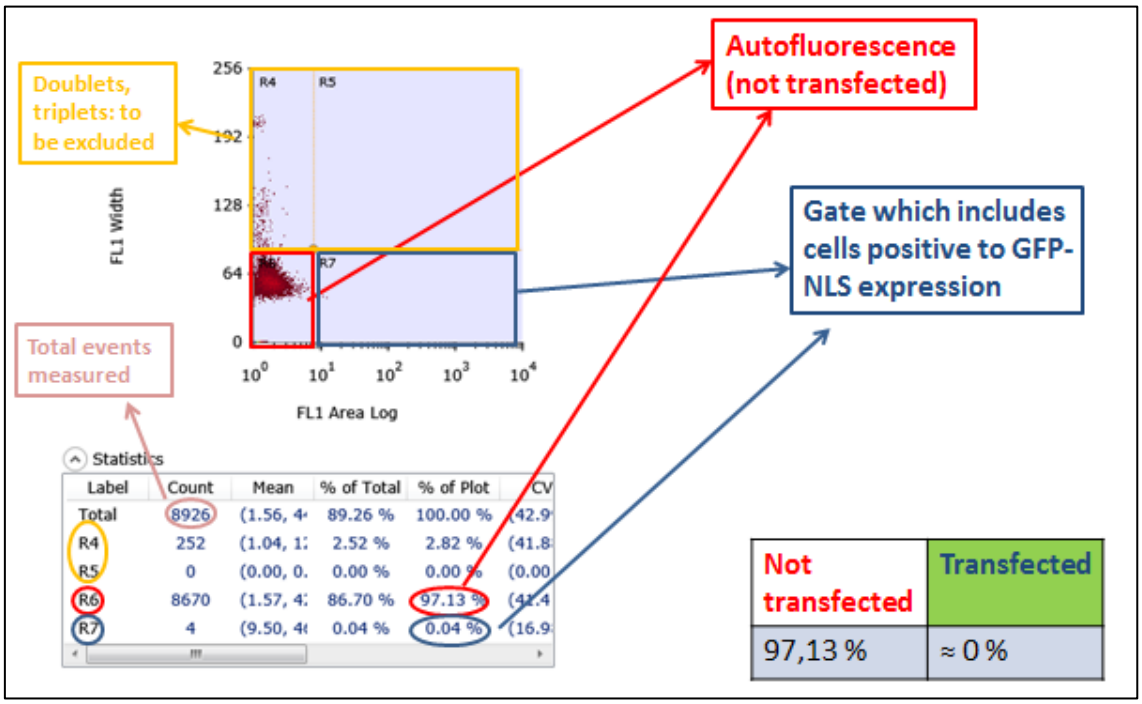

Figure 50 This is an example of analysis with a dot plot FL1 Width vs FL1 Area Log of non-transfected cells. Laser 488 (100 mV) was used to excite cells passing through the stream so that GFP could be excited and fluorescence signal was collected with a filter FL1 (525/30 nm).

3.9.2 Cell cycle analysis

Fluorescence intensity of dividing cells treated with propidium iodide (PI) is roughly proportional to DNA content and PI can be used to classify them into the G0/G1 pre-replicative phase, S replicative phase or G2/M post-replicative phase populations. PI is the most used compound to study cell cycle since this reagent binds to DNA in a stoichiometric manner such that there is a direct relationship between DNA content and PI fluorescence: cells that are in S phase will have more DNA than cells in G1 because they take up proportionally more dye and will fluoresce more brightly, and cells in G2 should approximately be twice as bright as cells in G1 **Figure 51**. Cells must be fixed or permeabilized to allow entry of the PI dye, which is otherwise actively pumped out by living cells. Alcohol is a dehydrating fixative that also permeabilizes cells allowing easy access of PI to the DNA, giving good fluorescence profiles. The following protocol was followed to analyze the cell cycle with a flow cytometric approach:

1) trypsinize adherent CHO cells ($5 \times 10^5 – 1 \times 10^6$) to detach;
2) add 1 mL complete DMEM medium and suspend cells; centrifuge 10 minutes at 1200 rpm;
3) aspirate supernatant and wash with 0,5 mL of PBS; centrifuge 10 minutes at 1200 rpm;
4) aspirate supernatant and re-suspend the pellet in 0,5 mL of PBS paying attention not to leave any cells clumps;

5) fix for 5 minutes with 1,5 mL 95% cold Ethanol (EtOH) by adding dropwise to cells while gently vortexing the tube;
6) dilute EtOH by adding 6 mL of PBS (at this step fixed cells can be stored for a week at 4 °C);
7) centrifuge the cells 15 minutes at 1200 rpm;
8) aspirate supernatant and re-suspend the fixed cells in 0,3 mL of staining solution (PI 50 µg/mL);
9) incubate at room temperature for 40 minutes (for a complete and more reproducible coloring it is recommended overnight at 4 °C); it is important to keep the cells covered with aluminum foil;
10) filter the cells and analyze by flow cytometry.

How to prepare the staining solution:

- Propidium Iodide (Sigma): 50 µg/mL;
- RNAse (Sigma): 20 µg/mL;
- Nonidet NP40: 0,1 %;
- PBS.

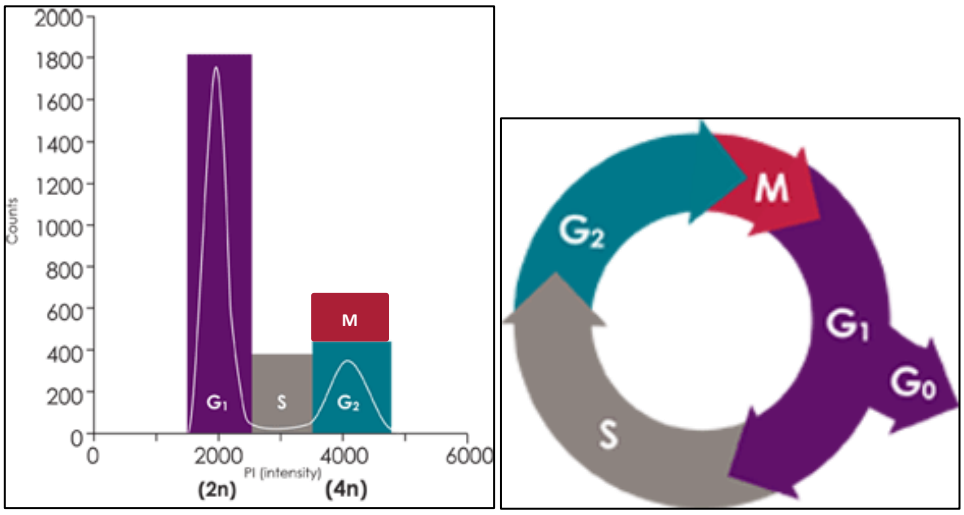

Figure 51 2n means diploid condition having a double set of chromosomes, 4n means a tetraploid (post replicative) condition having a 4 sets of chromosomes because of duplication of DNA in S-phase of cell cycle

3.9.3 How to study transfection efficiency in synchronized CHO cells

To test the role of cell cycle in transfection efficiency, cells were treated with mimosine, a drug that arrests cells at the border between G1 and S-phase. CHO cells were synchronized at the G1/S border and transfection occurred at different phases post mimosine release to evaluate, after the same amount of time, how transfection efficiency is influenced by the phases of the cell cycle at the time of transfection. The following protocol[36] (**Table 7**) was used to analyze GFP expression and cell cycle status upon transfections at various time-points during cell cycle:

1) pre-synchronization step by incubating cells in low serum-containing DMEM/F12 medium at 0.2% FBS for 48 h;
2) incubate cells for 14 h with DMEM/F12 + 10% FBS + 100 µM mimosine (Sigma);

3) to reinitiate the cycle, change the medium to mimosine-free DMEM/F12 medium + 2% FBS;
4) cells are transfected with GFP-NLS-SV40 plasmid at different hours post mimosine release and at the same time of transfection cells are fixed, DNA is labeled and the phases of the cell cycle are determined through flow cytometry analysis;
5) GFP expression is determined after a fixed amount of time post transfection.

<table>
<tr><td>1</td><td colspan="2">Pre-synchronization (48 hours) with DMEM F12 0.2% FBS</td></tr>
<tr><td>2</td><td colspan="2">Mimosine synchronization (14 hours) with DMEM F12 10% FBS and mimosine 100 µM</td></tr>
<tr><td>3</td><td colspan="2">Release from synchronization</td></tr>
<tr><td>4</td><td>GFP transfection (every hour for example)</td><td rowspan="2">Fixation, DNA labelling, flow cytometry analysis</td></tr>
<tr><td>5</td><td>Fluorescence measurement (after a fixed amount of time for each sample)</td></tr>
<tr><td>6</td><td colspan="2">Comparison and results</td></tr>
</table>

Table 7

4 Results

The aim of this Master's thesis project is to elucidate the mechanisms of nuclear entry of plasmidic DNA during transfection. To tackle this issue a nanoformulation made of a cationic peptide (protamine) and liposomes (Dc-Chol and DOPE) is used in comparison with the Lipofectamine Reagent® gold standard. Thus this work deals with two main problems:

1) how plasmidic DNA enters the nucleus;
2) what differences can be established between two different nanoformulations (Lipofectamine and Lipid nanoparticles combined with protamine) used for transfection.

4.1 Characterization of transfection phenotypes

Initially, cells transfected with Dc-Chol/DOPE/Protamine Nanoparticles and Lipofectamine were observed with confocal microscopy and characterized phenotypically.

4.1.1 Dc-Chol/DOPE/Protamine Nanoparticles

CHO cells were transfected with *Label* IT® Plasmid Delivery Control Cy™3 (2.7 kbp, double stranded, circular plasmid, Mirus Bio Corporation, Madison, WI, USA) using Dc-Chol/DOPE/Protamine and observed 24 h post transfection. Three different transfection phenotypes were identified:

1) Cells with red (Cy3 peak emission 570 nm) cytoplasmic spots **Figure 52**;
2) Cells with red diffused cytoplasmic signal **Figure 53**;
3) Cells with red diffused cytoplasmic and nuclear signal **Figure 54**.

The phenotype 1) shows, 24 h post transfection, vesicles of endocytosis containing the Cy3 plasmid molecules mostly accumulated in the perinuclear region. This phenotype represents the most common one among the cells (>95%) and it shows no red signal coming from inside the nucleus **Figure 52**. On the other hand the other two phenotypes present a diffused stain of either the cytoplasm (phenotype 2 - **Figure 53**) or both cytoplasm and nucleus (phenotype 3 - **Figure 54**).

In order to better characterize the red diffused signal observed in phenotypes 2) and 3), that together represent less than 5% of the total number of cells observed, an experiment of Fluorescence Recovery After Photobleaching (FRAP) on an area of the cell that was uniformly showing emission signal from Cy3-DNA was performed.

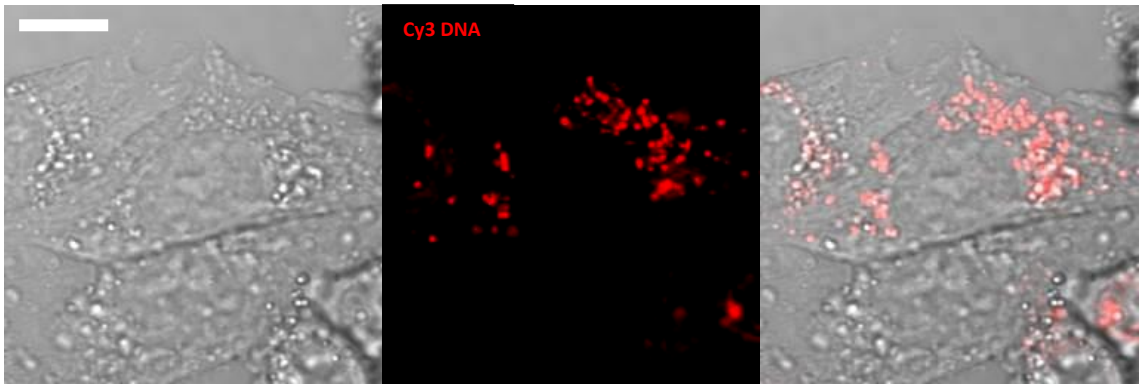

Figure 52 Phenotype 1): Cells with red cytoplasmic spots. Scale bar = 10 µm.

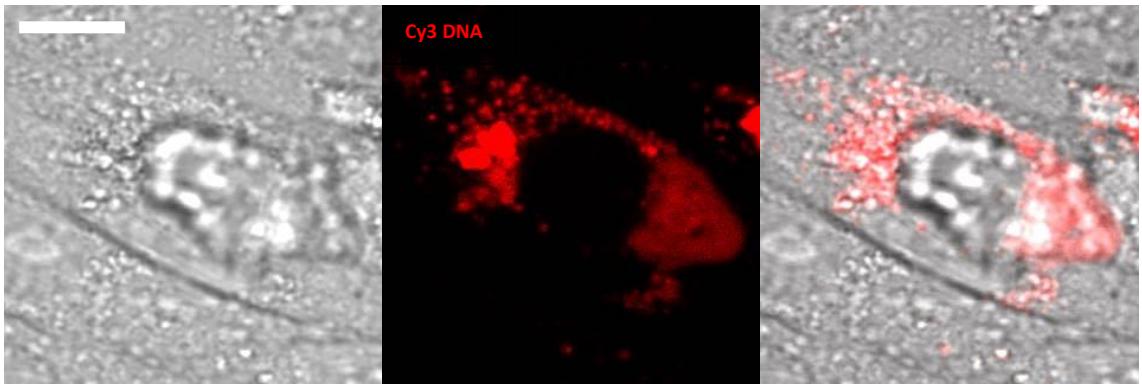

Figure 53 Phenotype 2): Cells with red diffused cytoplasmic signal. Scale bar = 10 µm.

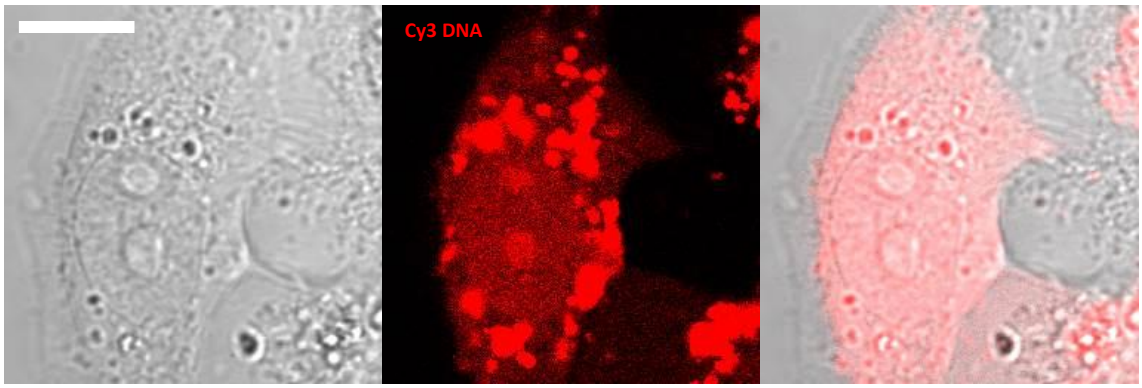

Figure 54 Phenotype 3): Cells with red diffused cytoplasmic and nuclear signal. Scale bar = 10 µm.

As can be seen in **Figure 55**, corresponding to phenotype 2), by applying a 3 s photobleach in the cytoplasm, no recovery is observed in the next ≈ 100 s. On the other hand, by applying a 5 s photobleach in the nucleus of a phenotype 3) cell **Figure 56**, partially recovery is observed soon after photobleaching with a loss of ≈ 25% of total fluorescence. These results show that the red signal coming from phenotype 2) and 3) may involve two different molecular species. The lack of fluorescence recovery of phenotype 2) can be related indeed to intact Cy3-plasmid or long fragments of Cy3-DNA. The partial recovery of fluorescence signal in phenotype 3) cells may be due to free Cy3-fluorophore or small fragments of Cy3-DNA. This is in agreement with the study of size-dependent DNA mobility conducted by Lukacs et al[16]. They showed, by using spot photobleaching, a reduction of diffusion coefficients of fluorescein double-stranded DNA fragments in the cytoplasm compared with those calculated in aqueous solutions and that

reduction was strongly dependent on DNA size. DNA diffusion coefficients in cytoplasm of 100-bp DNA fragments were, respectively, 3-fold and 19-fold higher compared to those of 250-bp and >2000-bp DNA fragments. The very slow diffusion of plasmid-size DNA fragments in cells is an important observation with regard to gene therapy. The diffusion of DNA in cytoplasm may be an important rate-limiting barrier in gene delivery utilizing non-viral vectors because of molecular crowding.

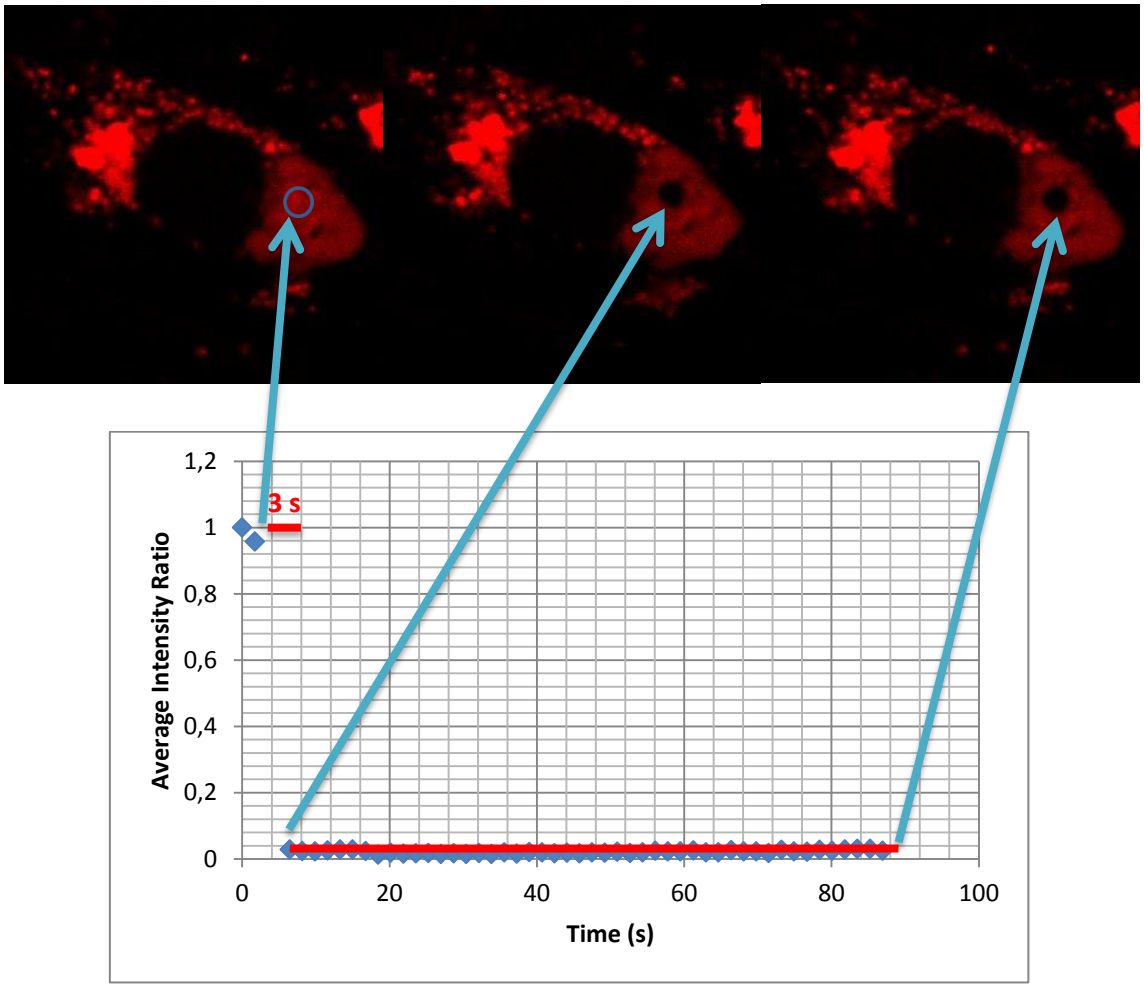

Figure 55 FRAP experiment in phenotype 2) cell. The absence of recovery (in <100 s) is an index of free intact Cy3 DNA plasmids

Phenotype 3) cells could represent good samples to study transport of plasmidic-DNA between cytoplasm and nucleus with FRAP experiments, but as **Figure 56** shows, the recovery time cannot be associated to a plasmidic-DNA species but very most likely to free Cy3 fluorophore.

Another important observation was that transfection of CHO-K1 cells with Dc-Chol/DOPE/Protamine actually provides a remarkable cytoplasmic release of DNA, as it was confirmed with confocal microscopy experiments with NBD fluorophore attached to DOPE. As **Figure 57** shows, there is a low colocalization between Cy3-plasmidic DNA and NBD-DOPE lipid in < 12 h post transfection. This indicates that a large amount of DNA may have escaped endocytic vesicles or lysosomal compartments and reached the cytoplasm. The cell represented in **Figure 57** belongs to phenotype 2) group, because of diffused red signal in the

cytoplasm. This observation was also showed by Caracciolo *et al.*[50] with DOTAP/Protamine LPD nanoparticles.

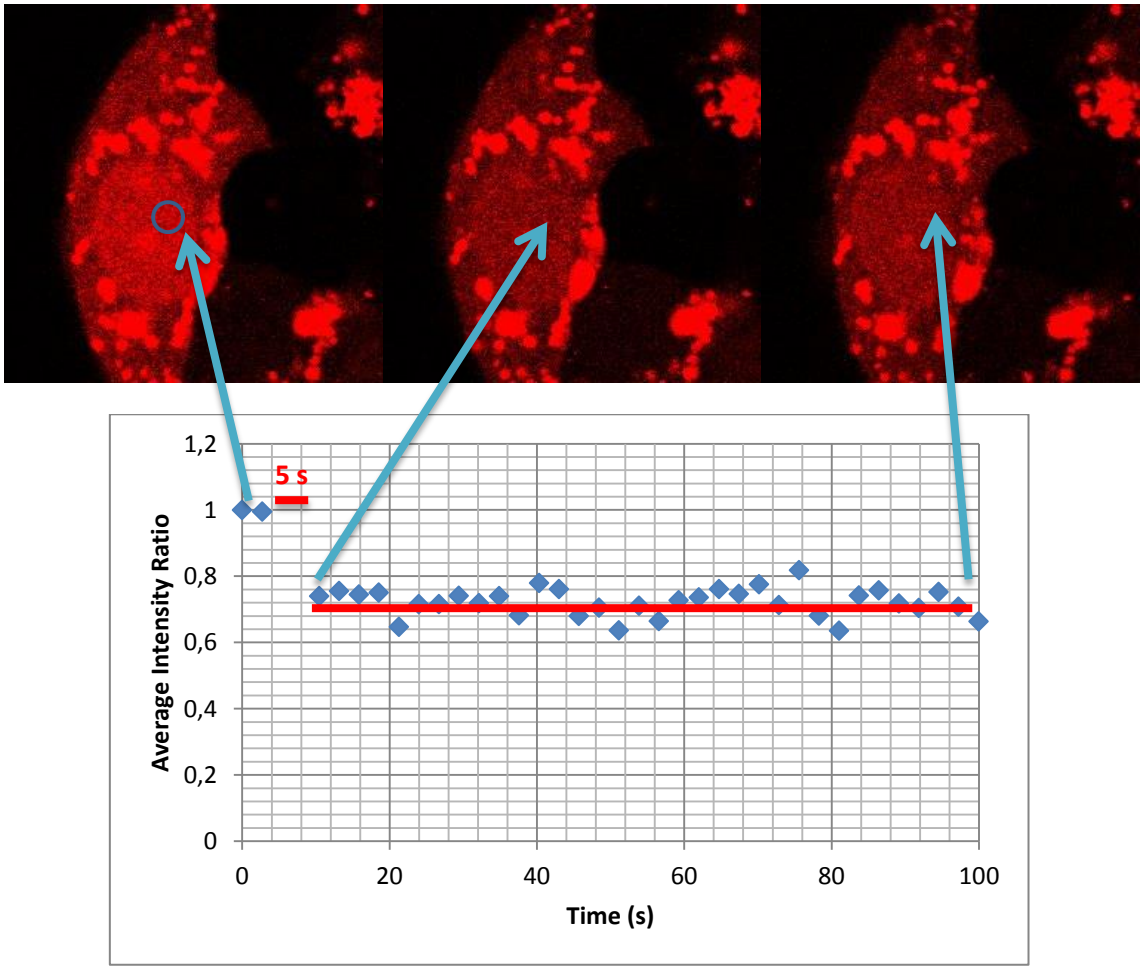

Figure 56 FRAP experiment in phenotype 3) cell. The rapid recovery is an index of small fragments of Cy3 DNA or free fluorophore

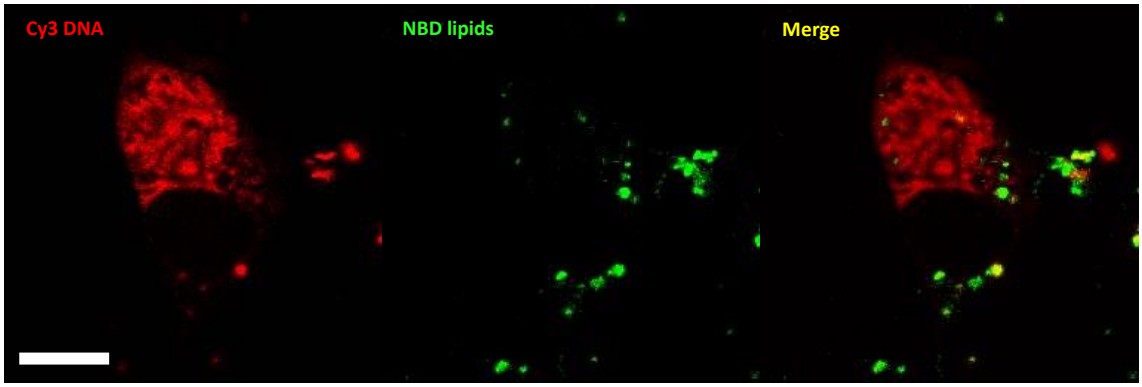

Figure 57 Green fluorescence from NBD lipids forming LPD complexes was clearly localized, while DNA (red fluorescence) had visibly spread into the cytoplasm. Scale bar = 10 µm.

At this point, it was important to evaluate which cell phenotypes are assoaciated with transfection in terms of protein expression. To investigate this aspect, a co-transfenction with Cy3-plasmidic DNA and an expression plasmid codyfing for a GFP-NLS protein (GFP with a

targeting sequence for nuclear entry) was performed. 24 h post co-transfection with Dc-Chol/DOPE/Protamine Nanoparticles cells were observed and qualitatively only a few cells (≈ 5%) were positive for expression of GFP-NLS protein. As previously described, most of the cells belong to a phenotype 1) group not expressing the heterologous gene (**Figure 58**) and those expressing the GFP-NLS protein seem to be phenotype 1) cells (**Figure 59**). This is interesting because phenotype 2) cells were expected to be more eligible considering the huge endosomal escape. This observation may indicate that endosomal escape doesn't always yield to a high transfection efficiency (in terms of expression of GFP-NLS protein) and that other mechanisms may be involved. It is also noteworthy to mention that "green" cells were often not positive to any red signal coming from the nucleus which would indicate the presence of the plasmid inside the nucleus: this may bring to hypothesize that the plasmid has already been degraded or that a few numbers of molecules entered the nucleus so that fluorescence signal is not strong enough to be detected.

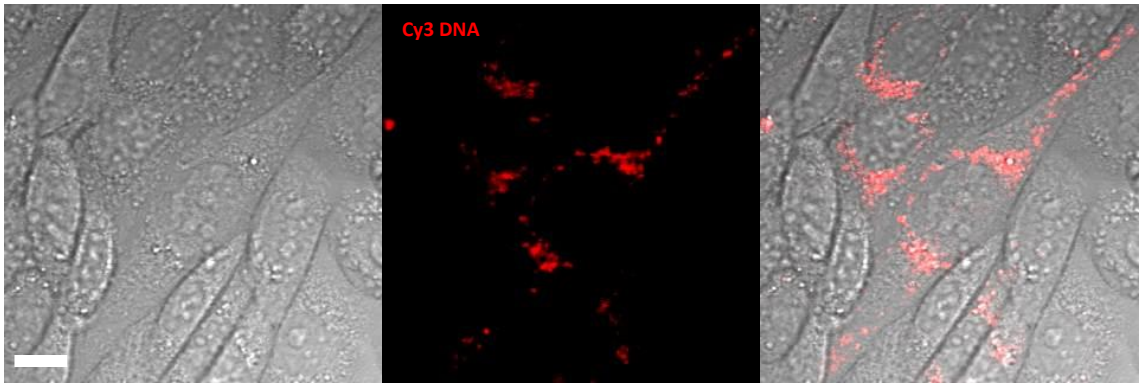

Figure 58 Phenotype 1) group cells not expressing the heterologous gene. Scale bar = 10 µm.

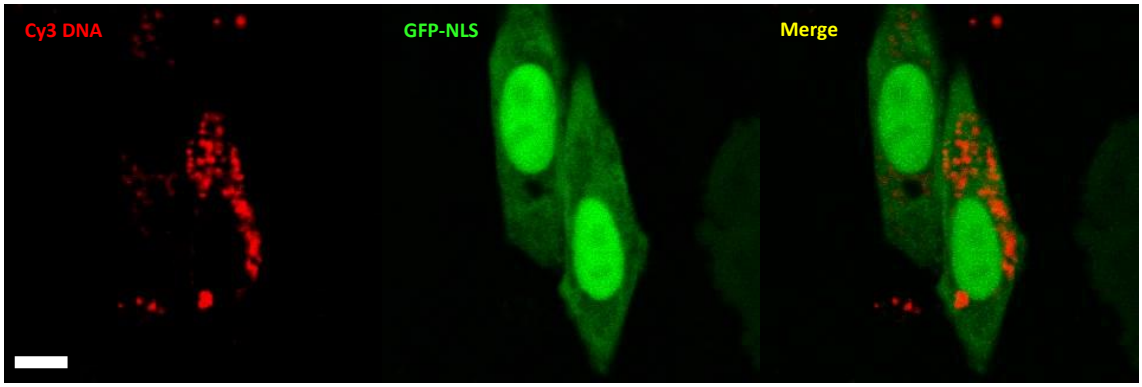

Figure 59 Phenotype 1) group cells expressing GFP-NLS protein**.** Scale bar = 10 µm.

In order to check if red signal coming from Cy3-plasmidic DNA could be detected inside the nucleus, the Hoechst dye was used to highlight the nuclear region. Some cells show red nuclear clusters localization when analyzed with a double channel observation (**Figure 60**) and a z-stack of images was collected to make sure the clusters are really inside the nucleus **Figure 61**. As can be seen in **Figure 61,** the red spot looked to be inside the nucleus but orthogonal views (in x-y, y-z and x-z planes) were necessary to confirm it and exclude the possibility that the red cluster was just in a very close proximity with the nuclear region.

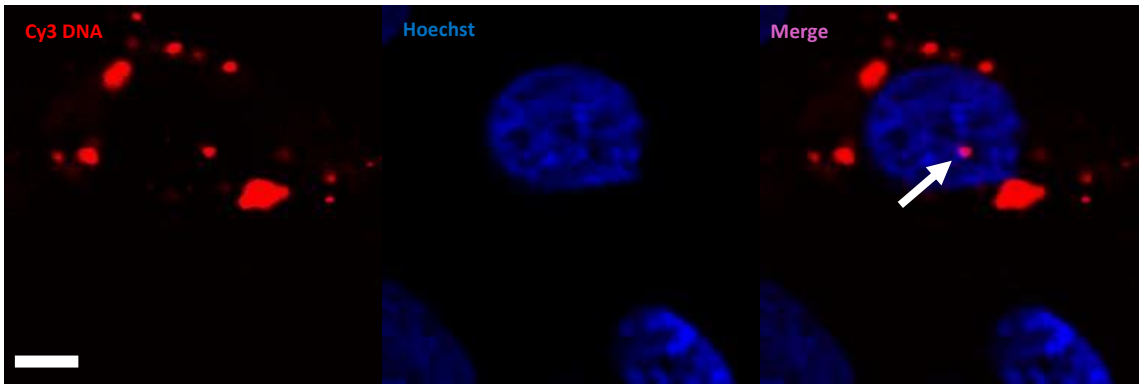

Figure 60 Some cells show red nuclear clusters localization when analyzed with a double channel observation. The arrow indicates a possible red object inside the nucleus. Scale bar = 5 µm.

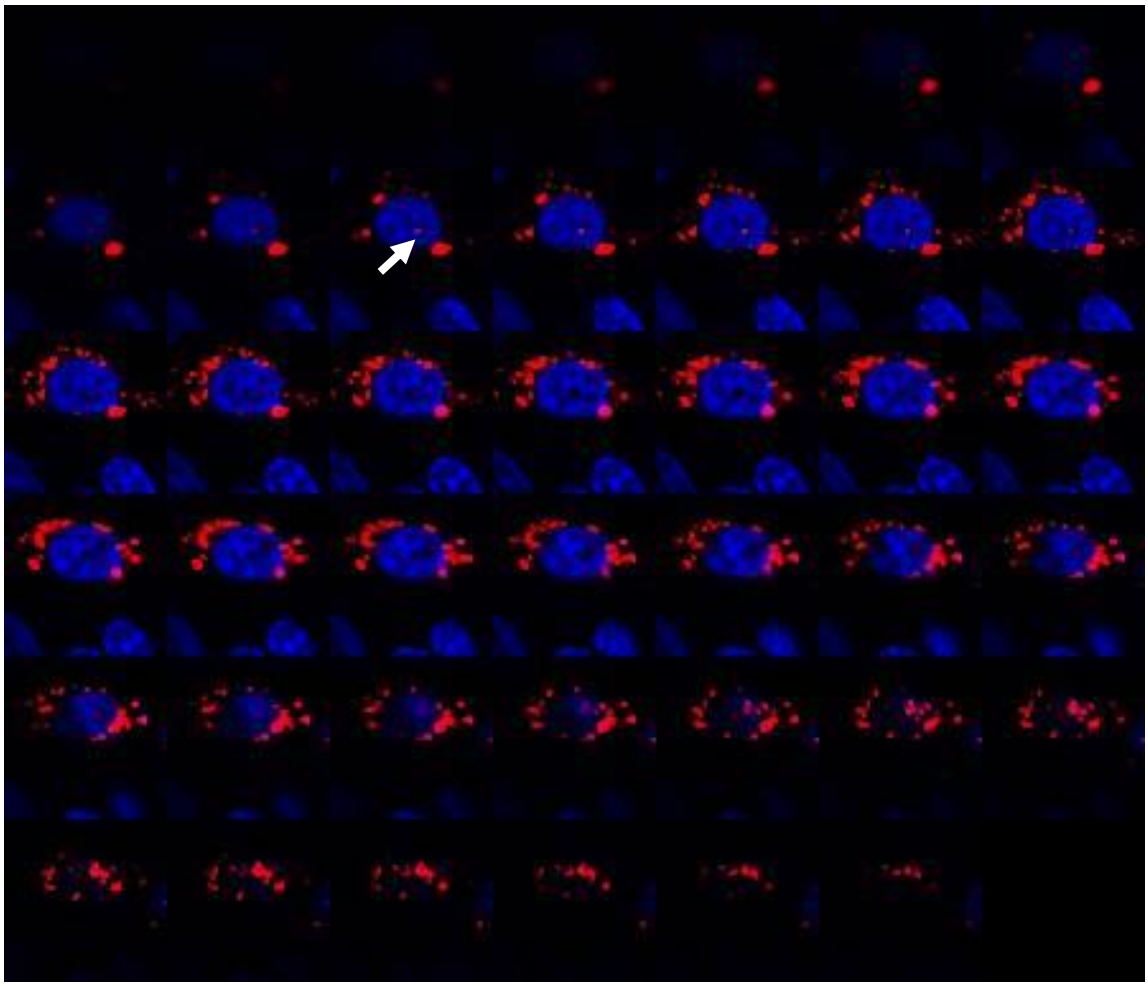

Figure 61 Z-stack of a cell (z = 0.25 µm). The arrow indicates a possible red object inside the nucleus.

As can be seen in the three orthogonal views in **Figure 62**, the red spot can be found on the boundary between nucleus and cytoplasm and this is the most representative situation among the analyzed cells. Another instrument useful to investigate the localization of red signal inside the nucleus is the fluorescence profile analysis of the two channels (red and blue) along a line passing through the nucleus in the three orthogonal projections. As can be seen in **Figure 62**, the blue fluorescence profile represents a good mean to establish the boundary of the nuclear compartment and, at the same time, the red peak can be identified and determined whether it

is included inside the borders of the blue nuclear region. In this case, the xy orthogonal projection shows a clear red peak inside the nuclear region, but the other two orthogonal views don't show the same result: the read peak is found to be located on the region where the "blue signal" is decreasing, and thus makes it difficult to believe that the red spot is really inside the nucleus. This situation probably shows an example of red Cy3-DNA cluster located in the periphery of the nucleus or in the cytoplasmic perinuclear region. On the other hand, a few cells present red spots that colocalize inside the nucleus **Figure 63,** and this is proved both through orthogonal views and fluorescence profile analysis along a line traced crossing the nucleus and the red spot **Figure 64** .

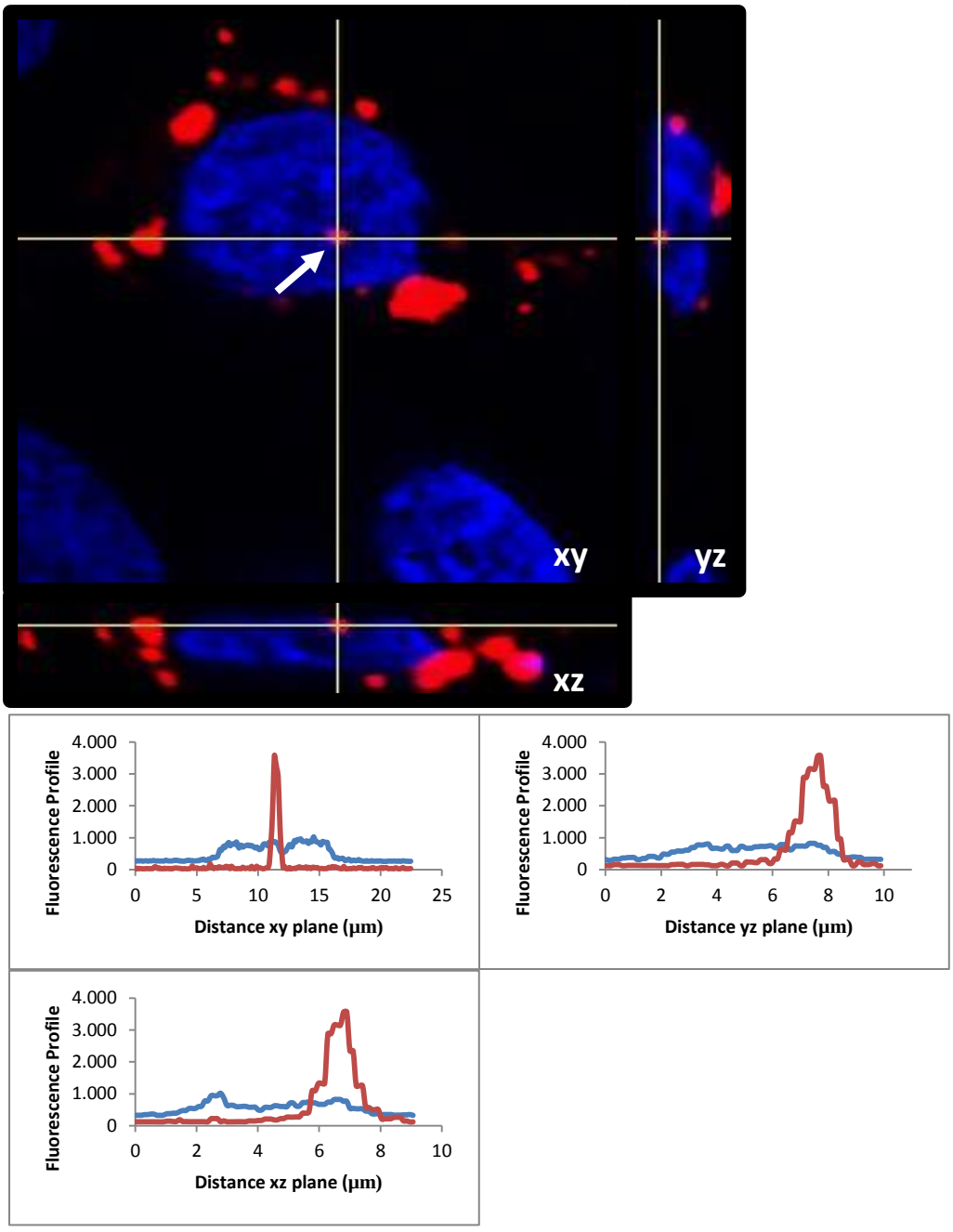

Figure 62 Orthogonal views (x-y, x-z, y-z) and fluorescence profile analysis of the red spot.

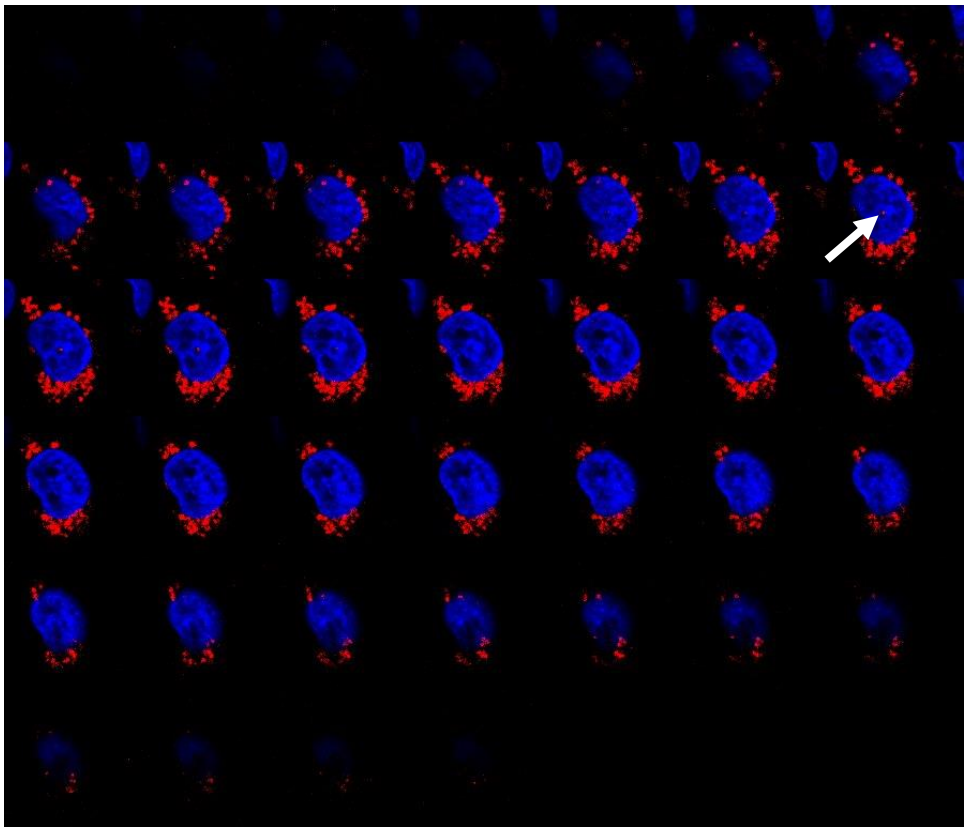

Figure 63

The two examples reported above are representative of the methodology used to check the localization of DNA-Cy3 clusters inside the nucleus. Data show that most of the cells present red clusters in the perinuclear region, as verified with orthogonal views and fluorescence profiles; other cells, though a few, show red puncta colocalizing with the inner region of the nuclear compartment. This brought to find an alternative way to investigate this phenomenon, in order to get more insights on the possible ways plasmids may exploit to reach the nucleus and transfect the cells to express an heterologous protein.

Figure 65 shows a summary of the most representative phenotype of the observed cells 72 h post transfection:

- red puncta spread in the cytoplasm (z-stack and orthogonal views showed that sometimes these spots can be found on the boundary between nucleus and cytoplasm or apparently inside the nucleus);
- little colocalization between DOPE-NBD and Cy3 plasmid indicating a large endosomal escape and presence of free plasmidic-DNA in the cytoplasm;

It is interesting that a very few cells are transfected after 48 h or 72 h and there is no positive correlation between red spots inside the nucleus (or on the boundary) and “green” GFP-NLS-expressing transfected cells. The high presence of red spots in the perinuclear region can be explained if we consider that escape from vesicles and lysosomes could take protamine associated plasmidic DNA in the nearby of the perinuclear region and trigger the nuclear pore complex mediated transport by exploiting the NLS signal of protamine or simply recruiting the key players of the cytoplasm-nucleus transport.

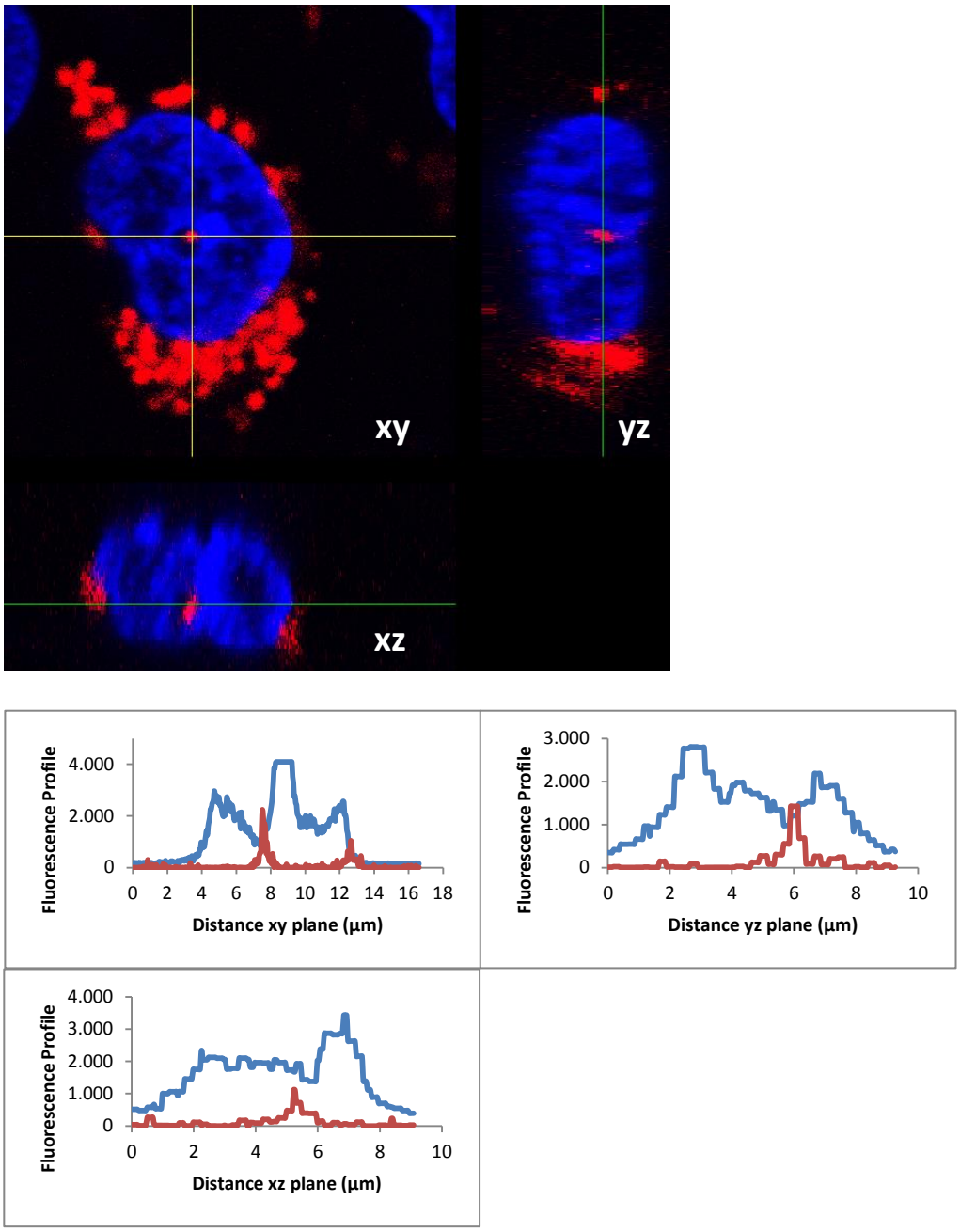

Figure 64 Orthogonal views (x-y, x-z, y-z) and fluorescence profile analysis of the red spot.

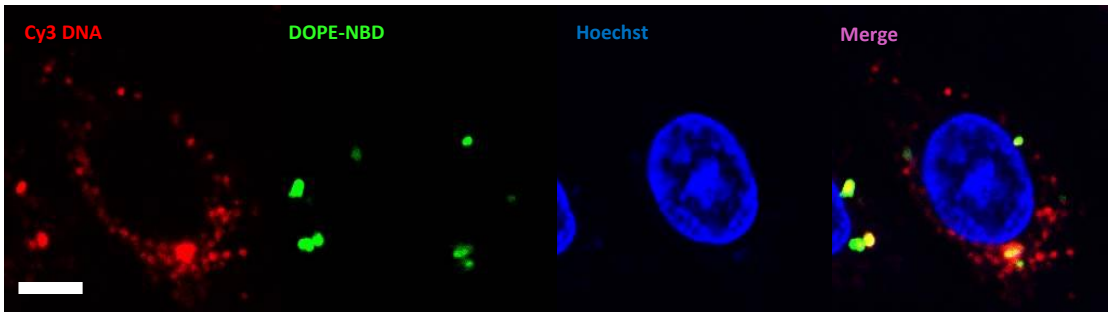

Figure 65 Summary of the most representative phenotype of the observed cells 72 h post transfection. Scale bar = 5 µm.

Before going on with the analysis of the transfection process, it was interesting to investigate a little bit further the presence of the red spots inside the nucleus. FM4-64, a dye that allows the labeling of the nuclear envelope, was used to get insights on these nuclear clusters by exploiting its capacity to undergo a spectral change of fluorescence and reveal a distinct microenvironment in the nuclear envelope (NE) of living cells. This dye localizes to the NE at physiological temperature, where it exhibits enhanced fluorescence when excited at 620-650 nm in contrast to 480-520 nm excitation in the endocytic pathway and in the endoplasmic reticulum. This is probably due to a different distribution of negatively charged lipids and a diverse phospholipid biosynthesis between NE and ER[56]. First, some images were collected to verify this **Figure 66**. The selectivity of the dye described before was achieved with a laser scanning confocal microscope using sequential excitation at 488 nm and 633 nm.

To analyze whether the red clusters described before are really inside the nucleus, cells were transfected as usual with the Dc-Chol/DOPE/Protamine Nanoparticles and Cy3-plasmidic DNA and then, before observation with confocal microscopy, stained with FM4-64. First of all, cells with red clusters were identified (**Figure 67**) and then z-stacks were collected in order to create orthogonal projections **Figure 68**.

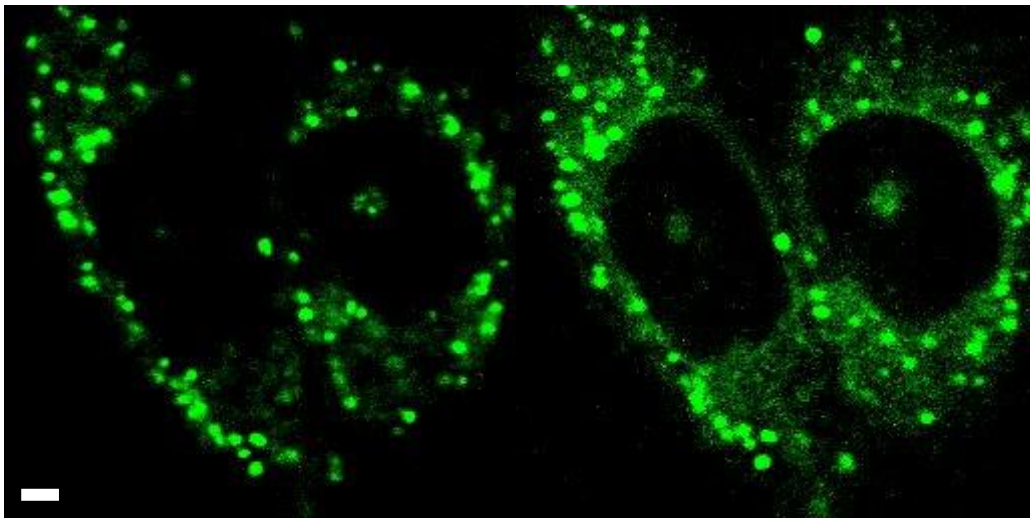

Figure 66 On the left FM4-64 stained cells were excited with a 488 nm Laser and on the right with a 633 nm Laser. Both emissions were collected above 700 nm. Scale bar = 2 µm.

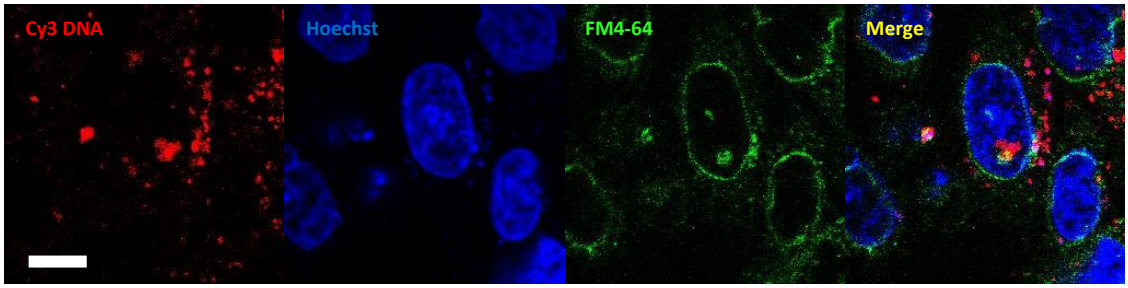

Figure 67 FM4-64 stained cells transfected with Cy3-DNA. Scale bar = 10 µm.

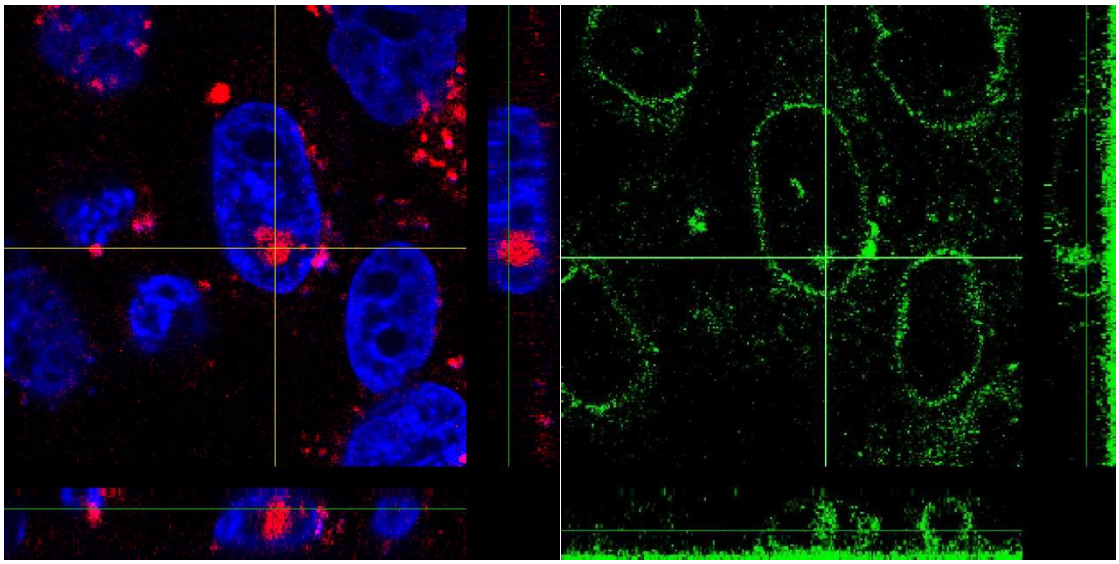

Figure 68 Z-stacks of FM4-64 stained cells transfected with Cy3-DNA (z = 0.25 µm)

As these pictures show, there is colocalization between Cy3-plasmidic-DNA, nucleus and FM4-64. It can be hypothesized that:

- some kind of nuclear envelope endocytosis might have happened;
- clusters of plasmidic-DNA and protamine may be trapped inside little channels spread among the nuclear envelope.

This last hypothesis is not to be excluded. Fricker *et al*.[59] identified long, dynamic tubular channels, derived from the nuclear envelope that extended deep into the nucleoplasm. The channels were cell-type specific (found also in more than 90% of CHO cells) and their morphology varied from single short tubs to multiple, complex, branched structures. Some of the channels transected the nucleus entirely, opening at two separate points on the nuclear surface. The presence of NPCs in the channel walls suggests a possible role for these structures in nucleus-cytoplasmic transport. It is interesting to formulate this hypothesis because it could explain the low transfection efficiency and lack of correlation between "green cells" and red spots localized inside the nucleus. The red DNA clusters could actually remain trapped inside these channels and may not reach the nucleoplasm, representing an additional obstacle for the DNA entry into the nucleus. It is also worthy of mention that these clusters, either those found inside the nucleus and those in the perinuclear region, often have sizes which are much higher than the diameter of the NPC sieve. This may lead to think that other mechanisms are involved in the process of nuclear entry if we exclude that all the red spots found inside the nucleus were actually clusters trapped within the nuclear channels described by Fricker.

As first proposed by Sorgi et al., protamine has four possible NLS-like regions made of basic amino acids: the precondensation of plasmidic DNA with protamine would actually enhance the trans-gene expression mediated by cationic liposomes. To establish the role of protamine in these red clusters of Cy3-plasmidic-DNA described before, different ratios (weight/weight) of Protamine/DNA were used during the preparation of the transfection nanoparticles. Specifically P/D ratios 2:1, 4:1 and 8:1 were used in comparison to the common one (P/D = 1:2) used until now. As can be seen in **Figure 69** nanoparticles with P/D = 2:1 (charge ratio P/D = 2,54) also showed red clusters spread in the cytoplasm and the perinuclear region. Staining

with Hoechst confirmed the presence of red spots inside the nuclear region (**Figure 70**) and the same happened for P/D = 4:1 (charge ratio P/D = 5,08 **Figure 71 - Figure 72**) and P/D = 8:1 (charge ratio P/D = 10,16 **Figure 73 - Figure 74**).

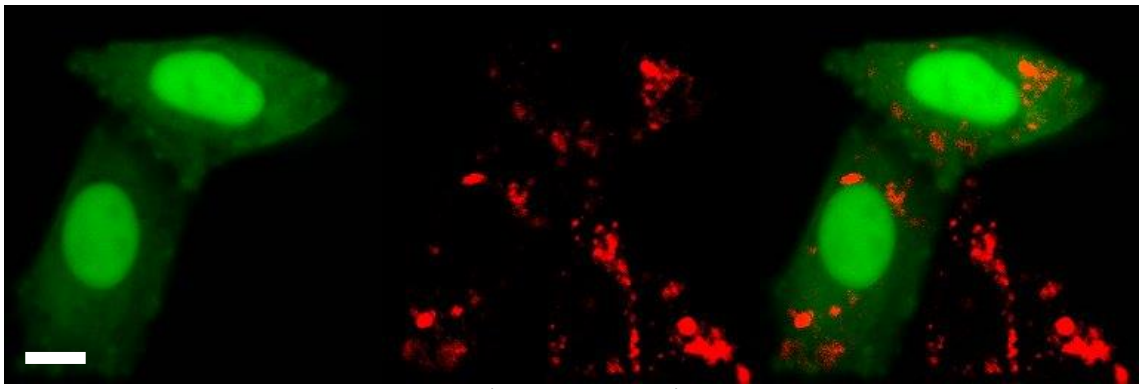

Figure 69 CHO cells transfected with a Protamine/DNA ratio (weight/weight) P:D=2:1. Scale bar = 10 µm.

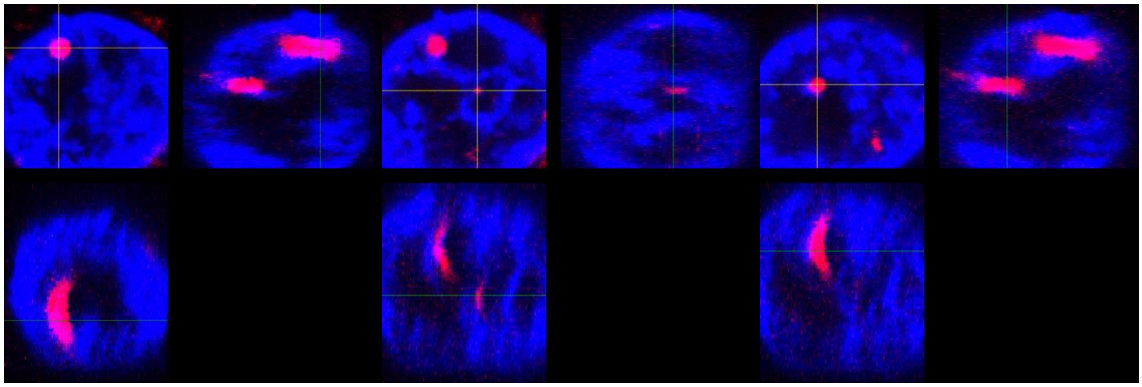

Figure 70 Z-stacks of CHO cells transfected with a Protamine/DNA ratio (weight/weight) P:D=2:1

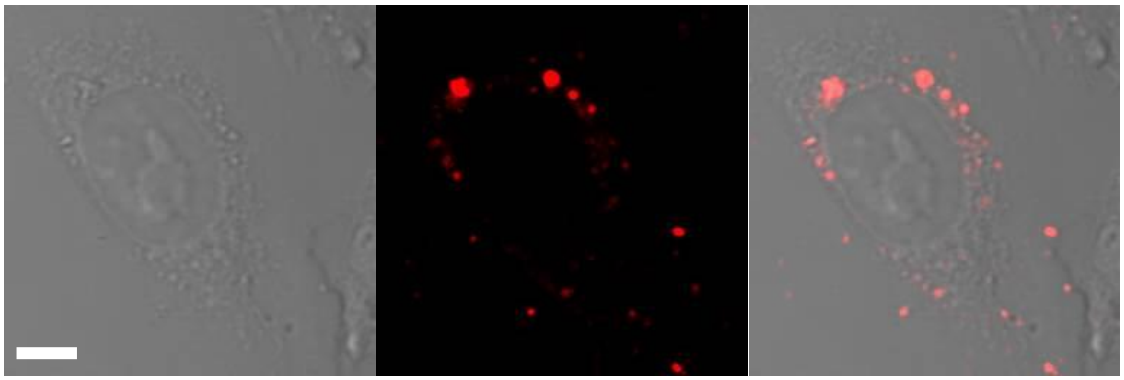

Figure 71 CHO cells transfected with a Protamine/DNA ratio (weight/weight) P:D=4:1. Scale bar = 5 µm.

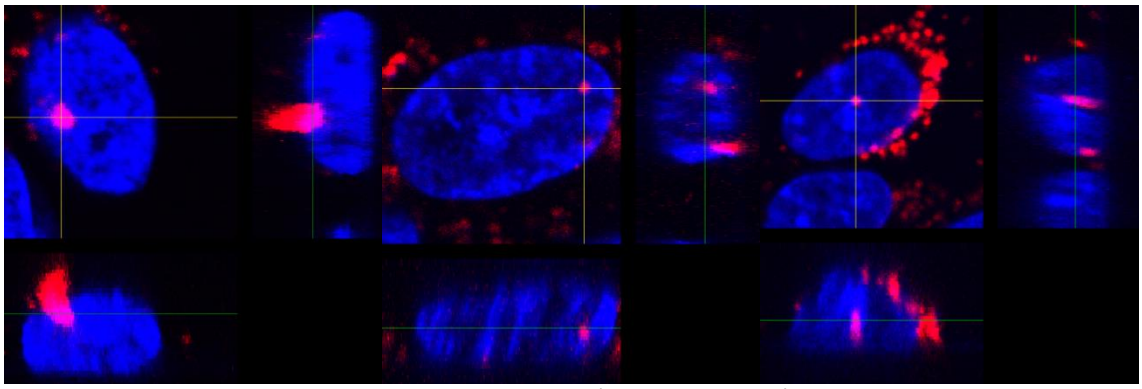

Figure 72 Z-stacks of CHO cells transfected with a Protamine/DNA ratio (weight/weight) P:D=4:1

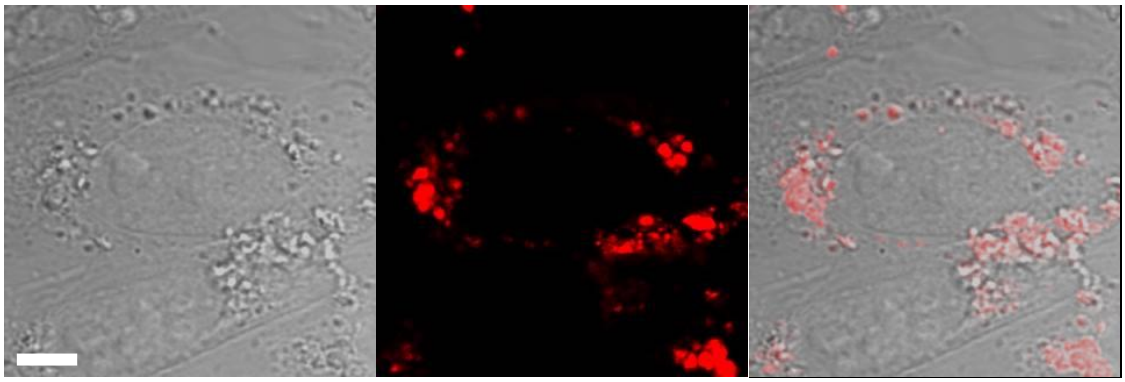

Figure 73 CHO cells transfected with a Protamine/DNA ratio (weight/weight) P:D=8:1. Scale bar = 5 µm.

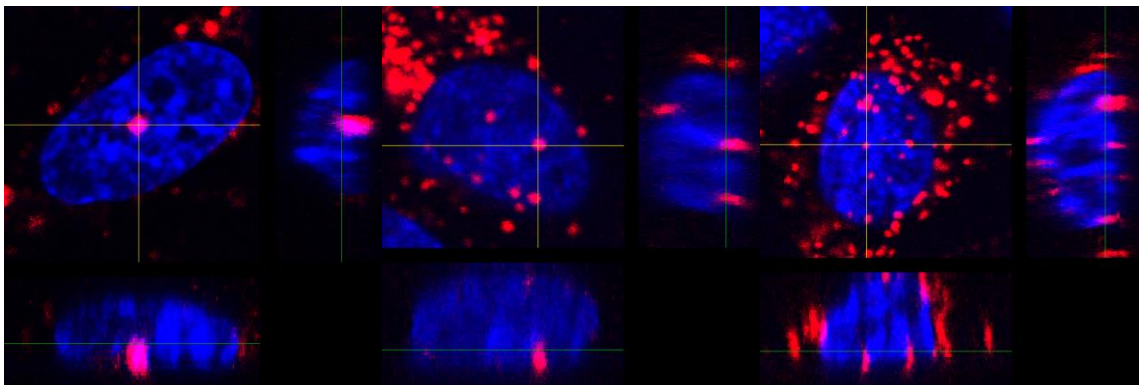

Figure 74 Z-stacks of CHO cells transfected with a Protamine/DNA ratio (weight/weight) P:D=8:1

Figure 75 shows the presence of red spots inside the nucleus of "green cells" transfected with a ratio w/w P/D = 2:1. In other words, a transfected cells expressing the GFP-NLS codifying plasmid shows red puncta inside the nuclear region. This was not representative of the cells examined but brought to relate these data with those of Masuda *et al.*[60] They microinjected inside the cytoplasm complexes of protamine and DNA at different charge ratios and observed that higher charge ratios improved the nuclear transfer of plasmidic DNA by protamine according to a model showed in **Figure 76** .

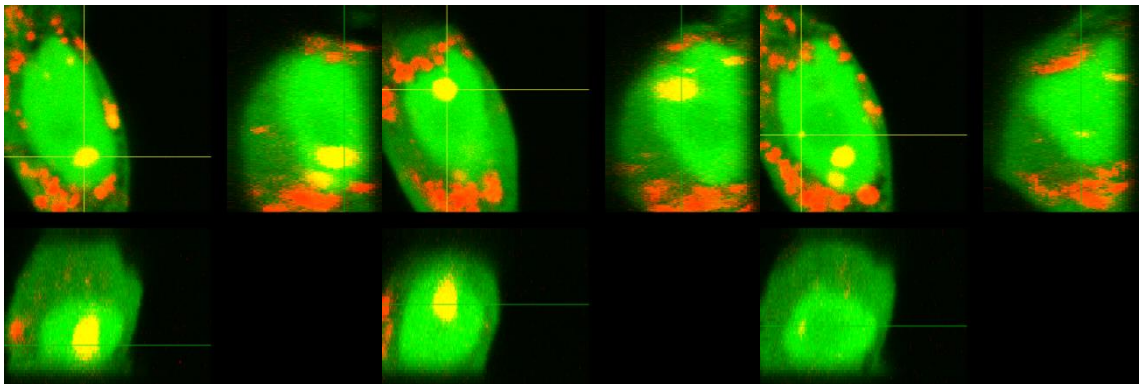

Figure 75 CHO cells transfected with a Protamine/DNA ratio (weight/weight) P:D=2:1

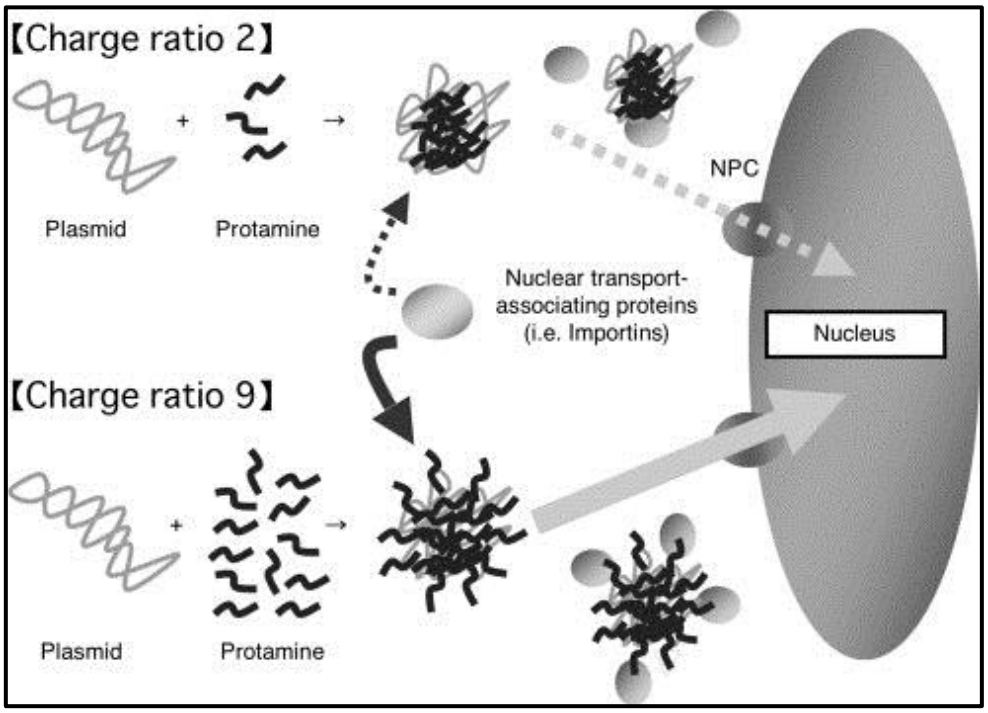

Figure 76 Schematic diagram illustrating the possible mechanism for the improved nuclear transfer of pDNA by protamine

Their proposed model supposes that at a low charge ratio, the recognition of the nuclear localization signal by the nuclear transport associating proteins is limited since all of the basic amino acids (arginines) of protamine may be engaged in the condensation of pDNA. When the charge ratio is increased, single protamine exhibits heterogenic functions: a partial domain involves in the pDNA condensation, and the other domain is displayed on the particle allowing them to be recognized as a nuclear localization signal. The P/D weight/weight ratios used in my experiments correspond to the following charge ratios: 0,64 – 2,54 – 5,08 – 10,16 and the observations with confocal microscopy actually showed that a larger number of red complexes were found in the perinuclear region (and inside the nucleus) as the charge ratio P/D increased (**Figure 70 – Figure 72 – Figure 74**). This may help explain why cells transfected P/D=2:1 sometimes showed green cells with red clusters inside the nucleus **Figure 75**.

As can be seen from the orthogonal views obtained from the z-stacks in cells transfected with P/D=4 and P/D=8, red clusters are often found inside the nuclei and in the perinuclear region and have sometimes much higher sizes than those observed at a lower P/D ratio. This may be caused by a major clustering of DNA and protamine when protamine is used at a higher ratio. These data are interesting because they show that higher charge ratios P/D increase the dimensions of the red clusters and the number of these complexes in the perinuclear region but this observation is not correlated with a higher transfection efficiency. The number of green cells was actually decreased compared to the usual P/D ratio used before.

Another striking observation obtained by visualizing transfected cells expressing GFP-NLS protein was that very often these cells were found to be in groups of even number, in couple or multinucleated cells (**Figure 77 - Figure 78**). This provided a hint that cell division could be involved in the process of nuclear entry. This is already known from the literature but the question was to find out if cell division represented the only way exploited by plasmidic DNA with this transfection formulation to enter the nucleus. This was important because of the lack of correlation between red spots inside the nucleus and “green cells”. It could be hypothesized that the red clusters showed so far could actually represent unavailable plasmidic DNA which cannot be transcribed. One reason could be the entrapment of the clusters inside the nuclear channels but another possible explanation could be the huge condensation of DNA and protamine that would inhibit plasmidic DNA release inside the nucleus and transcription. Maybe only little clusters or free plasmidic DNA molecules could actually be effectively transcribed and nuclear envelope breakdown during cell division represented the main way for DNA nuclear entry.

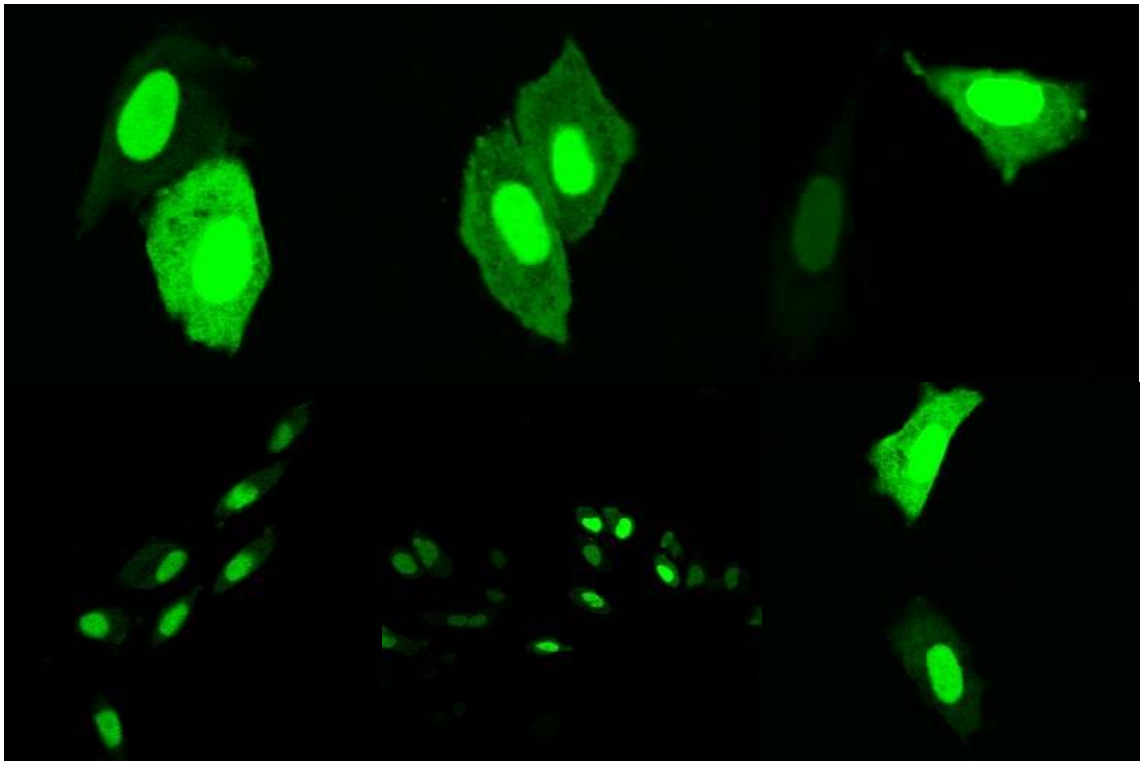

Figure 77 GFP-NLS expressing cells are often found in groups of even numbers, coupled or multinucleated.

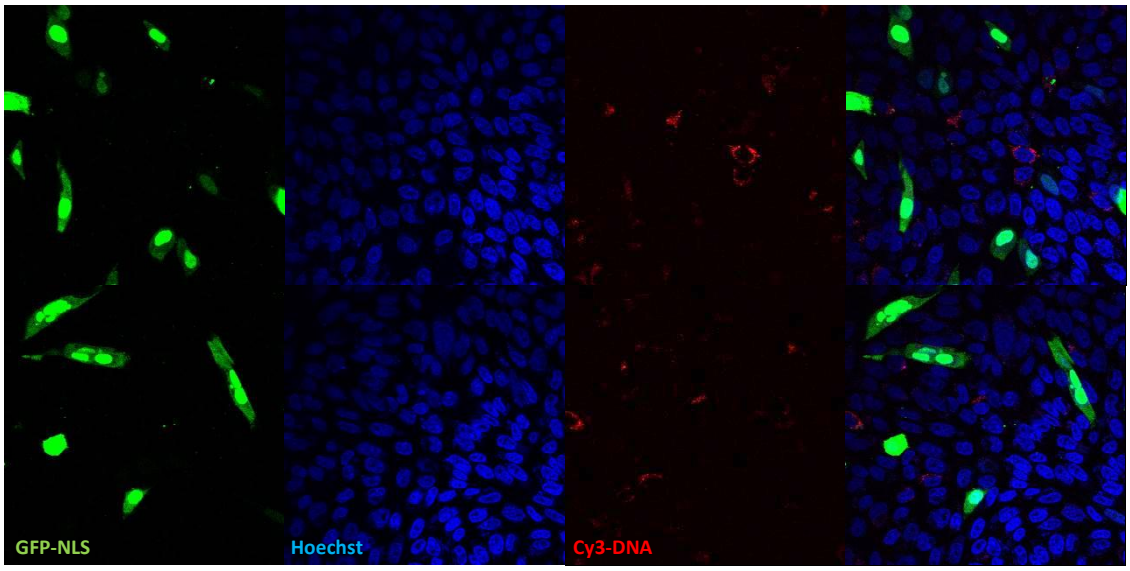

Figure 78 GFP-NLS expressing cells are often found in groups of even numbers, coupled or multinucleated.

4.1.2 Lipofectamine

So far the experiments and observations were conducted by precondensing DNA with protamine and finally with liposomes made of DC-Chol and DOPE. It was interesting to compare all these observations with a transfection gold-standard reagent: Lipofectamine. As the double transfection experiment in **Figure 79** shows, cells present a few number of red clusters and a higher number of little red puncta in the cytoplasm. Compared to the LPD nanoparticles, it was very difficult to find red signal coming from inside the nucleus or clusters of any size. As it is showed in **Figure 80**, putative nuclear red clusters are always found to be in the perinuclear region and never inside the nucleus.

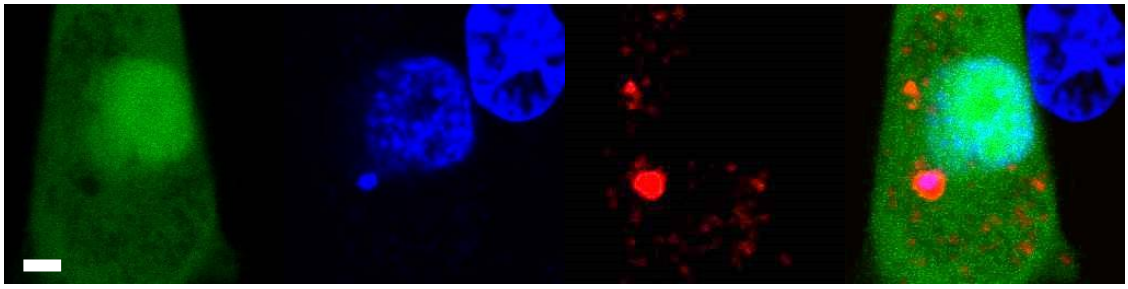
Figure 79 Cells transfected with Lipofectamine (Cy3 and GFP-NLS plasmids). Scale bar = 5 µm.

It was then interesting to check, whether the protamine was responsible for the higher chance of localization of nuclear red spots and an experiment of transfection using precondensation of DNA with protamine and then Lipofectamine liposomes show an increase in the number of cells positive for bigger red clusters in the cytoplasm and inside the nucleus **Figure 81**. These results encourage to think that protamine could be really involved in this process of DNA clustering but it always remains the doubt whether this clusters could actually provide bioavailable plasmidic DNA inside the nucleus. Also in this case, actually, red spots could be colocalizing in the nucleus but be trapped inside the channels. This may not be always the case

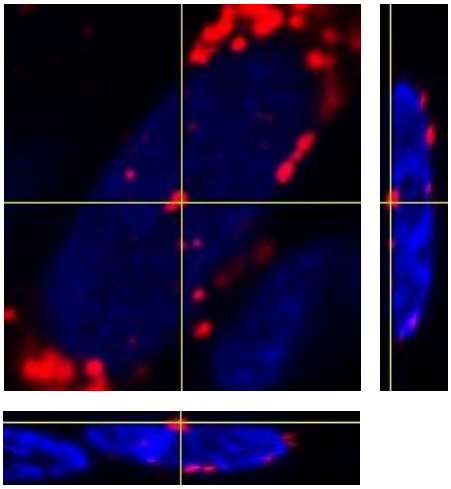

as it is showed in **Figure 82 - Figure 83**, where the red cluster is found in either a “blue” and “green” nucleus.

Figure 80 Orthogonal views of Lipofectamine transfected CHO cells

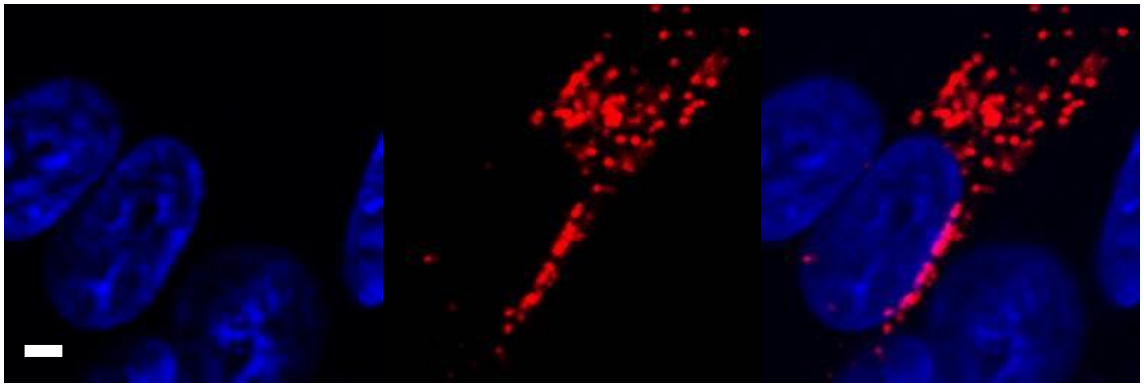

Figure 81 Cells transfected with Cy3 DNA/Lipofectamine and stained with Hoechst. Scale bar = 5 µm.

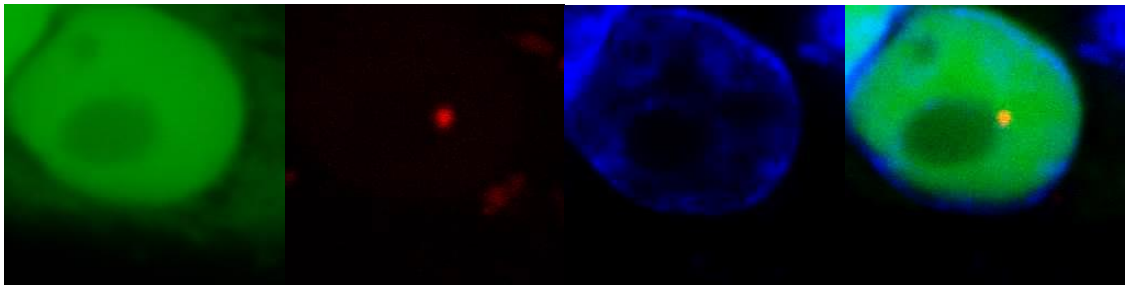

Figure 82 Red nuclear clusters in Lipofectamine transfected cells

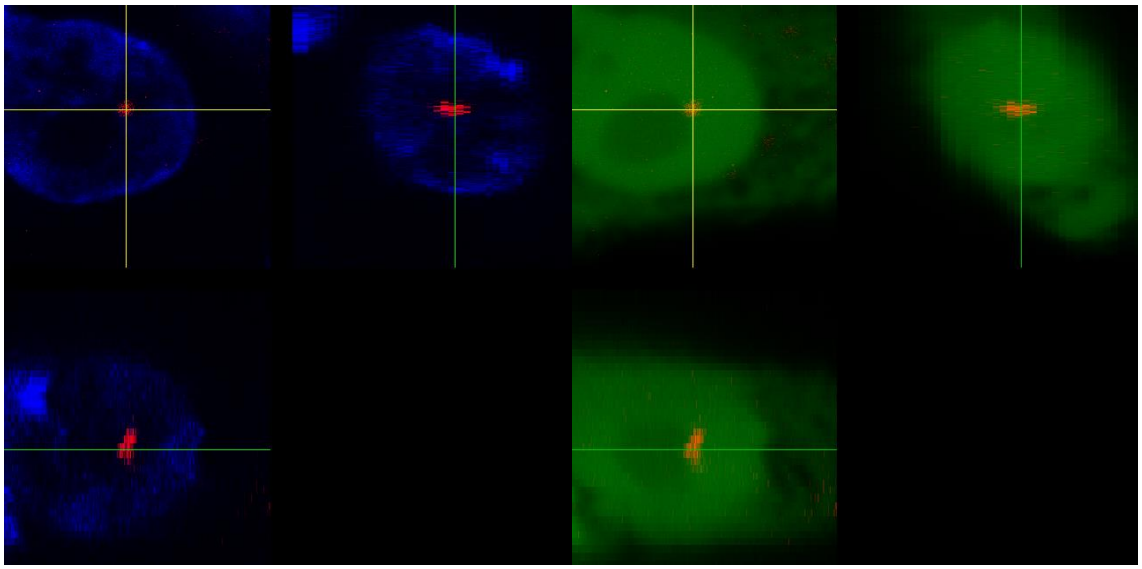

Figure 83 Z-stacks of Lipofectamine transfected cells with Cy3-DNA (z = 0.25 µm)

4.2 Transfection Efficiency measured with Flow Cytometry

A very clear observation between the two transfection nanoformulations was the different transfection efficiency in terms of "green" cells observed with confocal microscopy. As previously commented before, LPD nanoparticles are able to transfect only a few cells and often these cells are found in couple suggesting a role of cell division as a necessary prerequisite for plasmidic nuclear entry and transfection **Figure 84**. On the other hand, cells transfected with Lipofectamine reagent show a much higher transfection efficiency giving rise to a "green carpet" of cells suggesting the possibility that in this case cell division is not essential for transfection **Figure 85**. In order to quantify this difference, experiments with flow cytometry were performed to give a much higher statistical quantification of transfection efficiency between LPD nanoparticles and Lipofectamine reagent **Figure 86 - Figure 87**. As can be seen from the **Table 8** and **Table 9** Lipofectamine shows an average of 69,94% (24 h post transfection) and 65,04% (48 h post transfection), whereas LPD nanoparticles made of Protamine/DC-Chol/DOPE showed 6,11% and 5,02% of transfection efficiency after the same amount of time. These results are totally in agreement with previous confocal microscopy observations as can be seen in **Figure 84 - Figure 85**. A graph collecting together the results of transfection efficiency measured by flow cytometry is shown in **Figure 88** .

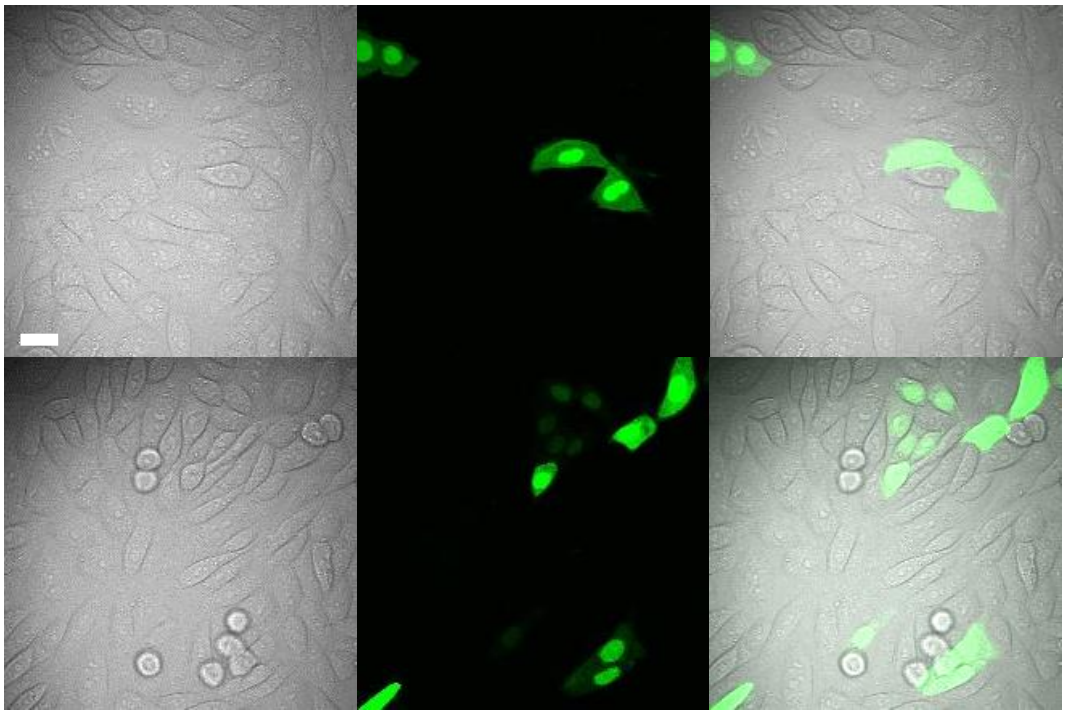

Figure 84 Confocal microscopy observation 24 h post LPD nanoparticles transfection of CHO cells. Scale bar = 20 µm.

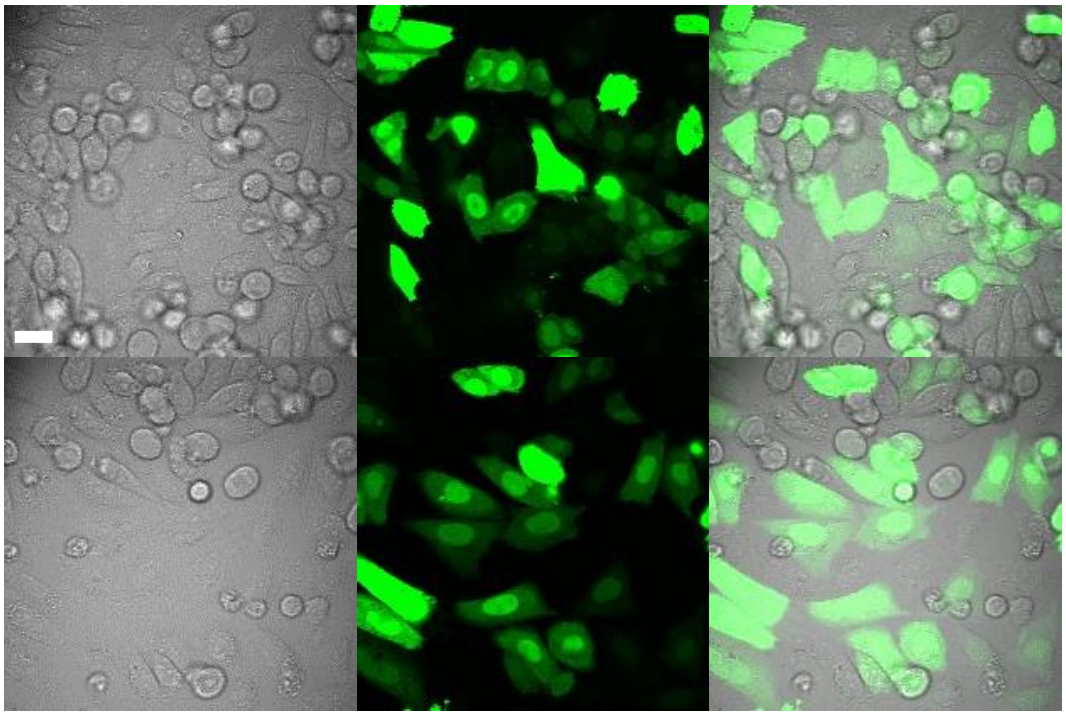

Figure 85 Confocal microscopy observation 24 h post Lipofectamine transfection of CHO cells. Scale bar = 20 µm.

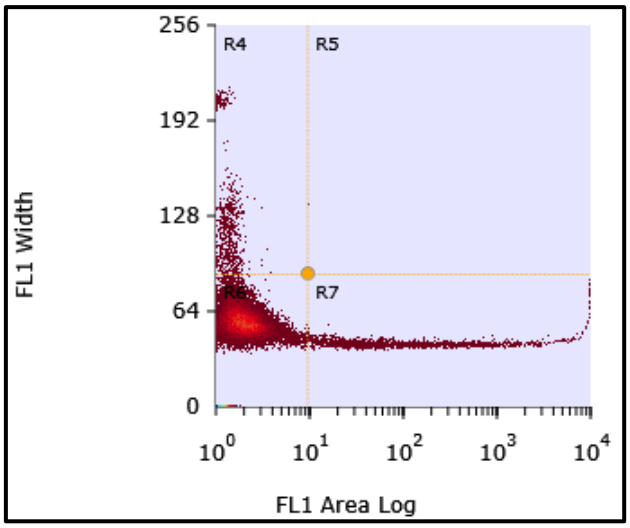

Figure 86 Plot that measures LPD nanoparticles-transfected cells.

24 h	48 h
5,69 %	5,24 %
7,21 %	5,19 %
5,82 %	5,24 %
5,71 %	4,69 %
6,11 %	**5,10 %**

Table 8

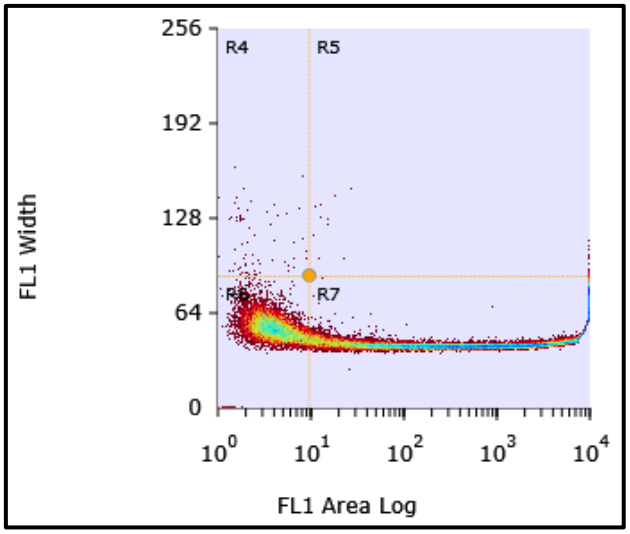

Figure 87 Plot that measures Lipofectamine-transfected cells.

24 h	48 h
77,87 %	67,78 %
61,71 %	63,66 %
77,75 %	66,93 %
61,21 %	61,81 %
69,94 %	**65,04 %**

Table 9

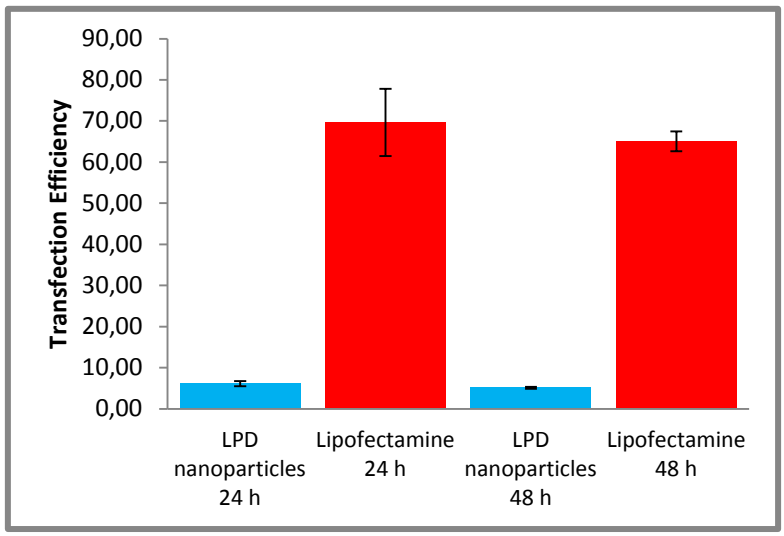

Figure 88 Histogram showing transfection efficiency measured with flow cytometry analysis.

4.3 CHO cells synchronization with mimosine

At this point it was very interesting to check the possibility that cell division represented the only way for LPD nanoparticles to transfect the cells and a protocol of cell synchronization and flow cytometry was established to test this hypothesis. These type of experiments have the aim to verify whether the "status" (in terms of cell position within the cell cycle) of cell populations prior to transfection is involved in transfection efficiency. For synchronization of CHO cells a drug called mimosine was used. Mimosine inhibits ribonucleotide reductase and thus lowers dNTPs levels available intra-cellularly, thus inhibiting entry of the cell into S phase. After mimosine treatment, the majority of cells are arrested at the border between G1 and S-phase. Through optimized addition and removal of the drug from the culture it is possible to generate a culture of highly synchronized cells. These synchronized cells were transfected at two different time points throughout the cell cycle and flow cytometry measurement was performed to determine the transfection efficiency at these various time points.

Figure 89 represents the synchronization protocol of CHO cells and **Figure 90** shows the progression through the cycle after release from mimosine. Cells were pre-synchronized for 48 h in 0.2 % FBS containing medium and then synchronized with mimosine for 14 h. Samples were taken for cycle analysis every 2 h after mimosine release (left to right, top to bottom), fixed with ethanol, stained with PI and then analyzed by flow cytometry. **Figure 91** shows the percentages of cells in each phase of the cell cycle during the progression through the cycle obtained by flow cytometry. It can be seen that the synchronization is not perfect because only 65% are synchronized in G1 phase at t = 0 h (post mimosine release) but longer treatment with mimosine is not recommended because of toxicity. Now I transfected synchronized cell populations at two different time points throughout the cell cycle. First, cells were transfected with LPD nanoparticles and Lipofectamine at 0 h and 8 h after release from mimosine and then observed at 12 h after (respectively 12 h and 20 h after release from mimosine). Since it is risky to have a population which has lost synchronization, the transfection has to be observed not too long after (like 24 h or more). These timings were chosen because the first one would allow most of the cells to reach the end of S-phase and beginning of G2-phase, thus avoiding the nuclear envelope

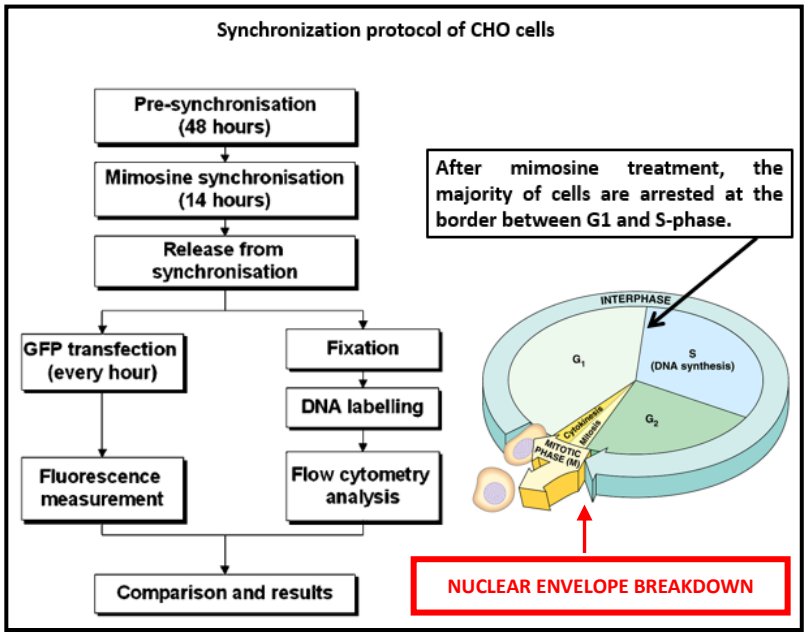

Figure 89 Synchronization and transfection protocol of CHO cells with mimosine to study transfection efficiency at different points of the cell cycle.

breakdown. The second timing, on the other hand, would allow most of the cells to go through mitosis and hence nuclear envelope breakdown.

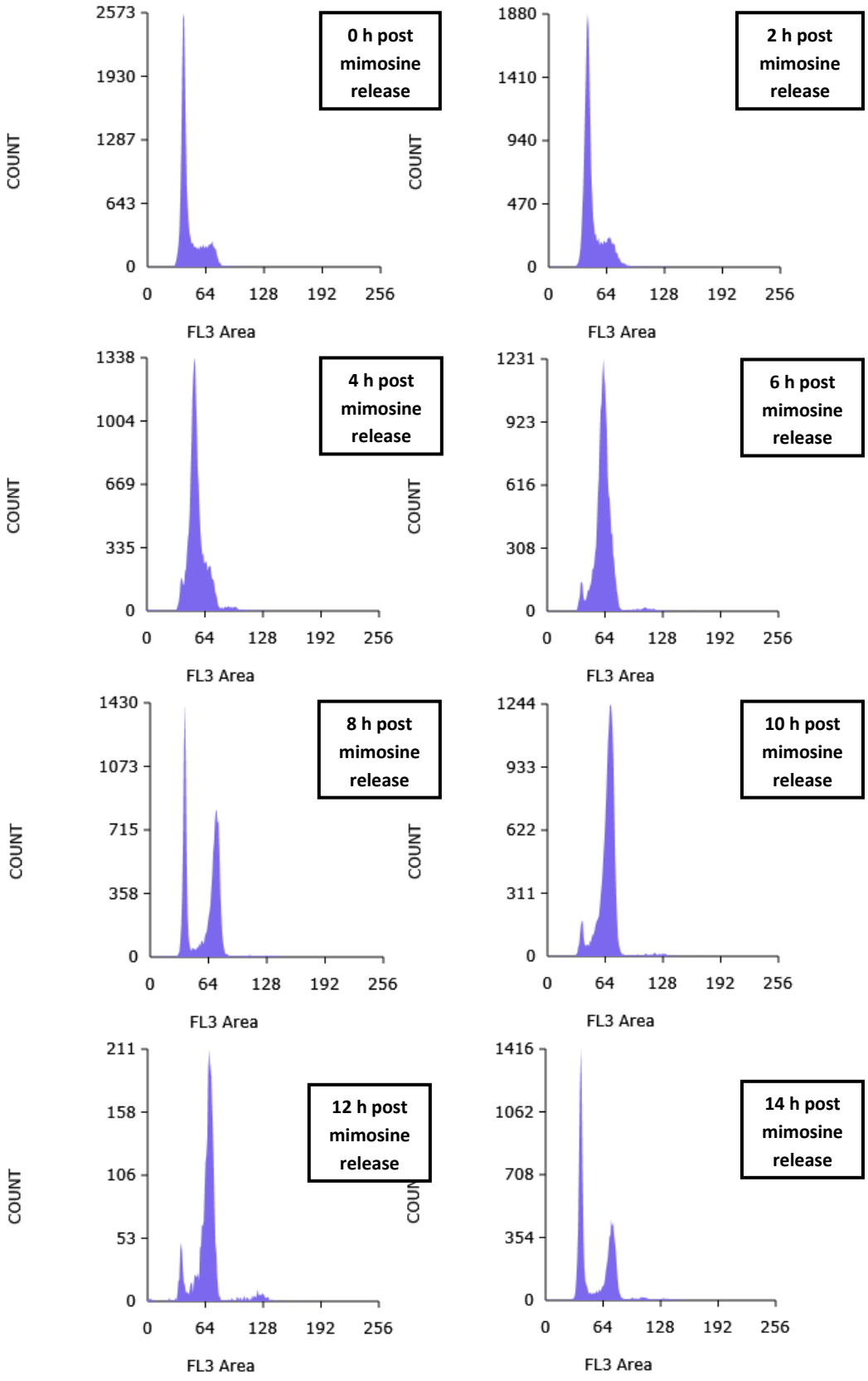

Figure 90 Progression of the cell cycle after mimosine release.

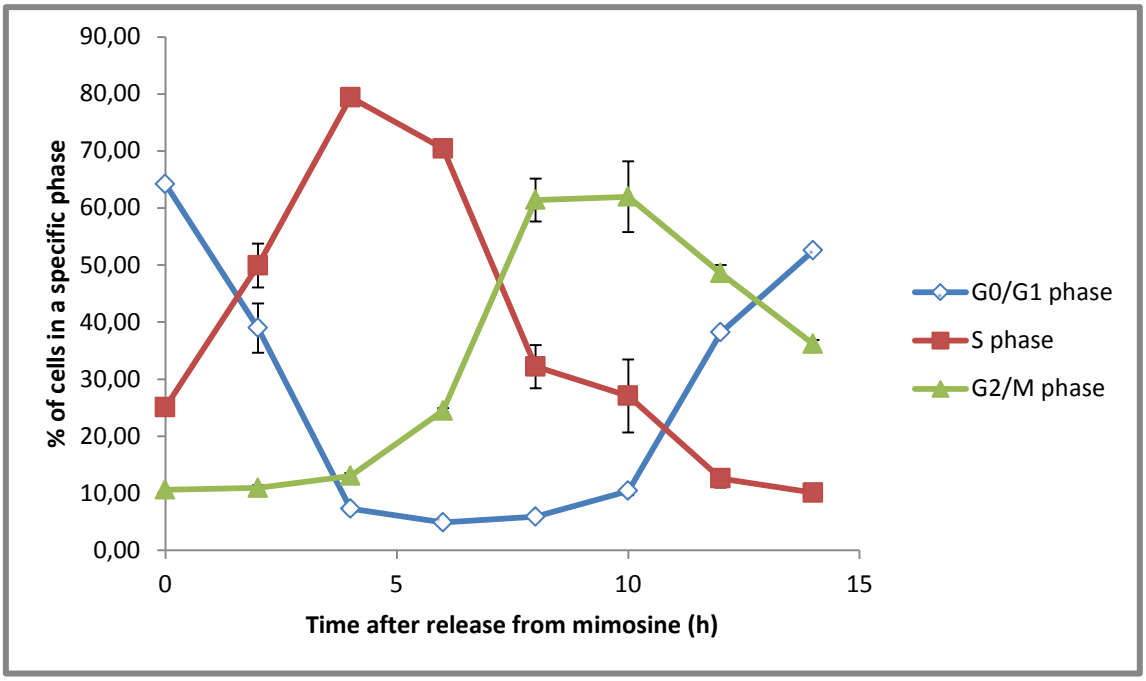

Figure 91 Percentage of CHO-K1 cells in specific phases of the cell cycle after mimosine-induced synchronization.

As can be seen in **Figure 92**, no increase of transfection efficiency is observed between these two combinations. One hypothesis is that transfecting at 8 h after release from mimosine does not give enough time for the plasmid to reach the nucleus and for the protein to be expressed. The experiment was then repeated by reducing both the selection of the second moment of transfection (from 8 h to 4 h after mimosine release) and the time interval to measure transfection efficiency by flow cytometry (from 12 h to 10 h and 8 h after transfection). These two precautions could help identifying the time necessary for the plasmid intracellular delivery plus protein expression and reducing the chance of "desynchronize" the population of cells.

As can be seen from **Figure 93** Lipofectamine reagent transfection actually shows an increase between the two different combinations of transfections after release from mimosine. On the other hand, transfection with LPD nanoparticles shows an increase only once. These results indicate that transfection with Lipofectamine of populations of cells at a higher S-phase percentage obtain a higher transfection efficiency measured with flow cytometry than populations of cells

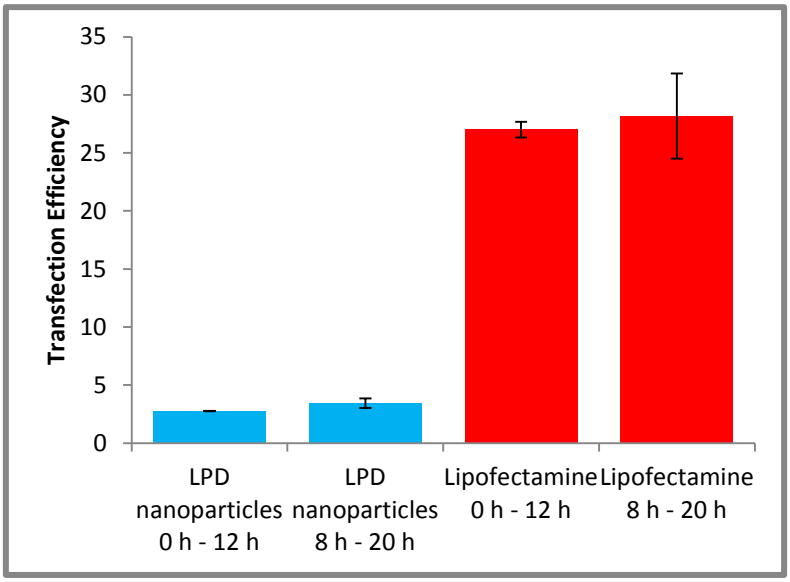

Figure 92 Histogram showing the transfection efficiency between Lipofectamine and LPD nanoparticles at two chosen timings after mimosine release.

transfected at a lower S-phase percentage. The first experiments also showed that a certain time is needed for the plasmidic-DNA complexes to enter the cell, escape from endosomes/lysosomes, become distributed within the cytoplasm, reach the nucleus and the protein be expressed. At mitosis, when the nuclear membrane disintegrates, and before it is rebuilt again, pDNA may become enclosed into the nuclear environment. Very most likely cells transfected at 0 h after release from mimosine don't have enough time to disrupt the nuclear membrane and pDNA also has a higher chance of being degraded in the lysosomes or in the cytoplasm. It is noteworthy to mention that this doesn't happen for LPD nanoparticles suggesting that maybe different mechanisms could be involved during transfection compared with Lipofectamine reagent.

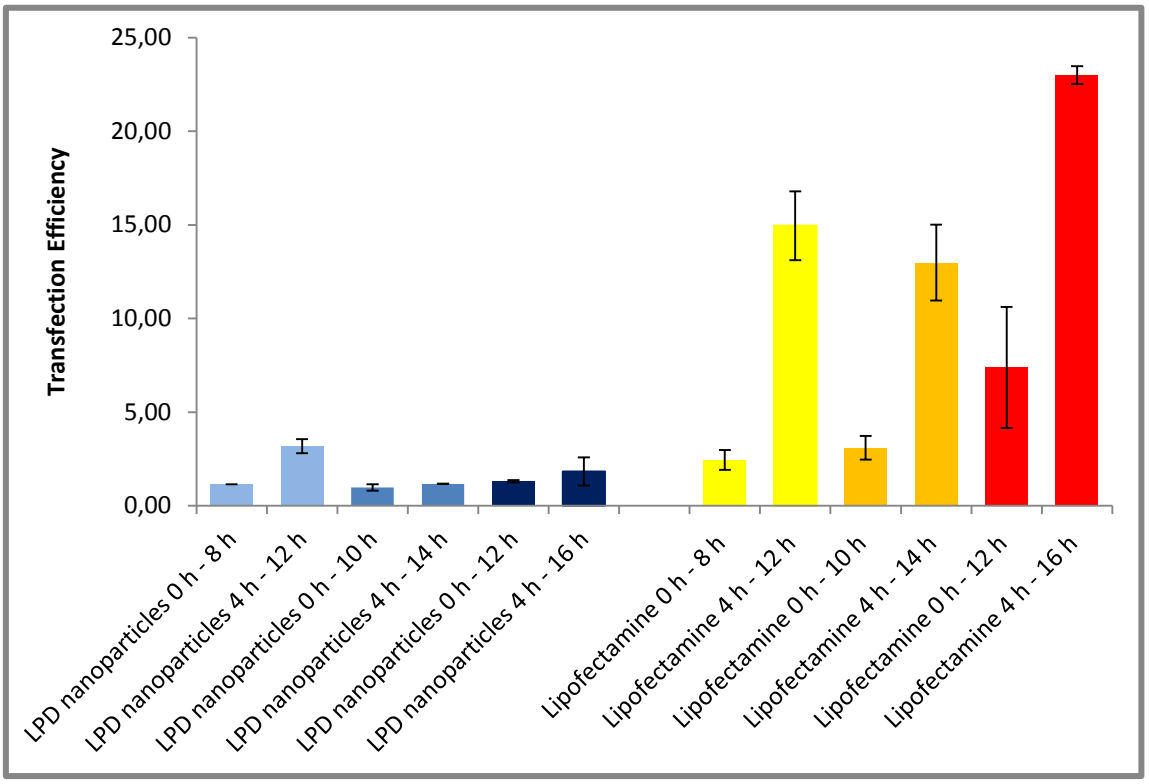

Figure 93 Histogram showing transfection efficiency of Lipofectamine and LPD nanoparticles at different temporal combinations after mimosine release in CHO-K1 cells.

These experiments provide useful proofs that mitosis actually enhance transfection efficiency but it is not able to tell whether this represents the only way possible since a certain degree of CHO cell population remained asynchronous (t = 0 h there's 25 % and 10% of cells in S- and G2-phase) and this probably is responsible for some protein expression when cells are transfected at t = 0 h after release from mimosine.

4.4 Live cell imaging with confocal microscopy

The previous experiments of flow cytometry, cell synchronization and transfection efficiency support the hypothesis of a positive correlation between successful gene transfer (in terms of protein expression) and “status” of the cell population (mitosis enhance transfection efficiency probably because plasmidic DNA can reach the nucleus and thus overcome the major barrier of the nuclear envelope). Flow cytometry provides excellent statistics, yet this method is indirect in comparison to single cell studies. It is actually possible to evaluate an entire population only at one specific time, meaning that the course of events is averaged over a certain period.

It was then decided to address the question of cell cycle correlation to exogenous protein expression by using time-lapse imaging methods that combines both the advantages of direct measurements with a statistical approach. An incubator and confocal laser scanning microscope were used to observe CHO-K1 cells over a period of over 24 h. Images were recorded every 5 minutes and subsequent analysis was performed by following the fate of singe cells **Figure 94**.

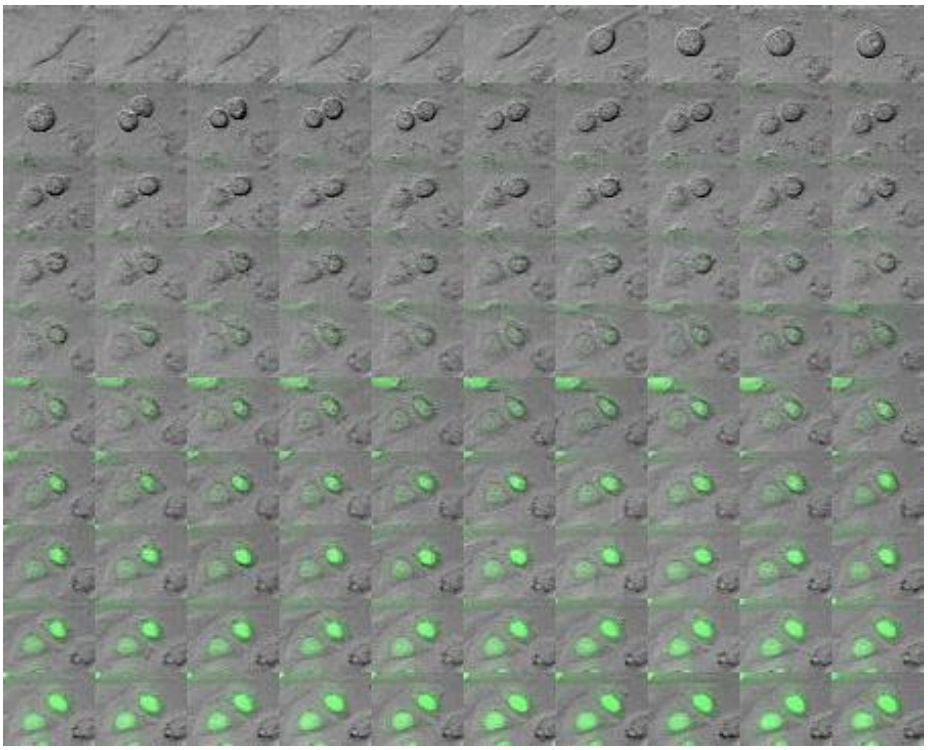

Figure 94 Time-lapse imaging of a CHO cell dividing and giving rise to two transfected “daughter” cells. Each frame is collected every 5 minutes with a 488 nm excitation Laser.

As usual, cells were transfected either with LPD nanoparticles or with Lipofectamine transfection reagent. GFP-NLS is used as reporter for successful lipoplex transfection. It is found that only cells entering mitosis were able to express the fluorescent protein reporter GFP-NLS. Concentration of the reporter to the relatively small nuclear volume leads to a faster increase in signal intensity above noise without requirement for protein expression to the same minimally detectable level in the cytoplasm. This reduces the uncertainty in determining

the moment of first expression. It is noteworthy to mention that cells up to at least 10 h post cell division could express the protein reporter indicating stability of pDNA in the cytoplasm **Figure 95**. This is important because it provides evidence that there must not be necessarily a small time window for transfection coupled to active mitotic activity. Lipoplexes and (especially) LPD nanoparticles may then be quite stable in the cytoplasm. Cell live imaging allows also to determine the length of the cell cycle by measuring two consecutive detachment timings of the cells. For CHO-K1 cells the cell cycle has a length of 14,4 ± 1,7 h (*n* = 35) which is in agreement with data coming from synchronization analysis previously described.

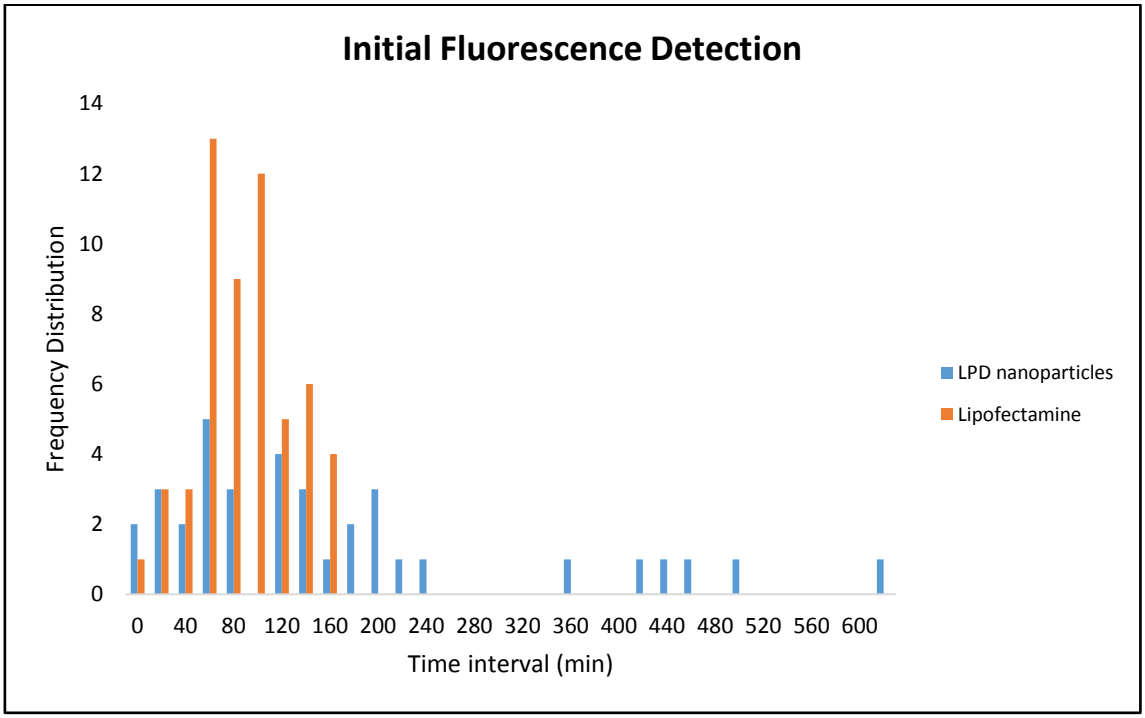

Figure 95 Frequency distribution histogram graph that shows the different initial fluorescence detection signals after division for CHO cells transfected with LPD nanoparticles and Lipofectamine.

Confocal fluorescence live cell microscopy confirm the different transfection efficiency between the two transfection nanoformulations. In order to see if any other differences could be appreciated, it was performed a fluorescence analysis of each couple of cells becoming "green" after mitosis over time **Figure 96**.

As can be seen from the graphs in **Figure 96**, the fluorescence profiles over time of the two "daughter" cells after mitosis between Lipofectamine and LPD nanoparticles show different trends. Cells transfected with Lipofectamine show a symmetry of fluorescent signal between the two daughter cells after cell division; by contrast, cells transfected with LPD nanoparticles present in 30% of analyzed samples a marked asymmetry of the fluorescent signal with the extreme case of just one "daughter" cell being transfected.

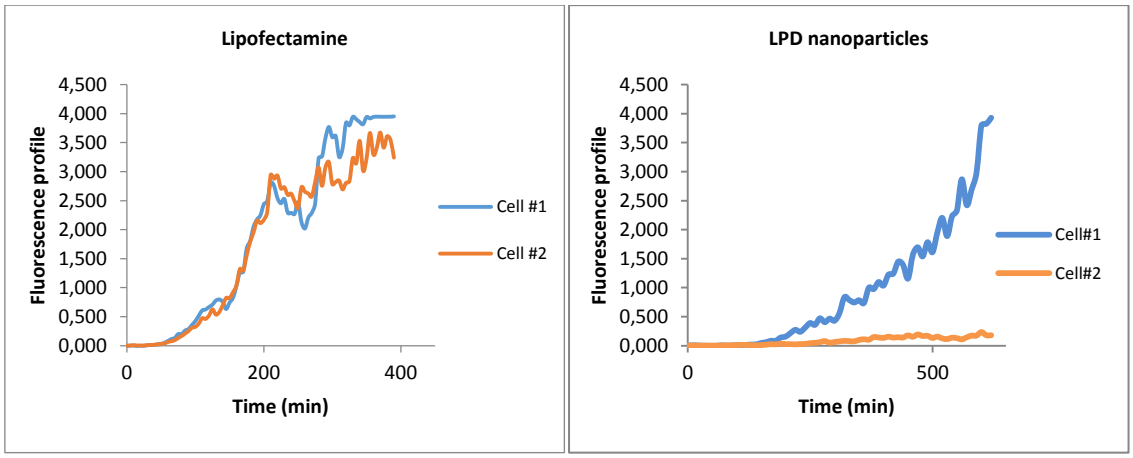

Figure 96 Fluorescence profile analysis of two daughter cells after mitosis for LIpofectamine-transfected cells (left) and LPD-nanoparticles-transfected CHO cells (right). These are two representative samples chosen to show the different trend between the two transfection nanoformulations.

An interesting observation comes from **Figure 95**: usually, in fact, longer time-lags are observed for LPD-nanoparticles-transfected cells before fluorescence signal can be detected, as compared to Lipofectamine. These observations may help elucidating the differences between the two formulations in terms of transfection efficiency: transfection with lipids/protamine could yield lower TE, compared to Lipofectamine, because of a lower bioavailability of pDNA, which may be clustered in a few “big” aggregates described before in the first part of the results. These clusters may help to explain the asymmetry observed with the fluorescence profile analysis (both in terms of lag time for initial fluorescence detection and counts of extreme cases where only one daughter cell becomes “green” after division). In other words, a limited number of pDNA molecules can be segregated into the two nuclei of the daughter cells after the nuclear envelope breakdown, giving rise to a pronounced asymmetry of the fluorescence signal between daughter cells.

5 Discussion

DNA complexes used during transfection must overcome several barriers to enter the plasma membrane, cytoplasm and nucleus of a target cell in order for the transgene to be translated into protein. As these complexes encounter each of these barriers, they are subject to a certain probability of success (or failure) in overcoming these obstacles. The cumulative probability of success for the entire journey influences the transfection efficiency for a given system. This is the reason why successful non-viral gene nanocarriers require a deep understanding of the mechanisms involved in their interaction with target cells that goes beyond the simple evaluation of final transfection efficiency. Design of efficient nanoparticles and studies focused on each single step of transfection are needed so that the main disadvantage of non-viral vectors, that is a relatively low efficiency compared to virus, can be efficiently improved. The findings reported in this study bring to several interesting conclusions and highlight further open questions that deserve investigation in future studies.

As previously said, there is the need to predict which of the intracellular barriers represent the main rate-limiting factor in the transfection process. In this project I focused on the cytoplasmic and nuclear compartments with the aim of increasing the overall understanding of the sequence of events encountered by lipid-mediated DNA delivery systems during their intracellular journey. The ability of a non-viral vector to escape from the endosomal compartment can strongly influence the carrier's transfection efficiency. Phenotype analysis of LPD systems (DC-Chol/DOPE/Protamine) confirms the evident property of endosomal escape and DNA release in the cytoplasm. Transfection with LPD nanoparticles, whose lipids and DNA are respectively labeled with NBD and Cy3, clearly shows spread into the cytoplasm and can give rise to cells with diffuse "red" cytoplasmic signal coming from plasmidic-labeld DNA. In this regard, FRAP experiments give quantitative contribute to understand which "species" of DNA are being observed: some cells actually show a phenotype with "red" cytoplasmic diffuse signal that, when photobleached in a limited region of interest, present a slow recovery of fluorescence, thus compatible with the presence of intact plasmidic DNA molecules. I believe it is interesting that no positive correlation is observed between this kind of phenotype and transfection efficiency (in terms of "green cells" observed by confocal microscopy). This prompts me to speculate that efficient endosomal escape does not necessarily bring to high TE, probably because of other factors that may influence the overall yield of this process. Vectors and cellular factors that enhance cytoplasmic DNA mobility may then have a role in increasing the efficacy of gene expression. Actually, the slow diffusion of plasmidic DNA in the cytosol has probably necessitated the evolution of efficient packaging and transport mechanisms to carry viral DNA across the cytoplasm. Interaction between viral proteins and the microtubular network and/or the actin cytoskeleton appears to account for the efficient nuclear targeting of viral particles. The vectorial transport of viruses to the nucleus could thus serve as a paradigm to design more efficient DNA delivery systems to improve non-viral gene delivery methods.

The observation of "red" DNA clusters inside the nucleus both with LPD nanoparticles and Lipofectamine (with an initial step of pre-incapsulation of DNA with protamine) represents a strong evidence of the putative role played by protamine. First of all, different methods were used to confirm the real localization of DNA clusters inside the nuclear compartment, such as

z-stack collections and 2-channel-fluorescence-profile analysis along the three axes. It is observed that the number of these clusters increases both in number and dimensions when the ratio (weight/weight) Protamine:DNA increases (from 0.5:1 to 8:1). Collectively, it is shown that protamine represents a good DNA condenser with the advantage of nuclear targeting improvement (because of the presence of NLS signals within protamine sequence). On the other hand, also in this case, no positive correlation is observed between red clusters inside the nucleus and "green" GFP-expressing cells (index of transfection efficiency). This observation inspired further investigations of the role and localization of these nuclear red clusters. In this regards, FM4-64 dye proved extremely useful to gain insights into this observation: the major practical advantage of dual-excitation imaging of FM4-64 resides in the ability to visualize the nuclear envelope (NE) in unaltered cells (without the need to transfect NE-resident fusion proteins). LPD nanoparticles were then used associated with FM4-64 showing colocalization between Cy3-DNA and FM4-64-NE. As described by Fricker *et al*.[59], this may be explained by the entrapment of DNA clusters inside tubular channels, of both inner and outer nuclear membranes, that extend deep into the nucleoplasm (up to more than 90% in CHO cells). One possible function of such invaginations is to bring a larger proportion of the nucleoplasm close to a nuclear pore. They actually esteem that three or four appropriately placed tubes would bring almost all of the nucleoplasm within a distance of 0.5 µm from the nuclear envelope. This means that even nucleoli, which are buried within the nucleus, may lie close to the envelope. Deep tubular invaginations into the nucleoplasm occur so often in mammalian interphase nuclei that may even have a role in entrapping big clusters, like the DNA-Cy3 ones observed colocalizing with FM4-64 stain. Actually, the lumen of nuclear channels is not empty but ribosomes, small vesicles and cytoskeletal elements have all been seen. Thus, these structures may very most likely bring cytoplasmic space closer to the interior of the nucleus. Taken together, the traditional view of the NE as an approximately spherical coat defining the nucleoplasm may not represent the best one.

The observation of "green" cells found in groups or couples prompted me to study how the "status" of the cell population influences transfection efficiency. Cell synchronization using mimosine was achieved in order to evaluate transfection at different phases of the cell cycle. Transfection efficiency was monitored by fluorescence quantification of GFP with flow cytometry and I show that CHO cells passing through mitosis yield higher transfection efficiency. The nuclear membrane disintegration may allow plasmid DNA to become enclosed within the nuclear environment before this latter is rebuilt again. It is interesting to highlight two observations: 1) transfection at 8 h (< 10% of the cells are in G1 phase) post mimosine release (PMR) does not yield to higher transfection efficiency compared to 0 h (65 % of the cells are in G1 phase) PMR transfection. The increase is observed only when 4 h (< 10 % of the cells are in G1) PMR cells are compared to 0 h PMR; 2) only Lipofectamine shows such a behavior. The first observation proves that a certain time is needed for the complexes to be distributed within the cells so that at least a few will be localized in the proximity of the nucleus. The 8 h PMR transfection timing may have failed because of insufficient time for DNA to reach the nucleus giving rise to a TE comparable with the 0 h PMR one. On the other hand 4 h PMR shows a different transfection behavior and represents the timing with the highest percentage of cells in S-phase (around 80%). This supports the hypothesis that "S-phase cells" obtain higher efficiency. The last observation supports the fact that LPD complexes may have different mechanisms or require longer time compared to Lipofectamine: this represents a

novel parameter that can be included when single transfection formulations are studied (so that further investigations can be conducted to give insights into the different mechanisms involved).

In this work, GFP-expressing plasmids are used to evaluate the capacity of the transgene to be transcribed and translated into a protein. This is particular useful to verify the TE of cells when using microscopy. Though simple and practical, this method does not allow a quantitative evaluation of cell populations and other methods like protein assays (e.g. luciferase gene expression) and fluorescence plate reader measurements of GFP help to overcome this problem. In this work FACS analysis is employed to calculate transfection efficiency and, considering that most of the analysis described in the literature to prove the high efficiency of protamine are conducted with luciferase gene expression analysis, it would be interesting to check whether a similarity (in terms of general percentage or relative ratios) are maintained between these two methods when comparing different transfection formulations. This coupling may be useful to reinforce reliability of measured data.

Another method to study the differences between different transfection agents is time lapse fluorescence microscopy. Detailed image analysis coming from time lapses provide new insights on the single cell level while simultaneously achieving appropriate statistics. Flow cytometry method indicates a primary rout for transfection involving nuclear envelope breakdown but does not allow verifying the existence of mitosis-independent pathways. First, temporal relation between protein expression and cell division and second fluorescence profile analysis over time allow providing important parameters to compare, in this case, Lipofectamine with LPD nanoparticles. It was found that all transfected cells go through mitosis before becoming “green”. This is a striking observation that confirms the need for a cell to enter mitosis in order to be transfected. This is in partial disagreement with a similar work by Kirchenbuechler *et al*.[61], that in HeLa cells reports a ≈ 3% of the cells expressing the protein without preceding proliferation. Moreover, cells entering mitosis up to at least 10 h post division express the fluorescent protein reporter GFP-NLS. This indicates an impressive stability of the plasmid in the cytoplasm of at least 10 h.

These last experiments provide a new tool to study the dependence between cell division and DNA transfection compared to flow cytometry. The latter can provide only indirect support due to the averaging over entire cell populations and time frames (and, in this case, difficulty to have a 100 % fully synchronized cell population). Time lapse studies provide new and more interpretable evidence for correlation of cell division and protein expression based on statistics at the single cell level. This means it is possible to reveal the lag time needed for protein expression and evaluate if all cells go through mitosis before being transfected. Moreover through the temporal evolution of the fluorescence profile, it can be established whether two “daughter” cells show a similar protein expression pattern or not. Lipofectamine system gives rise to a marked symmetry compared to LPD nanoparticles. The latter present, in 30% of the cases, the feature that only one “daughter” cell gets transfected. This observation can help speculate possible mechanisms that may be different between the two systems. I may argue that the red clusters of DNA and protamine observed by confocal microscopy can represent less “bio-available” plasmidic DNA compared to Lipofectamine. For instance, the extreme case of just one daughter cell becoming green, may bring to think that there is a very little genetic material bio-available at the moment of cell division. The existence of red clusters of

DNA/protamine in the nucleus in not-transfected cells further supports this hypothesis (nuclear envelope breakdown). In addition, the longer time needed to detect the first expression signal reflect the necessity for a longer time to release DNA from these clusters or even inhibition of transcription (because of possible disturbance induced by protamine). These last hypotheses may help explain why I did not observe an increase in TE evaluated by flow cytometry analysis of transfected and synchronized CHO cells. Collectively, all these results provide good means to evaluate possible differences in transgene expression between two nanoformulations in terms of differences in intracellular fate of pDNA.

This work stimulates to:

1) further investigate the role of protamine as part of transfecting agents and examine in depth the putative role of nuclear channels in DNA clusters entrapment;
2) study additional transfection formulations by coupling flow cytometry with live cell imaging;
3) prove, with other experiments, whether cell division is the only requisite for efficient transfection;
4) develop new transfection methods capable of releasing DNA in early mitosis.

These results and perspectives are of great interest for the community of scientists working with cationic lipids and other non-viral nanoparticles as DNA-transfecting agents. A better understanding of the mechanisms of cellular and nuclear delivery are necessary in order to overcome the obstacle of low transfection efficiency (compared to viruses) and for guiding the rational engineering of a new generation of non-viral vectors better tailored to both *in vitro* and *in vivo* applications.

6 References

1. Kay, M. a. State-of-the-art gene-based therapies: the road ahead. *Nat. Rev. Genet.* **12,** 316–328 (2011).

2. Ibraheem, D., Elaissari, a. & Fessi, H. Gene therapy and DNA delivery systems. *Int. J. Pharm.* **459,** 70–83 (2014).

3. Luo, D. & Saltzman, W. M. Synthetic DNA delivery systems. *Nat. Biotechnol.* **18,** 33–37 (2000).

4. Elsabahy, M., Nazarali, A. & Foldvari, M. Non-viral nucleic acid delivery: key challenges and future directions. *Curr. Drug Deliv.* **8,** 235–244 (2011).

5. Yin, H. *et al.* Non-viral vectors for gene-based therapy. *Nat. Rev. Genet.* **15,** 541–555 (2014).

6. Khalil, I. a, Kogure, K., Akita, H. & Harashima, H. Uptake pathways and subsequent intracellular trafficking in nonviral gene delivery. *Pharmacol. Rev.* **58,** 32–45 (2006).

7. Hama, S. *et al.* Quantitative comparison of intracellular trafficking and nuclear transcription between adenoviral and lipoplex systems. *Mol. Ther.* **13,** 786–794 (2006).

8. Lechardeur, D. & Lukacs, G. L. Nucleocytoplasmic transport of plasmid DNA: a perilous journey from the cytoplasm to the nucleus. *Hum. Gene Ther.* **17,** 882–889 (2006).

9. Pichon, C., Billiet, L. & Midoux, P. Chemical vectors for gene delivery: Uptake and intracellular trafficking. *Curr. Opin. Biotechnol.* **21,** 640–645 (2010).

10. Lima, M. C. P. De. Cationic lipid – DNA complexes in gene delivery : from biophysics to biological applications. **47,** 277–294 (2001).

11. Wiethoff, C. M. & Middaugh, C. R. Barriers to Nonviral Gene Delivery. **92,** 203–217 (2003).

12. Medina-Kauwe, L. K., Xie, J. & Hamm-Alvarez, S. Intracellular trafficking of nonviral vectors. *Gene Ther.* **12,** 1734–1751 (2005).

13. Belting, M., Sandgren, S. & Wittrup, A. Nuclear delivery of macromolecules: Barriers and carriers. *Adv. Drug Deliv. Rev.* **57,** 505–527 (2005).

14. El-Sayed, A. & Harashima, H. Endocytosis of gene delivery vectors: from clathrin-dependent to lipid raft-mediated endocytosis. *Mol. Ther.* **21,** 1118–30 (2013).

15. Dowty, M. E., Williams, P., Zhang, G., Hagstrom, J. E. & Wolff, J. a. Plasmid DNA entry into postmitotic nuclei of primary rat myotubes. *Proc. Natl. Acad. Sci. U. S. A.* **92,** 4572–4576 (1995).

16. Lukacs, G. L. *et al.* Size-dependent DNA mobility in cytoplasm and nucleus. *J. Biol. Chem.* **275,** 1625–1629 (2000).

17. Dauty, E. & Verkman, a. S. Actin cytoskeleton as the principal determinant of size-dependent DNA mobility in cytoplasm: A new barrier for non-viral gene delivery. *J. Biol. Chem.* **280,** 7823–7828 (2005).

18. Geiger, R. C., Taylor, W., Glucksberg, M. R. & Dean, D. A. Cyclic stretch-induced reorganization of the cytoskeleton and its role in enhanced gene transfer. *Gene Ther.* **13,** 725–731 (2006).

19. Vaughan, E. E. & Dean, D. a. Intracellular trafficking of plasmids during transfection is mediated by microtubules. *Mol. Ther.* **13,** 422–428 (2006).

20. Melchior, F. & Gerace, L. Mechanisms of nuclear protein import. *Curr. Opin. Cell Biol.* **7,** 310–318 (1995).

21. Glover, D. J., Leyton, D. L., Moseley, G. W. & Jans, D. A. The efficiency of nuclear plasmid DNA delivery is a critical determinant of transgene expression at the single cell level. *J. Gene Med.* **12,** 77–85 (2010).

22. Smoyer, C. J. & Jaspersen, S. L. Breaking down the wall: The nuclear envelope during mitosis. *Curr. Opin. Cell Biol.* **26,** 1–9 (2014).

23. Grunwald, D., Singer, R. H. & Rout, M. Nuclear export dynamics of RNA-protein complexes. *Nature* **475,** 333–341 (2011).

24. Speese, S. D. *et al.* Nuclear envelope budding enables large ribonucleoprotein particle export during synaptic Wnt signaling. *Cell* **149,** 832–846 (2012).

25. Wente, S. R. & Rout, M. P. The Nuclear Pore Complex and Nuclear Transport. *Cold Spring Harbor Perspectives in Biology* **2,** a000562–a000562 (2010).

26. Lam, A. P. & Dean, D. A. Progress and prospects: nuclear import of nonviral vectors. *Gene Ther.* **17,** 439–447 (2010).

27. Cohen, S., Au, S. & Panté, N. How viruses access the nucleus. *Biochim. Biophys. Acta - Mol. Cell Res.* **1813,** 1634–1645 (2011).

28. Miller, A. M. & Dean, D. a. Tissue-specific and transcription factor-mediated nuclear entry of DNA. *Adv. Drug Deliv. Rev.* **61,** 603–613 (2009).

29. Vaughan, E. E., DeGiulio, J. V & Dean, D. a. Intracellular trafficking of plasmids for gene therapy: mechanisms of cytoplasmic movement and nuclear import. *Curr. Gene Ther.* **6,** 671–681 (2006).

30. Miller, A. M. & Dean, D. A. Cell-specific nuclear import of plasmid DNA in smooth muscle requires tissue-specific transcription factors and DNA sequences. *Gene Ther.* **15,** 1107–1115 (2008).

31. Tachibana, R., Harashima, H., Shinohara, Y. & Kiwada, H. Quantitative studies on the nuclear transport of plasmid DNA and gene expression employing nonviral vectors. *Adv. Drug Deliv. Rev.* **52,** 219–226 (2001).

32. Chan, C.-K. & Jans, D. a. Using nuclear targeting signals to enhance non-viral gene transfer. *Immunol. Cell Biol.* **80,** 119–130 (2002).

33. Gasiorowski, J. Z. & Dean, D. a. Mechanisms of nuclear transport and interventions. *Adv. Drug Deliv. Rev.* **55,** 703–716 (2003).

34. Munkonge, F. M., Dean, D. a., Hillery, E., Griesenbach, U. & Alton, E. W. F. W. Emerging significance of plasmid DNA nuclear import in gene therapy. *Adv. Drug Deliv. Rev.* **55,** 749–760 (2003).

35. *Cooper GM. The Cell: A Molecular Approach. 2nd edition. Sunderland (MA): Sinauer Associates; 2000. The Eukaryotic Cell Cycle. Available from: http://www.ncbi.nlm.nih.gov/books/NBK9876/*.

36. Grosjean, F., Batard, P., Jordan, M. & Wurm, F. M. S-phase synchronized CHO cells show elevated transfection efficiency and expression using CaPi. *Cytotechnology* **38,** 57–62 (2002).

37. Tseng, W. C., Haselton, F. R. & Giorgio, T. D. Mitosis enhances transgene expression of plasmid delivered by cationic liposomes. *Biochim. Biophys. Acta - Gene Struct. Expr.* **1445,** 53–64 (1999).

38. Brunner, S. *et al.* Cell cycle dependence of gene transfer by lipoplex, polyplex and recombinant adenovirus. *Gene Ther.* **7,** 401–407 (2000).

39. Akita, H., Ito, R., Khalil, I. a., Futaki, S. & Harashima, H. Quantitative three-dimensional analysis of the intracellular trafficking of plasmid DNA transfected by a nonviral gene delivery system using confocal laser scanning microscopy. *Mol. Ther.* **9,** 443–451 (2004).

40. Kamiya, H., Fujimura, Y., Matsuoka, I. & Harashima, H. Visualization of intracellular trafficking of exogenous DNA delivered by cationic liposomes. *Biochem. Biophys. Res. Commun.* **298,** 591–597 (2002).

41. Kamimura, K., Suda, T., Zhang, G. & Liu, D. Advances in gene delivery systems. *Pharmaceut. Med.* **25,** 293–306 (2011).

42. Sorgi, F. L., Bhattacharya, S. & Huang, L. Protamine sulfate enhances lipid-mediated gene transfer. *Gene Ther.* **4,** 961–968 (1997).

43. Tsuchiya, Y., Ishii, T., Okahata, Y. & Sato, T. Characterization of Protamine as a Transfection Accelerator for Gene Delivery. *J. Bioact. Compat. Polym.* **21,** 519–537 (2006).

44. Balhorn, R. The protamine family of sperm nuclear proteins. *Genome Biol.* **8,** 227 (2007).

45. Balhorn, R., Brewer, L. & Corzett, M. DNA condensation by protamine and arginine-rich peptides: analysis of toroid stability using single DNA molecules. *Mol. Reprod. Dev.* **56,** 230–234 (2000).

46. Warrant, R. W. & Kim, S.-H. [alpha]-Helix-double helix interaction shown in the structure of a protamine-transfer RNA complex and a nucleoprotamine model. *Nature* **271,** 130–135 (1978).

47. Biegeleisen, K. The probable structure of the protamine-DNA complex. *J. Theor. Biol.* **241,** 533–540 (2006).

48. Torchilin, V. P. Recent advances with liposomes as pharmaceutical carriers. *Nat. Rev. Drug Discov.* **4,** 145–160 (2005).

49. Rädler, J. O., Koltover, I., Salditt, T. & Safinya, C. R. Structure of DNA-cationic liposome complexes: DNA intercalation in multilamellar membranes in distinct interhelical packing regimes. *Science* **275,** 810–814 (1997).

50. Caracciolo, G. *et al.* Factors determining the superior performance of lipid/DNA/protammine nanoparticles over lipoplexes. *J. Med. Chem.* **54,** 4160–4171 (2011).

51. Mandal, B. *et al.* Core-shell-type lipid-polymer hybrid nanoparticles as a drug delivery platform. *Nanomedicine Nanotechnology, Biol. Med.* **9,** 474–491 (2013).

52. Pozzi, D. *et al.* Mechanistic evaluation of the transfection barriers involved in lipid-mediated gene delivery: Interplay between nanostructure and composition. *Biochim. Biophys. Acta - Biomembr.* **1838,** 957–967 (2014).

53. Ishikawa-Ankerhold, H. C., Ankerhold, R. & Drummen, G. P. C. Advanced fluorescence microscopy techniques-FRAP, FLIP, FLAP, FRET and FLIM. *Molecules* **17,** 4047–4132 (2012).

54. Goldys, E. M. *Fluorescence Applications in Biotechnology and Life Sciences*. (John Wiley & Sons, 2009).

55. Loura, L. M. S. Lateral distribution of NBD-PC fluorescent lipid analogs in membranes probed by molecular dynamics-assisted analysis of förster resonance energy transfer (FRET) and fluorescence quenching. *Int. J. Mol. Sci.* **13,** 14545–14564 (2012).

56. Zal, T., Zal, M. A., Lotz, C., Goergen, C. J. & Gascoigne, N. R. J. Spectral shift of fluorescent dye FM4-64 reveals distinct microenvironment of nuclear envelope in living cells. *Traffic* **7,** 1607–1613 (2006).

57. Reits, E. a & Neefjes, J. J. From fixed to FRAP: measuring protein mobility and activity in living cells. *Nat. Cell Biol.* **3,** E145–E147 (2001).

58. Kang, K., Lee, S. B., Yoo, J. H. & Nho, C. W. Flow cytometric fluorescence pulse width analysis of etoposide-induced nuclear enlargement in HCT116 cells. *Biotechnol. Lett.* **32,** 1045–1052 (2010).

59. Fricker, M., Hollinshead, M., White, N. & Vaux, D. Interphase nuclei of many mammalian cell types contain deep, dynamic, tubular membrane-bound invaginations of the nuclear envelope. *J. Cell Biol.* **136,** 531–544 (1997).

60. Masuda, T., Akita, H. & Harashima, H. Evaluation of nuclear transfer and transcription of plasmid DNA condensed with protamine by microinjection: The use of a nuclear transfer score. *FEBS Lett.* **579,** 2143–2148 (2005).

61. Kirchenbuechler, I., Kirchenbuechler, D. & Elbaum, M. Correlation between cationic lipid-based transfection and cell division. *Exp. Cell Res.* (2015). doi:10.1016/j.yexcr.2014.11.019

7 Acknowledgments

The end of this Master's Thesis project does not represent for me only the end of a laboratory research experience and the accomplishment of an educational duty but also the end of 5 long years of studying and living between both the University of Pisa and Scuola Normale Superiore.

It is hard to believe that a long time has passed, though it looks like yesterday when I first enrolled at University, but the good thing is to feel like A LOT has changed in me and around me. If I could describe all these years with one word, that would be "change". I have been feeling like not having a static situation for a long time and I think this is something (very most likely the most important) that has always kept me alive and lively. A lot of things have happened since I moved to Pisa and I am pretty sure I felt intensely most of the possible emotions that a person can ever experience. Maybe, only now, I can say that I am grateful for all the good and bad times and for all the people that have been there, both those who still are and those who are not any more.

There are a lot of people I feel like thanking for this last year I spent at the laboratory NEST, both inside and outside the job environment. First of all I have to thank my supervisor Francesco for having me accepted as his Master's student trainee. I appreciate all the conversations we have had together. I like his being always positive and hardly ever pessimistic. I like his calm and tranquility but most of all I value a lot his always being there and constant participation during all the time I spent at NEST. Last but not least, I am happy of the project's topic he entrusted to me because, though along the way it has not always been easy to remember it, it was very interesting and stimulating from my biological point of view. I want to thank also Giulio Caracciolo from Rome for his support and passion for his job.

Then I want to thank my dear friend Daniele who has helped me a lot through all this period and I am grateful for all the discussions and suggestions he has given me along the whole path, both this last year and especially for all these 5 years I spent in Pisa. He is one of the best memories I will always have of my experience in Scuola Normale Superiore (when I focus on the positive things) and he will always be one of the best "teachers" I have ever had around me. I appreciate his constant help and attempt to answer to all my "whys". Most of the times he helped me satisfy all my doubts and contributed to give a sense to a lot of things that for me were completely nonsense (especially in Mathematics and Physics obviously). I will always be thankful for the huge help he has given to me. Also I thank him for having me brought pizzas at nights when I had to perform cell cycle analysis experiments.

After that, I want to thank a lot of people in the laboratory and a special acknowledgment goes to those who had (almost) always a smile on their face: Sara Antonini, Sara Macchi, Melissa, Domenica, Enrico, Laura, Paola, Claudia, Fulvio, Cecilia, Domenico, Teresa, Pierluigi, Carmine, Francesco, Riccardo, Rosy, Barbara and Gianmarco. I am grateful they also managed to get smiles out of me as well. I think "our job" is not easy, is not easy at all, and I value to have met people who were not completely self-absorbed, who were kind and (at least sometimes) sensitive to other people around them. They helped me go through some difficulties and discouragements and I wish to find these qualities (kindness, availability, tranquility), even a little bit, even if not in everyone, everywhere I will go. I am easily influenced by people around

me and I think that, especially in a laboratory and in the research field, a very few things and attitudes can help improve tremendously the job environment and overcome the ordinary (and daily-routine) frustrations.

Another special acknowledgment goes to some other people that have sustained me in (many) other ways and for (many) other reasons. I want to thank (again) my supervisor Francesco, Emanuela Colla, Vittoria Raffa and Prof. Antonino Cattaneo. These last few months were kind of a burden for me because of all the uncertainties and doubts about the next future steps. I am grateful for all the nice and long conversations we have had. I totally understand it must not be easy to deal with people who are insecure and (almost always) doubtful like me and I value every single moment you have spent with me talking. I want to thank you for all the many recommendation letters you have provided me for the many applications I have submitted during all these months (internships, job positions, PhDs applications, summer schools). I will never take for granted all of the help you have given to me and will always be grateful for this. Thank you.

Eventually, I want to thank my friends Francesco B., Francesco C., Gioacchino, Andrea, Tommaso, Alexia and Lucia with whom I enjoyed life outside the laboratory. Thank you for the amusement, reliability, stimuli and (when needed) seriousness you have given to me. I thank also many other friends: Lorenzo, Guglielmo, Dario, Alessia, Irene, Valeria, Nicola, Giovanna, Antonio F., Giada G., Michele Sab., Antonio C., Michael, Leonard, Estelle, Natacha, Oury, Nicolas, Elisabetta, Vanessa, Filippo Q., Janis, Anne, Ludovica, Giada M., Francesco S., Giulia L., Vincenzo, Michele San., Michele B., Floris, Marie. I obviously thank also my family for caring about me and always sustaining me.